Understanding the interplay of structure and dynamics in neuronal networks

by
Sarah E. Feldt

A dissertation submitted in partial fulfillment
of the requirements for the degree of
Doctor of Philosophy
(Physics)
in The University of Michigan
2009

Doctoral Committee:

Associate Professor Michal R. Żochowski, Chair
Professor Mark E. Newman
Professor Leonard M. Sander
Assistant Professor Victoria Booth
Assistant Professor Jennifer P. Ogilvie

To Bozenna Pasik-Duncan, whose example, encouragement, and friendship inspires me to continue along this academic path.

ACKNOWLEDGEMENTS

As with any work of this nature, this could not have been done alone. I'd like to thank all of the members of the Zochowski lab, especially Rhonda Dzakpasu for teaching me the cell culture protocol, Jane Wang and Eva Olariu for their work on the structural labeling, and Liz Shtrahman for her help with the electrical recordings. I also would not have made it through those first few years in the lab without the patient guidance of Ben Singer and Jack Waddell who answered more of my questions than they probably should have, and were excellent friends and role models as well. I've also been blessed with wonderful officemates: Andrew Bogaard, Casey Schneider-Mizell, and David Adams. Their willingness to work though ideas on the board and take coffee and ice cream breaks has been essential for this work and my sanity.

Of course the main member of the Zochowski lab who deserves my thanks is my advisor Michal. His enthusiasm for our work and belief in my abilities has made all the difference during my time as a graduate student. I cannot stress enough how important it has been to have an advisor who has treated me as a colleague and not just a student. Thank you.

This work also involved collaborations with others and I'd like to thank my all of collaborators for their contributions. Joshua Berke and Vaughn Hetrick provided the experimental data from freely moving mice, and Jane Wang contributed the model data presented in Chapter III. The EEG data presented in Chapter IV came from Klaus Lehnertz, Hannes Osterhage, and Florian Mormann. It should also be noted

that Chapters II and III are derived from work published in [37, 38]. Chapter IV was published in [36].

Graduate school also would not have been what it was without all of those late nights bonding over Jackson homework with Eva, Evan, Steve, Rachel, and Casey. I couldn't have asked for a better study group or friends. I also can't imagine my time here without the Cronies who are too numerous to name but have provided continuous supported and encouragement. Special thanks goes to Brandon Erickson and Matt Largo for making sure that I wrote in complete sentences and remained fed throughout the production of this dissertation. Additionally, I want to recognize Ryan Muldoon for never letting me lose sight of the fact that science is fun, and that I really do love my work, even when it's hard.

Finally I'd like to thank my parents, Jan and Andy Feldt, for their support and belief in me throughout the years. Despite living a thousand miles away, they've managed to feed me through the mail and support my coffee habit, and I wouldn't be who I am today without them.

TABLE OF CONTENTS

LIST OF FIGURES

Figure

LIST OF ABBREVIATIONS

AMD	average minimum distance
CE	causal entropies
CED	causal entropy difference
DIV	days *in vitro*
EEG	electroencephalogram
FCA	Functional Clustering Algorithm
IBI	interburst interval
ISI	interspike interval
MEA	multi-electrode array
NMI	normalized mutual information
PBS	phosphate buffered saline
STDP	spike timing dependent plasticity
SWN	small-world network

CHAPTER I

Introduction

Networks are an important part of everyday life. Friends, family, and co-workers comprise our network of social interactions. The simple act of clicking on a link to a web page allows us to traverse the complicated network of the world wide web. The hierarchy of who eats who in the animal world is described by a network known as a food web. In all of these cases, I've described a network that can be classified by its nodes (elements) and the links between them (interactions). This allows us to speak of the topology, or structure, of the network: the specific way in which the nodes are connected. The nodes of the network can also have properties which change over time, leading to the observation of network dynamics. For example, consider the spread of a computer virus over the internet; the computers are the nodes of the network, and the state of the computers (infected, susceptible, protected, etc.) describe dynamics of the network as they change over time as the virus spreads and software to protect against the virus is installed.

In the examples above, not only are the elements of the network different (people, web pages, animals, computers), but the types of interactions connecting them are different as well. In certain cases, the link between the two nodes might only exists in one direction: the snake eats the mouse, but the mouse will never eat the snake. In

this case, we refer to the network as being directed, meaning that each link between nodes contains additional information about the direction of the interaction. Links can also be weighted in which case the weight of the link can give information about the strength of the interaction.

In considering the topology of a network, we must also question what happens to this structure as a function of time. If the topology of the network is approximately constant over the time scales that we are interested in studying, we call this network a static network, in which the connections and connection strengths between nodes do not change. An example of this type of network would be the air transportation network in which cities are connected if there is a direct flight between them. Because the flight schedules are highly correlated with social and economic factors which evolve on large time scales, this network can be considered to be largely constant over time [52]. If the topology of the network is not constant over the time scales in which we are interested, we call this an evolving network. (These networks are also sometimes referred to dynamic networks, but we will use the phrase evolving networks to avoid confusion with networks comprised of dynamical elements as discussed below.) For example, recent work has investigated the effects of the addition and deletion of email addresses over time to the structure of the network of email address books [146]. This changing structure has important implications in the spread of computer viruses through email.

Finally, it is important to remember that many networks exist to perform a specific function, and often we must concern ourselves with the properties of the individual nodes in addition to how they are connected. Specifically, we are interested in the case in which the network is composed of dynamical elements whose properties change as a function of time. As a simple case of a dynamic network, consider a network

composed of oscillators. If the links between the nodes represent coupling between the phases of the oscillators, then it becomes clear that the specific topology of the network will affect the phases of the individual oscillators. In fact, much work has studied the effects of network topology on the synchronization properties of oscillators [101, 16, 9].

In this dissertation, I will be interested in networks whose connections can evolve over time and whose nodes are dynamical. While there are multiple examples of evolving dynamical networks, I will focus much of the work presented here to a specific class: networks of neurons.

1.1 The brain: a complicated network of neurons

The human brain is a prime example of a complicated, evolving and dynamic network. The brain is comprised of two types of cells: glial cells and neurons. Glial cells help provide support and nutrition for the neuronal network which is responsible for information processing. Thus, to study brain function, we are interested in the neuronal network where the nodes of the network are neurons, and the synapses between neurons provide the links. A schematic of a typical neuron can be seen in Fig. 1.1. The dynamics of the neurons are characterized by the voltage of their cell membrane and the firing of action potentials. An action potential is an all or

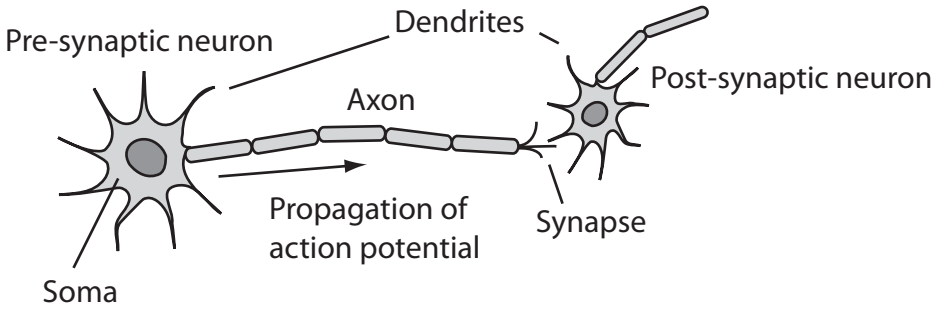

Figure 1.1: Schematic of a neuron. Neurons are connected through synapses forming a complicated network through which action potentials can be transmitted.

nothing event that lasts 1-2 ms and is characterized by the rapid depolarization and subsequent hyperpolarization of the cell membrane as seen in Fig. 1.2. The generation of an action potential is often referred to as a spike or firing of the neuron. Upon firing, a neuron will go into a short refractory period during which it cannot fire another action potential.

Action potentials are the result of changes in ion concentrations within the cell body that control the membrane potential of the cell. The cell membrane of a neuron is comprised of multiple ion channels which control the flux of various ions through the membrane. These channels are ion specific and voltage gated, meaning that they open and close depending upon the potential of the membrane. An action potential can largely be characterized by examining the flux of Na^+, K^+, and Ca^{2+} through the channels. When a neuron receives input from other neurons, the cell membrane of the soma becomes depolarized, and if this depolarization exceeds some threshold amount, a rapid opening of Na^+ channels occurs, leading to an influx of Na^+. This depolarization also activates K^+ channels on a slower time scale which causes an outflux of K^+, corresponding to the hyperpolarization of the membrane. The opening of Na^+ channels also corresponds to an opening of Ca^{2+} channels causing an influx of Ca^{2+} which helps to open the K^+ channels and aid the repolarization of the cell. While the intracellular changes in Na^+ and K^+ concentrations are negligible overall, there is a considerable increase in the Ca^{2+} concentration. Thus by monitoring the Ca^{2+} within the cell as a function of time, one can observe the firing activity of the cell. However, the Ca^{2+} dynamics operate on a much slower time scale than the action potential so Ca^{2+} signals cannot necessarily be used to distinguish single spikes if a neuron fires repeatedly.

Neurons communicate with each other through the firing of these action potentials.

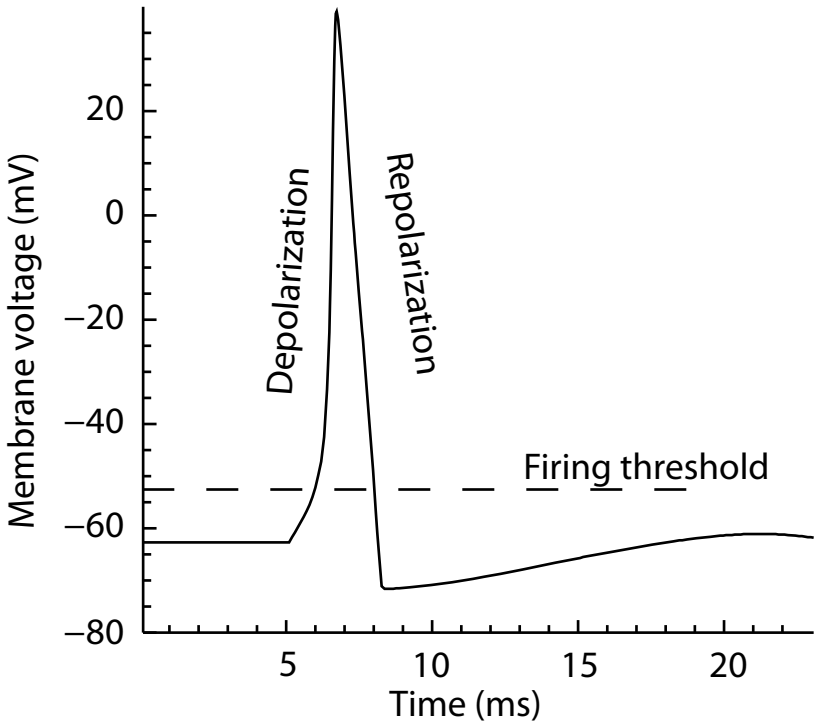

Figure 1.2: Schematic of an action potential. When a neuron receives enough input to depolarize its membrane past some threshold amount, the membrane potential will undergo a rapid depolarization followed by a rapid hyperpolarization due to the flow of ions through the voltage-gated channels in the cell membrane. This all or nothing event is called an action potential and travels down the axon of the neuron where it can be transmitted to other neurons through synapses.

An action potential is generated in the soma of a neuron and travels down the axon and through synapses to the dendrites of other neurons. The transmission of the signal through the synapse can be electrical in which case the synapse is called a gap junction, but most synapses are chemical synapses. In this case, the axon and dendrite of the two neurons are separated by what is called the synaptic cleft, which is simply the name given to the physical space separating them. When the action potential reaches the synapse, it initiates the release of neurotransmitters that diffuse into the synaptic cleft and bind to receptors on the post-synaptic terminal. This initiates the opening of ion channels in the post-synaptic cell which will either cause that cell to depolarize (an excitatory synapse) or hyperpolarize (an inhibitory synapse). The post-synaptic cell integrates the input from all of its connections and

then, dependent on the resulting polarization, will generate an action potential and continue the transmission of the signal.

1.1.1 Anatomical structure influences dynamics

Since a neuron determines if it will fire an action potential based upon the input it receives from other neurons, the specific topological or anatomical structure of the network will greatly impact the firing patterns of the neurons. Due to the fact that many network topologies cannot be analytically studied, much work initially focused only on networks with either local or all-to-all coupling. For example, consider the Hopfield neural network model [58] which traditionally involves symmetric all-to-all coupling. Only recently have mathematical tools been developed that allow this model to be studied analytically for topologies with neither all-to-all nor sparse coupling [149]. Random graphs are also attractive to study because analytical solutions can be obtained [137], but random graphs do not describe most real-world network structures [95]. A more realistic topology is given by a small-world network (SWN). In fact, it has been shown that the anatomical structure of the neuronal network of *C. elegans* has small-world properties [148]. These networks are characterized by high clustering with a short path length, and much recent work has focused on their synchronization properties [147, 57, 78, 9].

To study the effects of synchronization under different topologies, consider a network of neurons positioned on a 2D lattice and examine the dynamics of the network as we transition the connections between neurons from local to random. To do this, we will use the idea of a Watts-Strogatz SWN [148]. A neuron initially sends connections to neurons located within a certain radius. Each of these connections is then rewired with a probability, p. Thus, by varying p from 0 to 1, it is possible to transition the structure of the network from purely local connections to an entirely

random connectivity. For intermediate values of p, the network will exhibit small-world properties: high clustering due to local connections, but a small path length due to the addition of global random connections. The dynamics of the network will also vary according to the connectivity of the network. For a purely local network with $p = 0$, if we stimulate a group of neurons in the center of the network, the activity will propagate outward in a circular traveling wave. For SWNs, we will see a very different behavior. The network will display sustained asynchronous activity with small clusters of neurons active at any given point in time. This behavior changes yet again for a random network, as all of the neurons will synchronize their activity and fire in entire network bursts.

Different parts of the brain perform different functions based on different types of neural activity patterns, thus it is not surprising that the anatomical structure of different brain regions is also varied. For example, the neocortex is composed of cortical columns whose neurons have similar responses to incoming stimuli. These columns combine to create the various functional regions of the cortex [64]. While the functional regions of the cortex are connected locally through interneurons, few long range connections exist between functional regions, giving the neocortex a small world structure [22].

The connections between regions of the cortex tend to be bi-directional, but the hippocampal formation, which is associated with learning and memory, has a different type of gross neuronal organization. Here, connections between areas tend to be uni-directional, forming loops with important applications for information processing. In a somewhat simplified description of hippocampal structure, sensory information from the cortex enters the hippocampus through the entorhinal cortex. Cells in this region project their outputs to the dentate gyrus which in turn sends its output to

the CA3 region of the hippocampus. From here, the cells project to the CA1 region, which sends output back to the entorhinal cortex both directly and though a structure called the subiculum [4]. The difference in structure between the hippocampus and other neocortical regions is largely believed to be derived from the fact that the type of information processing done in the hippocampus is different from that in other brain regions.

There are also observed differences in anatomical brain structure between healthy and pathological cases. For example, epilepsy is often associated with mossy fiber sprouting and the re-organization of axons in the dentate gyrus [103]. Here, the axons of neurons in the granular layer of the dentate gyrus grow aberrant connections to neighboring cells, resulting in a re-organization of network structure that has been associated with an increased excitability (ease of firing) of the network [134]. This increased excitability is associated with the abnormal hypersynchronous activity of neurons during seizures. Patients with Alzheimer's disease also show structural changes in the brain characterized by an overall excess atrophy of the cortex, specifically in the mesial and lateral temporal lobes [83]. Additionally, Alzheimer's disease can be predicted by the amount of shrinkage of the hippocampus as a function of age, as this structure shows considerable loss in those who develop the disease [56].

It should also be noted that individual neuron properties can also influence neuronal dynamics. While in certain cases of epilepsy the observed increase in excitability has been associated with structural changes due to mossy fiber sprouting, the excitability of a neuron is also due to variables not associated with structure. The excitability of a neuron can be thought of in terms of the resting potential of the neuron and the threshold value which much be crossed for the generation of an action potential. Thus, the raising (lowering) of the resting potential or lowering (raising)

of the threshold value will have implications on the dynamics of the neuron, as it changes whether or not a neuron will fire based on a specific amount of input. This, in turn, will affect the overall network dynamics and propagation of action potentials.

1.1.2 Dynamics influence anatomical structure

In addition to the anatomical structure and dynamic properties of neurons influencing their firing patterns, the specific temporal firing relationship between two neurons can also impact the strength of the connection between them. The famous phrase summarizing the work of Hebb: "Neurons that fire together wire together." is a prime example of how related firing patterns between a pair of neurons is linked to the strength of the connection between the neurons. Here, I refer to a phenomenon called synaptic plasticity [55]. The strength (efficacy) of a synapse connecting two neurons change can change over time, dependent upon the firing patterns of the neurons. Thus, in an excitatory connection, if the efficacy of the synapse is increased, the firing of the pre-synaptic neuron will have a larger depolarizing effect on the post-synaptic neuron, making it more likely for that neuron to fire. This idea has been further developed into a theory known as spike time dependent plasticity (STDP) [1]. Here, the strength of a synapse is increased if a post-synaptic neuron fires within some small window of time after the pre-synaptic neuron. However, if the post-synaptic neuron fires before the pre-synaptic neuron, the strength of the synapse is decreased. Thus, the brain is an evolving network whose evolution is dependent upon its dynamics.

1.1.3 Functional structure

The ability of a synapse to evolve through STDP has important implications for learning and memory, as it provides a mechanism for the brain to change its

properties and store new information. But how does the brain code this information? One hypothesis which again emphasizes the importance of firing patterns of neurons is the temporal correlation hypothesis [51, 124]. In this case, correlated activity of neurons allows for feature binding and coding of objects. An example of this mechanism can be seen in Fig. 1.3. Different subsets of neurons code for different attributes (features) of an object, such as shape or color. Thus in order to identify the purple circle of Fig. 1.3(a), the groups of neurons that code for purple and for a circle will show correlated activity in their firing patterns. If instead the brain wishes to code for the purple rectangle of Fig. 1.3(b), the group of neurons that code for purple will show correlated activity with the group of neurons that code for a rectangle. Similarity, to code for the green circle in Fig. 1.3(c), the activities of neurons coding for a circle and those coding for green will become correlated. Other hypotheses involve coding schemes based upon the firing rates of neurons where different rates of firing code for different stimuli, and it is likely that both types of coding schemes are present in neural activity [99, 82]. Regardless of the specific coding schemes involved, populations of neurons are likely to be involved in the coding as the brain is robust to noise, individual neuron response variability, and changes in the specific network structure [74].

This leads to the classification of a different type of network structure called functional structure. In this case, similarities between the dynamics of nodes determine the links of the network. This means that neurons with highly correlated firing patterns or rate variations could be considered to be functionally connected. Thus, while the nodes are the same as in the anatomical network, the links between the nodes have a different meaning, implying that the structure of the functional network can be different than the structure of the anatomical network. Since we have

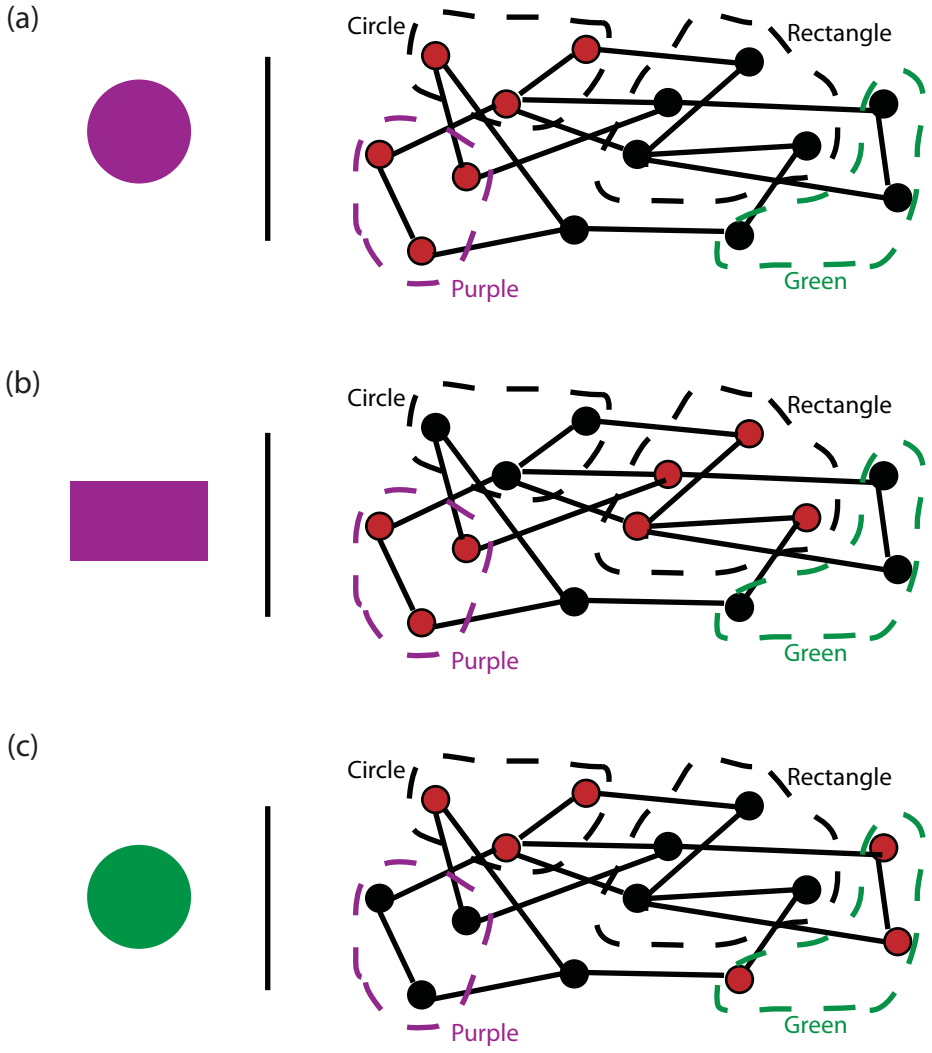

Figure 1.3: An example of the temporal correlation hypothesis. Here different subsets of neurons fire with correlated activity patterns to bind various features such as shape and color to code for an object. The groups of neurons which will fire with correlated activity are shown in red for (a) a purple circle, (b) a purple rectangle, and (c) a green circle.

already determined that anatomical structure influences network dynamics, it seems reasonable to assume that there is a link between the anatomical structure and the functional structure. However, how to determine this link is unclear, especially given that individual neuron properties also influence network dynamics.

We've seen that the relationships between firing patterns of neurons can have important implications in normal brain activity during memory and learning. However, neuronal dynamics are important under pathological conditions as well. For example, epilepsy is characterized by the repeated occurrence of seizures, which are the result of the hypersynchronous firing of groups of neurons. In a common form of epilepsy called focal epilepsy, a seizure starts in a specific area of the brain, known as the focal region, before spreading to other areas of the brain. The ability to identify this focal region has important implications for the treatment of the disease, which often requires the surgical removal of the focus. Thus the detection of the functional structure of the network is essential, as this allows for the identification of the focal region and treatment of the disease.

1.2 Linking structure and dynamics

We have now clearly identified three interconnected features of neuronal networks in which we are interested: anatomical structure, dynamics, and functional structure. The question therefore becomes: How can we gain information about one area, given information about another? The human brain contains $\sim 10^{11}$ neurons, each of which has $\sim 10^4$ synapses connecting it to other neurons. This makes determining the anatomical structure of the brain nearly impossible. Additionally, we know that the connections between neurons are dynamics themselves, changing over time through processes such as STDP. Moreover, the average person loses $\sim 3 \times 10^7$ neurons each

year, indicating that the structure of the brain must be robust to the loss of any single neuron. It is also now known that new neurons are created through neurogenesis in certain brain regions, resulting in an ever changing anatomical structure.

As a result, what one often observes when studying the brain is not the underlying structure of the neurons, but the dynamics of populations of neurons or firing patterns of small samples of individual neurons. Advances in recording techniques such as fMRI allow for one to observe large scale interactions between activity in different brain regions. Technology such as EEG recordings allows for the observation of the average activity of smaller populations of neurons. Finally, recent advances involving the placement of tetrodes into brain tissue of freely moving animals allow for the identification of the firing patterns of single neurons. Recent advances in optical imaging techniques also allow for the identification of single neuron dynamics, although the time scales involved make single spike detection not always feasible.

With the above types of information about the dynamics of our system, we can start to determine the functional structure of our network. However, in order to do this, we must have measures that quantify the temporal relationships between the firing patterns of neurons and develop methods for determining when to place a link between nodes of our functional network. Additionally, we would like to have some way of relating the functional structure of our network to the anatomical structure.

Figure 1.4 shows the interaction between the different types of structure and dynamics in neuronal networks. This dissertation lays a framework for investigating the relationships between these different but related features of the network. I present new techniques for detecting functional structure from network dynamics and employ these techniques to analyze both experimental and model derived data. The use of modeling along with the analysis of experimental data allows for the comparison of

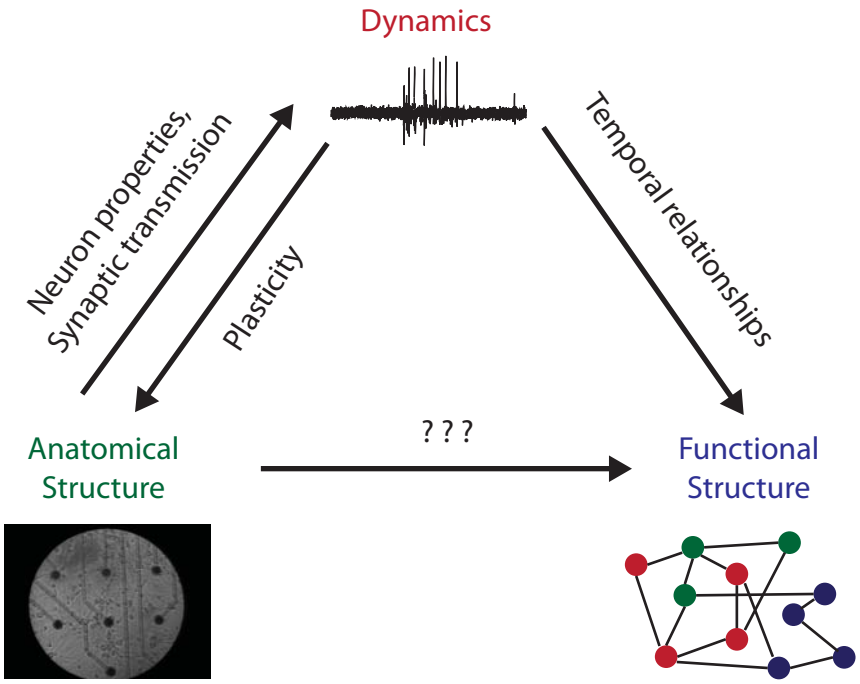

Figure 1.4: The relationships between different types of structure and dynamics in neuronal networks.

network dynamics and functional structure with the underlying network topology and neuronal properties. As the amount of information about neuronal networks grows, the methodology presented here will be useful in linking the elements of structure and dynamics in these complex systems.

1.2.1 Data analysis: relating dynamics to functional structure

In the second chapter, I present a new algorithm for extracting functional structure from networks with nodes whose dynamics can be characterized by discrete events in time. This algorithm is called the Functional Clustering Algorithm (FCA) and utilizes the fact that the nodes of the network are dynamic in order to group nodes with similar temporal representations. The advantage of this algorithm is that no prior knowledge of the number of functional groups is needed, as the procedure progressively combines data traces and derives the optimal clustering cutoff in a simple and intuitive manner through the use of surrogate data sets. The algorithm is

presented in the context of grouping spike train data, as it is particularly useful in detecting functional groups of neurons based on the temporal relationships between their firing events. I also introduce a new similarity metric called the average minimum distance (AMD) that is designed to detect co-firing events in neural data. I compare the performance of the FCA and AMD to that of the gravitational method which was also designed to detect functional groupings in spike train data, and a standard hierarchical clustering algorithm combined with a calculation of modularity. I show that in both cases, the FCA performs better than the previously established methods when applied to simulated spike train data with a known structure.

The third chapter focuses on the analysis of data using the FCA and a metric called causal entropies (CE) which detects directional relationships between firings of neurons. I apply these metrics to both experimental and model derived data in an attempt to link anatomical network changes with observed changes in neuronal dynamics during hippocampal memory formation processes. In the experimental case, I analyze spike train data obtained from the hippocampus of freely moving mice as they explored and learned a novel environment. I observe state-dependent clustering patterns and the development of directional relationships that are consistent with known neurophysiological processes involved in memory consolidation. When the measures are applied to simulated data from a simple STDP motivated model of memory formation, I show that the model provides a consistent explanation of the anatomical network modifications which underlie the activity changes observed in the experimental data.

These two chapters are a combination of work published in [37] with Jack Waddell, Vaughn Hetrick, Joshua Berke, and Michal Zochowski and work submitted to Philosophical Transactions A [38] with Jane Wang, Vaughn Hetrick, Joshua Berke,

and Michal Zochoswki. The model data in the third chapter comes from Jane who is also a member of the Zochowski lab, and the tetrode data comes from the Berke laboratory in the Psychology Department at the University of Michigan.

1.2.2 Modeling: relating anatomical structure to dynamics

The fourth chapter presents a model of coupled networks as a simple model to explore network interactions in focal epilepsy. In this case, the anatomical structure of the networks is known and can be linked to the resulting dynamics. However, the effects of the properties of the neurons on the network dynamics can also be studied. Here, I vary the properties of the neurons in one network and study how changes in the dynamical properties of the nodes can affect the overall network dynamics. I observe that the networks progress through resonance and driving dynamics, dependent upon the properties of the neurons. Through studying the phase synchronization between the collective signals of the two networks as they transition between these states, I attempt to explain a seemingly paradoxical result observed in epileptic patients indicating that the level of phase synchrony declines below normal levels during the state preceding seizures (preictal state).

One network is chosen to be the focal network and slowly transitioned from normal activity to a bursting state mimicking a seizure through an increase in the excitability of neurons in that network. I show that the transition from the interictal (between seizures) to preictal (preceding a seizure) and then to the ictal (seizure) state may be divided into separate dynamical regimes: the formation of slow oscillatory activity due to resonance between the two interacting networks observed during the interictal period, structureless activity during the preictal period when the two networks have different properties, and bursting dynamics driven by the network corresponding to the epileptic focus. Based on this result, I hypothesize that the beginning of the

preictal period marks the beginning of the transition of the epileptic network from normal activity towards seizing. I also show that this effect is robust over a large range of coupling strengths and delays between the two networks, indicating that, in this case, the dynamics of the neurons affect the overall functional structure of the network more than the specific anatomical structure.

The EEG data presented in this chapter comes from Klaus Lehnertz, Florian Mormann, and Hannes Osterhage at the University of Bonn in Germany, and this work was published with the above collaborators and Michal Zochowski in [36].

1.2.3 Experiments: relating dynamics to both anatomical and functional structure

In the fifth chapter, I discuss experimental results obtained from dissociated rat hippocampal cultures. Dissociated cultures are a good reduced system in which to study neuronal networks because the individual properties of the neurons are retained, but certain gross properties of the network structure can be controlled and monitored and the resulting neuronal dynamics can be recorded. I present an analysis of cultures grown under two different conditions: a high glial group where the glial cells in the culture are allowed to divide and multiply, and a low glial group in which the glial network remains constant over time. I show that the resulting dynamics between the two groups are different, indicating that the glial network has an impact on neuronal dynamics. Additionally, the cultures are studied as they age, and the changes in dynamics are linked to changes in both the glial and neuronal networks.

I then use the FCA presented in Chapter II to study the functional groupings resulting from the neuronal activity under the different growth conditions. I show that neuronal activity in the high glial group shows increasing global synchronization as opposed to local synchronization displayed by the low glial group. Additionally,

the levels of this synchronization are explored as the cultures age and the dynamics evolve. Finally, the FCA is used to explore the functional groupings at different temporal levels within network bursts.

The work presented in this chapter is currently being prepared for publication.

CHAPTER II

Functional Clustering: methodology

The detection of structural network properties has been recently recognized to be of great importance in aiding understanding of the properties of a variety of man-made and natural networks [133, 3, 95, 120]. However, two significantly different notions of network structure have to be identified. One is the physical (or anatomical) structure of the network. In this case, community structure refers to groups of nodes within a network which are more highly connected to other nodes in the group than to the rest of the network. Multiple techniques exist which utilize a knowledge of the network topology (adjacency matrix) to extract this hidden structure [49, 72, 96, 26].

The other type of structure is functional structure, which refers to a commonality of function of subsets of units within the network, generally observed by monitoring the similarities in the dynamics of nodes [39, 43]. Thus the structural proximity (i.e existence of physical connection between the network elements) is replaced with the notion of functional commonality (or proximity), which can rapidly evolve based on the observed dynamics. The concept of identifying functional relationships between nodes has been gaining popularity [47, 127, 31], as many networks with dynamic nodes (e.g., genetic, internet, neuronal, etc) exist with the goal of uniting to perform a specific task or function.

In order to successfully capture the (physical or functional) community structure of a network, a clustering algorithm should have two important properties: the ability to detect relationships between nodes in order to form clusters, and the ability to determine the specific set of clusters which optimally characterize the network structure. While some clustering methods have been designed to extract the structure directly from the dynamics of the neurons [46, 5, 28, 76, 47, 119], most methods rely on using a similarity measure to compute distances in similarity space between neurons, and then use structural clustering methods to determine the functional groupings [19, 17, 13, 65, 102, 31]. However, a major problem becomes identifying statistically significant community structures from spurious ones. To achieve this goal, current structural clustering techniques involve an optimization of the network modularity [94, 97] or require a prior knowledge of the number of communities [95, 49, 40, 152, 93, 8].

In this chapter, we develop a novel clustering method that does not depend on structural network information, but instead derives the functional network structure from the temporal interdependencies of its elements. We refer to this method as the Functional Clustering Algorithm (FCA). The key advantage of this algorithm is that it incorporates a natural cutoff point to cease clustering and obtain the functional groupings without an *a priori* knowledge of the number of groups. Additionally, the algorithm can be used with a variety of different similarity measures, allowing it to detect functional groupings based on multiple features of the data. While the algorithm is generic and applies to any type of discrete event data, we introduce the algorithm in the context of an application to spike train data as the inspiration for the algorithm comes from neuroscience, and spike trains are a simple example of discrete event data.

2.1 The Functional Clustering Algorithm

Here we introduce the Functional Clustering Algorithm (FCA) which is tailored to detect functional clusters of network elements. The FCA dynamically groups pairs of spike trains based on a chosen similarity metric, forming progressively more complex spike patterns. We will also introduce a new similarity measure which is used for the data analyzed in this dissertation, but any pairwise similarity measure can be chosen. The specific choice of the metric should depend on the nature of the data being analyzed and the type of functional relationships which one chooses to detect.

A general description of the FCA is as follows (see the subsequent sections for detailed descriptions and Fig. 2.1 for a schematic of the algorithm):

1. We first create a matrix of pairwise similarity values between all spike trains.

2. We then use surrogate data sets to calculate 95% confidence intervals for each pairwise similarity. These significance levels are used to calculate the scaled significance between each pair of similarity values (see Sect. 2.1.2 for the definition of scaled significance).

3. The pair of trains with the highest significance is then chosen to be grouped together, and the scaled significance of this pair is recorded. A unique element of the FCA is that the two spike trains which are grouped together are then merged by joining the spikes into a single new train (see Fig. 2.1(a)). This allows for a cumulative assessment of similarity between the existing complex cluster and the other trains.

4. The trains which are being joined are then removed, the similarity matrix is recalculated for the new set of trains, new surrogate data sets are created, and a new scaled significance matrix is calculated.

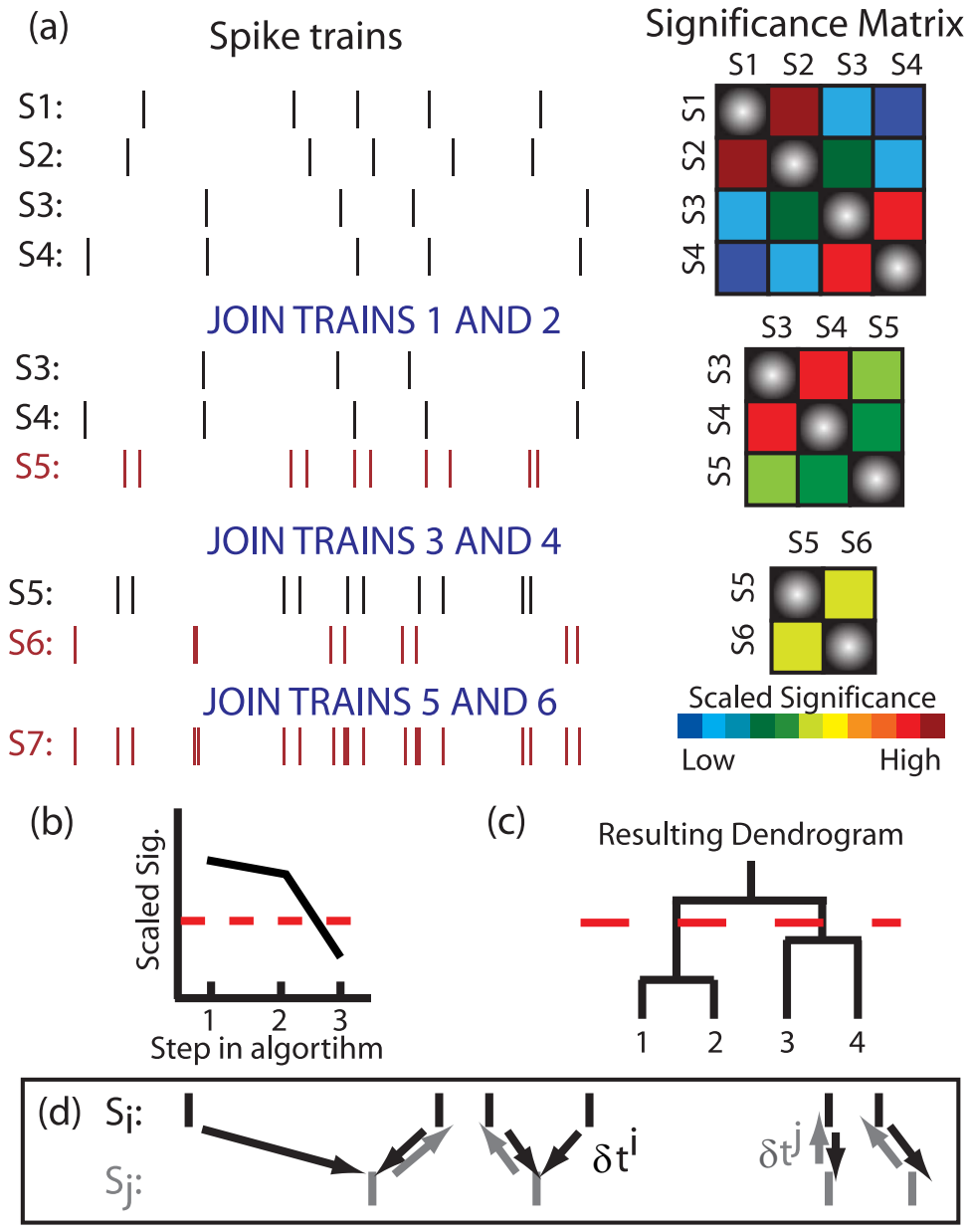

Figure 2.1: Functional Clustering Algorithm. (a) An example of the algorithm applied to four spike trains. Two trains are merged in each step by selecting the pair of neurons with the highest scaled significance value and effectively creating a new neuron by temporally summing their spike trains. The procedure is repeated until one (complex) spike train remains. (b) We cease clustering when the trains being grouped are no longer significant; here the dotted red line denotes the significance cutoff. (c) The subsequent dendrogram obtained from the FCA. The dotted line denotes the clustering cutoff. (d) Schematic of the average minimum distance between spike trains.

5. We repeat the joining steps $(3-4)$, recording the scaled significance value used in each step of the algorithm until the point at which no pairwise similarity is statistically significant, indicating that the next joining step is not statistically meaningful. We refer to this step as the clustering cutoff (dashed red line in Fig. 2.1). At this point, the functional groupings are determined by observing which spike trains have been combined during the clustering algorithm.

A key advantage of this algorithm is that the ongoing comparison of the similarity metric obtained from the data with that from the surrogates causes the algorithm to have a natural stopping point, meaning that one does not need an *a priori* knowledge of the number of functional groups embedded in the data. Gerstein et al [47] also developed an aggregation method based on grouping neurons with significant coincident firings, but this method results in the formation of strings of related neurons which must be further parsed to determine functional groupings. We now discuss the details of the implementation of the FCA in the following sections.

2.1.1 Average minimum distance

For the data presented here, we use a new similarity metric which we call the average minimum distance (AMD) to determine functional groupings. The AMD is useful in capturing similarities due to coincident firing between neurons. Note that other metrics could be chosen, depending upon the nature of the recorded data. To compute the AMD between two spike trains S_i and S_j, we calculate the distance δt_n^i from each spike in S_i to the closest spike in S_j as shown in Fig. 2.1(d). We then define

$$D_{ij} = \frac{1}{N_i} \sum_n \delta t_n^i \tag{2.1}$$

$$D_{ji} = \frac{1}{N_j} \sum_n \delta t_n^j \tag{2.2}$$

where $N_{i/j}$ is the total number of spikes in S_i or S_j respectively. Finally, we define the AMD between spike trains S_i and S_j to be

$$\Theta_{ij} = \frac{D_{ij} + D_{ji}}{2}. \tag{2.3}$$

2.1.2 Calculation of Significance

In order to determine the significance between two trains, we create 5,000-10,000 surrogate data sets and calculate pairwise similarities for each surrogate set. The surrogate spike trains are created by adding a jitter to each spike in the train. This jitter is drawn from a normal distribution [113], similar to the technique developed by Date [27]. The method of adding jitter to spikes (also known as dithering or teetering) to create surrogate data sets is commonly used when analyzing neural data and has been shown to eliminate correlations between spike timings [122, 107]. Creating the surrogate trains in this manner preserves the frequency of each train while keeping the gross properties of the interspike-interval distribution.

We examine the distribution of similarity values and create the cumulative distribution function (CDF) to determine the 95% level of significance. The scaled significance (Fig. 2.2) is measured in units defined as the distance from the midpoint of the CDF to the 95% significance cutoff. Thus, a scaled significance value equal to one denotes the 95% significance level, and values higher than one are significant while values lower than one are deemed insignificant.

2.2 Comparison to Other Algorithms

In order to verify the performance of the FCA and compare it to that of existing clustering methods, we created simulated spike trains with a known correlation structure. Specifically, we created a set of 100 spike trains derived from a Poisson distribution that consist of four independent groups, 20 spike trains each, and 20

uncorrelated spike trains. The spike trains within these four groups are correlated (see Fig. 2.2(a)). To create the correlated groups, we first created a master spike train and used this train to create new trains by randomly deleting spikes from the master train with a certain probability. Thus, the resulting train was also a Poisson process with a firing rate dependent upon the deletion probability. The master train was 5000 time steps long, with each neuron spiking an average of 250 times during the duration of the train. To further randomize the timings of the spikes copied from the master train, we added jitter (drawn from a normal distribution with a standard deviation of 1) to the spike times. Each correlated group was composed of 20 trains from the same master. The average correlation within the group was computed by first calculating the pairwise cross-correlations between all trains and then averaging over the group. The firing rate of the independent trains was set to match that of the correlated trains.

We first applied the FCA to the simulated data described above (Fig. 2.2(b-c)) using a jitter drawn from a normal distribution with a standard deviation of 10 to create the surrogate data. In Fig. 2.2(b), we show the scaled significance at each joining step in the algorithm. The dashed red line marks the significance cutoff (single 95% confidence interval); points above this line are statistically significant, and the clustering cutoff is given by the point where the curve drops below this line. Fig. 2.2(c) shows the resulting dendrogram with the dashed red line denoting the clustering cutoff. The algorithm correctly identifies the 4 groups of neurons as well as the 20 independent neurons.

2.2.1 Comparison to the Gravitational Method

We then compared the performance of the FCA to that of the gravitational method [46, 5, 28, 76]. This method performs clustering based on the spike times of neuronal

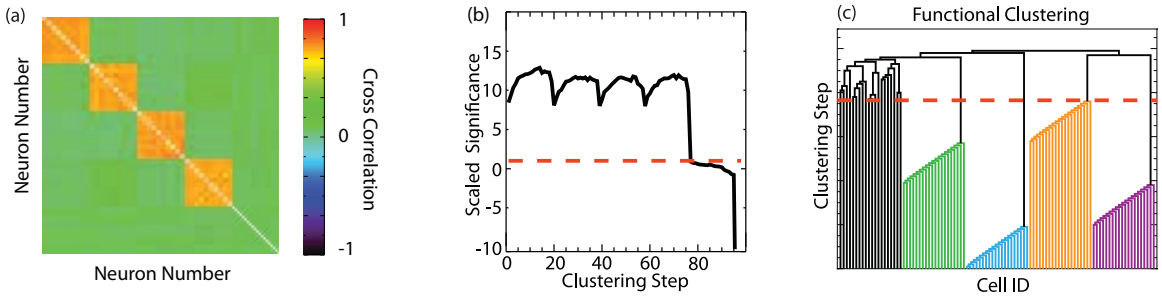

Figure 2.2: Performance of the FCA on simulated data. (a) The cross-correlation matrix showing the correlation structure of the simulated data. (b) The scaled significance used in each step of the FCA. The dashed red line denotes the point at below which clustering is no longer significant. (c) Dendrogram resulting from Functional Clustering. The algorithm easily identifies the correct groups.

firings by mapping the neurons as particles in N-dimensional space, and allowing their positions to aggregate in time as a function of their firing patterns. Particles are initially located along the trace of the N-dimensional space and given a 'charge' which is a function of the firing pattern on the neuron. The charge q_i on a particle is given by

$$q_i(t) = \sum_k K(t - T_k) - \lambda_i \tag{2.4}$$

where $K(t) = exp(-t/\tau)$ for $t > 0$ and $K = 0$ otherwise, T_k are the firing times of the neuron, and λ_i is the firing rate of the neuron, normalized so that the mean charge on a particle is zero. The position vector, $\mathbf{x}$, of the particle is then allowed to evolve based upon the following rule:

$$\mathbf{x}_i(t + dt) = \mathbf{x}_i(t) + \kappa dt \sum_{j \neq i} q_i q_j \frac{\mathbf{x}_j - \mathbf{x}_i}{|\mathbf{x}_j - \mathbf{x}_i|} \tag{2.5}$$

where κ is a user defined parameter that controls the speed of aggregation. One then calculates the Euclidean distance between particles as a function of time and looks for particles which cluster in the N-dimensional space (i.e., the distance between the particles becomes small).

Fig. 2.3 depicts the results of applying the gravitational method to the simu-

lated data described above for cases of high correlation ($C \approx 0.63$) within groups (Fig. 2.3(a,c)) and also for low correlation ($C \approx 0.13$) within clusters (Fig. 2.3(b,d)). In Fig. 2.3(a-b) we plot the pairwise distances between particles as a function of time in the algorithm. Blue traces denote distances between intra-cluster trains, green between inter-cluster ones, and red between any train and an independent train. To visualize the results of the method, we have sliced these plots as indicated by the dashed vertical line and represent the distances at this point in time as matrices in Fig. 2.3(c-d). While, for the case of high correlation between the spike trains, the algorithm separates the 4 groups correctly (black squares in Fig. 2.3(c)), one is unable to distinguish between inter and intra-cluster trains for the low correlation case. Furthermore, these plots must be visually inspected for the cutoff (i.e. time point at which they stabilize) and the clustering results may significantly depend on its position, as the algorithm has no inherent stopping point and the rate of aggregation is parameter dependent. Even then, the detection of the formed clusters may require the application of an additional N-dimensional clustering algorithm to detect the clusters formed in the N-dimensional space. Another drawback of this method is that as the particles aggregate into clusters, the clusters start interacting due to the nature of the algorithm, causing inter-cluster distances to become significantly lower than those with random trains, which does not match the correlation structure of the data.

The FCA performed the correct clustering of the data for the case of the high correlation and only made an occasional error for data with the low correlation.

2.2.2 Comparison to Complete Linkage and Modularity

We next compare the performance of the FCA to a method which maps spiking dynamics onto a structural space and then uses a structural clustering method to

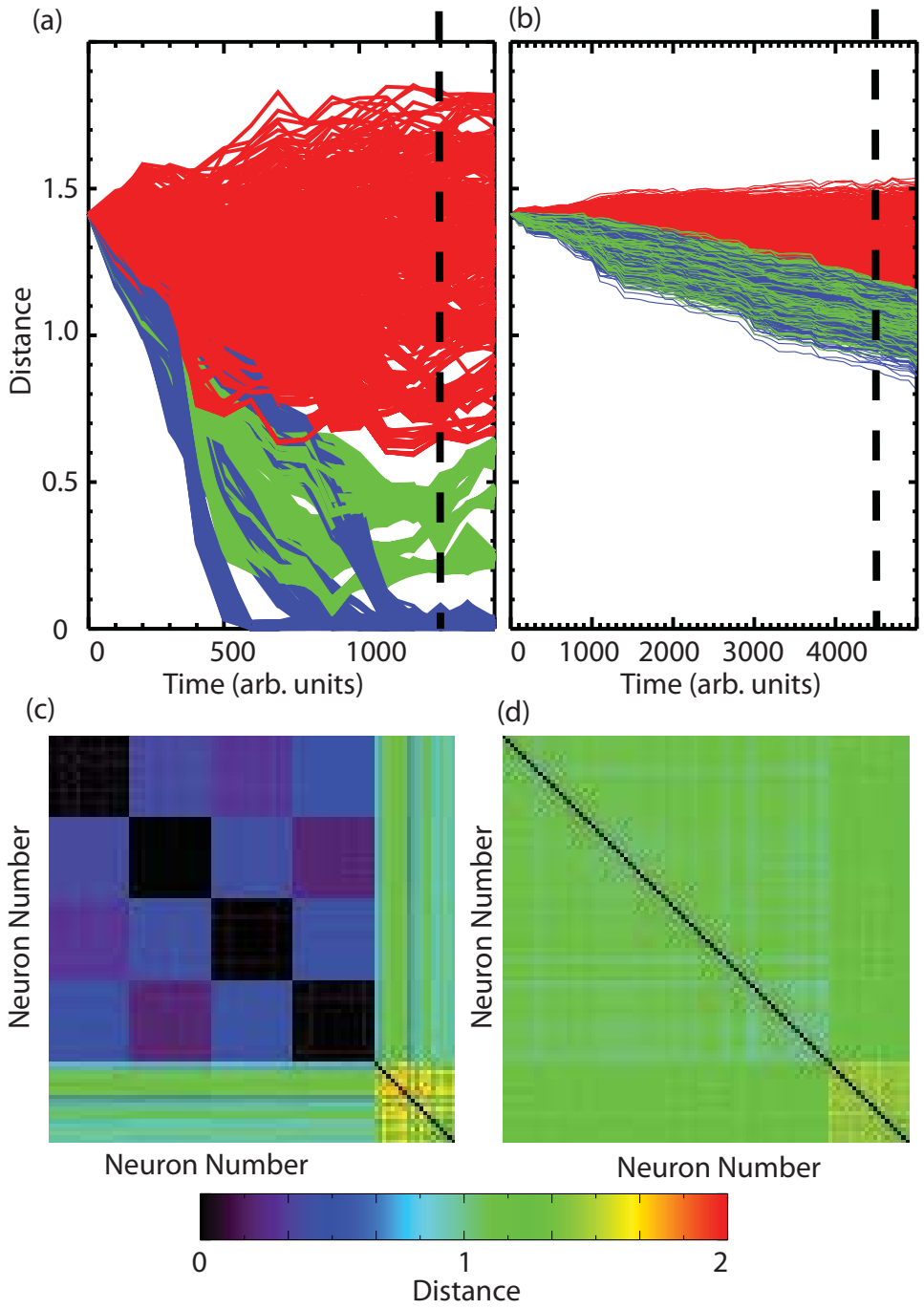

Figure 2.3: Application of the gravitational method to simulated data. (a,b) Pairwise distances as a function of time in the stimulation for high correlation within clusters (a) and low correlation within clusters (b). Blue traces: intra-cluster distances, green traces: inter-cluster distances, red traces: distances between any train and an independent train. (c,d) Matrix version of distances for the point in time denoted by the dashed vertical line in (a),(b) respectively. Note that for the low correlation case, one can not detect the formation of individual clusters.

determine functional groupings. The structural clustering method used is a standard hierarchical clustering technique called complete linkage. Since this algorithm has no inherent cutoff point at which clustering is stopped, we combine it with a calculation of the weighted modularity [97], which is a commonly used measure to determine the best set of groupings when dealing with hierarchical clustering methods. We have also tried other methods (single-linkage, GN algorithm [19, 49]), but complete linkage gave the best results of the other methods attempted. Please see [17, 19] for a review of standard hierarchical clustering techniques.

The complete linkage algorithm again clusters trains based upon a similarity measure. In this algorithm, a similarity matrix is created and the elements with the maximum similarity are joined. However, the clusters are formed through virtual grouping of the elements and there is no re-calculation of the similarity measure; the similarity between clusters is simply defined to be the minimum similarity between elements of the clusters. For the data presented in this paper, we use the absolute value of the normalized cross-correlation matrix as our similarity matrix, since this is what is commonly used to do examine community structure in neuroscience applications. To compute this matrix, spike trains are first convolved with a gaussian kernel and the signal is demeaned (the mean value of the signal is subtracted). The cross-correlation is given by

$$\hat{C}\left(S_i, S_j\right) = \left| \frac{C\left(S_i, S_j\right)}{\sqrt{C\left(S_i, S_i\right) \cdot C\left(S_j, S_j\right)}} \right|, \tag{2.6}$$

where C is the linear cross correlation function

$$C\left(S_i, S_j\right) = \int_{-\infty}^{\infty} S_i\left(t\right) S_j\left(t\right) dt. \tag{2.7}$$

Since the complete linkage algorithm has no inherent method of determining the clustering cutoff, we compute the (weighted) modularity [97] for each step of the

algorithm. The modularity measure was originally tailored to detect the optimal community structure based upon structural connections between nodes (i.e. adjacency matrix), however it can also be used to detect optimal clustering based on not structural, but dynamical relations, where the adjacency matrix is substituted with the correlation matrix. The modularity is given by

$$Q = \frac{1}{2m} \sum_{ij} \left(A_{ij} - \frac{k_i k_j}{2m} \right) \delta\left(c_i, c_j\right) \tag{2.8}$$

where A_{ij} is our similarity matrix, $k_i = \sum_j A_{ij}$, $m = \frac{1}{2} \sum_{ij} A_{ij}$, and $\delta\left(c_i, c_j\right) = 1$ if i and j are in the same community and zero otherwise. The maximum value of the modularity is then used to define the clustering cutoff.

The complete linkage dendrogram is shown in Fig. 2.4(b) and the modularity for this clustering is plotted in Fig. 2.4(a). The clustering cutoff is defined as the maximum of the modularity [94, 97], however the scaling of the modularity, even in this simple case, provides ambiguous results. The numerical maximum of the modularity is observed for the clustering step marked by the dashed red line in Fig. 2.4 - significantly above the clustering step that starts linking random spike trains. Even if we relax this definition and assume that the set of high modularity values is equivalent, the exact location of the cutoff is ambiguous as shown by the area enclosed in the transparent red box. Note that the FCA does not have this ambiguity, as the cutoff is quite clear and the algorithm correctly identifies the groups embedded in the spike train data.

To further explore the performance of the FCA in comparison with complete linkage and modularity, we monitor the performance of both methods for progressively lower correlations within the four clustered groups (Fig. 2.5). We did not perform this analysis for the gravitational method since that algorithm has no predetermined stopping point and cluster identification must be assessed by the user. As before, the

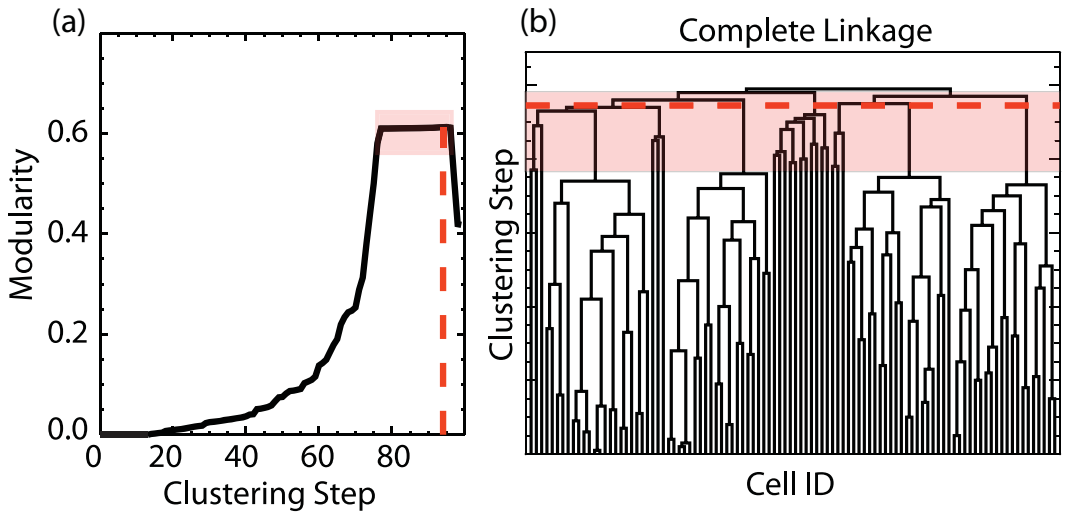

Figure 2.4: Comparison with complete linkage and modularity. (a) Modularity calculation for the clustering obtained using complete linkage. The transparent red box marks the ambiguous cutoff area. (b) Dendrogram indicating clustering by complete linkage. Here the clustering cutoff is ambiguous and the algorithm fails to identify the appropriate structure.

inter-cluster correlation is controlled through progressive, random deletion of spikes from a master train. In order to compare the performance of the two algorithms, it is necessary to compare the obtained clusterings to the known structure of the data. To assess the correctness of the retrieved clusters as compared to the actual structure of the network, we calculate the normalized mutual information (NMI) [42, 26] as a function of the average correlation within the constructed groups. The NMI is a measure used to evaluate clustering algorithms and determine how well the obtained clustering, C', matches the original structure, C. To compute the NMI, one first creates a matrix with c rows and c' columns, where c is the number of communities in C and c' is the number of found communities in C'. An entry, N_{ij}, is defined to be the number of nodes in community i that have been assigned to the found community j. If we denote $N_{i/j} = \sum_{j/i} N_{ij}$ and $N = \sum_{ij} N_{ij}$ then we can define

$$NMI\left(C, C'\right) = \frac{-2\sum_i \sum_j N_{ij} ln\left(\frac{N_{ij}N}{N_i N_j}\right)}{\sum_i N_i ln\left(\frac{N_i}{N}\right) + \sum_j N_j ln\left(\frac{N_j}{N}\right)}. \tag{2.9}$$

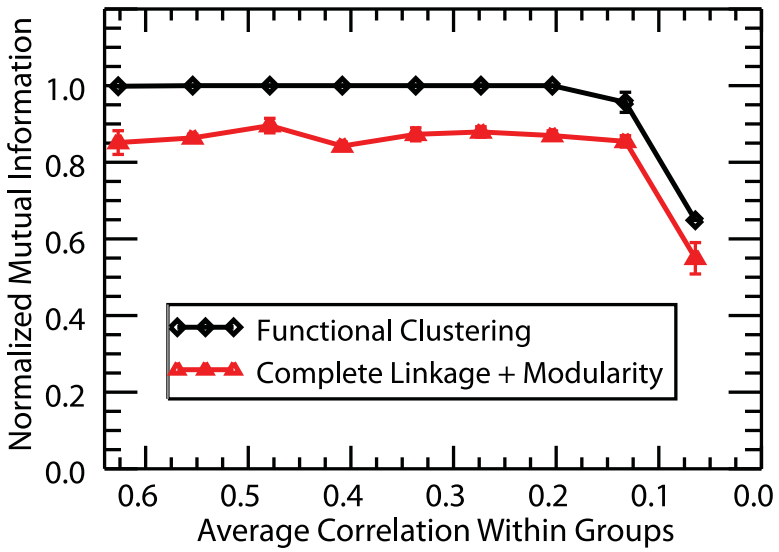

Figure 2.5: Normalized mutual information as a function of average group correlation. The measure takes a maximal value of one when the established clustering structure matches the predetermined groups and $NMI \to 0$ when the obtained clustering structure is independent of the original groupings. Functional Clustering identifies the correct group structure for almost all values of correlation while complete linkage and modularity consistently create erroneous structure.

This measure is based on how much information is gained about C given the knowledge of C'. It takes a minimum value of 0 when C and C' are independent, and a maximal value of 1 when they are identical.

In Fig. 2.5 we use the NMI to compare the obtained clustering with the known structure of the simulated data. As shown in the figure, complete linkage and modularity consistently fail to identify the correct structure. This is because the maximum of the modularity occurs for a point in the algorithm where various independent spike trains have been joined, creating erroneous group structure. However, the FCA correctly identifies neurons for almost all values of correlation. Please note that the 80% level of correctness using complete linkage and modularity for higher intercluster correlation values is due to the fact that we had only 24 independent groups (20 spike trains + 4 independent clusters) in the tested network. A higher number of independent neurons would lead to a poorer performance of that method (due to the

erroneous grouping of independent neurons) and thus higher relative effectiveness of the FCA.

2.3 Summary

In this chapter, I presented a new Functional Clustering Algorithm to perform grouping based on relative activity patterns of discrete event data sets. The FCA has many advantages over many traditionally used clustering methods as it directly detects functional groupings based on temporal relationships between network events. The FCA also incorporates the use of surrogate data sets to determine the significance of the obtained groupings, giving the algorithm a natural stopping point. This means that no *a priori* knowledge of the number of functional groups is required. The calculation of the significance used at each clustering step of the algorithm also provides information quantifying the relationship between neurons in each of the joined groups.

The algorithm was applied to simulated neural spike train data with a known correlation structure and shown to perform better than existing algorithms that did not have a natural stopping point (the gravitational method) or provided ambiguous results about when to cease clustering (complete linkage and modularity). The algorithm also consistently performed better than complete linkage and modularity as the correlation structure of the simulated data was progressively weakened.

Additionally, it should be emphasized that the algorithm is generic and can be applied to any network whose nodes participate in discrete temporal events. Possible other networks to which the algorithm could be applied include networks of oscillators where the trajectory passes through a Poincaré section, failure events on networks of routers, or fluctuation events in a power grid network. Thus, the Func-

tional Clustering Algorithm is a valuable new method for the detection of functional groupings in dynamic network data as will be demonstrated using experimental and model derived neuronal spike train data in the next chapter.

CHAPTER III

Functional Clustering: applications to brain dynamics

In the previous chapter, I introduced a new algorithm and similarity metric designed to detect functional groupings in discrete event data. In this chapter, I will use the developed methods to analyze both experimental and model derived data to explore the relationship between structure and dynamics during brain function.

The problem of understanding neuronal correlates of brain function has been addressed extensively over many decades but still remains unsolved. While a vast amount is known about the basic anatomy and physiology of the brain, the dynamics and interactions of neuronal ensembles which underlie various cognitive tasks are yet to be understood. This is largely due to the anatomical complexity of the neuronal networks which comprise the brain. The cortex alone contains 10^{10} neurons and 1.5×10^{14} synapses, making it impossible to derive any detailed properties of its connectivity. It is not even clear that having a detailed knowledge of the connectivity would be sufficient to understand brain function, as it significantly evolves on times scales ranging from tens of milliseconds to years, through processes such as constant rewiring [129] (i.e. creation, annihilation and modulation of synapses), neuronal loss and/or adult neurogenesis [2]. Additionally, even if the anatomical connectivity were known, this would not necessarily lead to an understanding of the spatio-temporal

patterning of neural activity which is the basis of function [44]. It therefore becomes imperative to define other approaches which rely more on functional commonality (i.e. coding the same aspects of cognitive tasks) as opposed to anatomical connectivity. Moreover, since it is known that brain function is distributed over large neuronal ensembles, or even more globally, between different brain modalities, it is important to understand how these ensembles self-organize to generate desired functions (movement, memory storage/recall, etc.) [55, 47, 125, 151].

From the experimental perspective, the emergence of new multiunit electrophysiological and/or optical imaging techniques has been crucial as they provide (extremely sparse) information on distributed neural activity during various cognitive tasks. Thus, the research task has been partially redefined to first understand the functional (dynamical) network correlates which underlie given cognitive phenomena, and then based on these, to understand the anatomical structures and physiological processes which lead to them. Thus, in short, we are asking two questions: what macroscopically observed neural interactions are the hallmark of a given cognitive process, and, what anatomical or pharmacological environment underlies these interactions? This, in turn, requires the formulation of new metrics that will allow for the identification of emerging dynamical patterns during brain function. However, since it is quite difficult to experimentally link the observed dynamical changes to the underlying structural changes, extensive modeling efforts must also be done where one can directly observe how known structural changes induce differences in functional relationships between neurons. While the knowledge gained from this modeling does not give direct evidence linking the experimentally observed changes in functional behavior with underlying structural changes, it can provide confirmation that the experimental data is consistent with certain hypotheses.

In order to define these new metrics, we must turn back to cognitive sciences to identify which dynamical neuronal patterns are important. It is assumed that functional neural ensembles form and disintegrate dynamically [84, 34, 141, 126], through spatio-temporal patterning of spiking activity of many individual neurons. The temporal correlation hypothesis [140, 51, 124, 33] postulates that correlated neuronal activity mediates rapid feature binding and thus the formation of intermittent functional ensembles in the brain. Therefore, the identification of these functional neural ensembles can potentially be reduced to the identification of temporally correlated groups of neurons. However, it is also clear that the formation of these ensembles is mediated through rapid anatomical/physiological changes. It has been established that the temporally ordered co-activation of neural populations leads to rapid synaptic changes via spike timing dependent synaptic modification (STDP) processes [15, 129, 1, 130]. Since these synaptic modifications are directional, one would also expect changes in directional relationships between firing patterns of neurons.

Here, we focus on the formulation of quantitative links between the anatomical and dynamical macroscopic network processes which underlie initial memory formation in the brain. We analyze hippocampal tetrode recordings obtained from freely moving mice which are exposed to a novel environment and look for two effects: 1) the enhancement of directional timing relationships between neuronal pairs, and 2) a decrease in the overall temporal distance between firings of subpopulations of cells during memory formation. Based on previous work [142, 30], we hypothesize that an increase in the number of pairs showing significant directional interdependencies is indicative of the strengthening of direct connections between interacting neurons, whereas a decrease in the temporal distance indicates an overall increase of fidelity of neuronal representation of the new environment through the increase in the cor-

relation of their activity [100]. Finally, we link these two effects in a modeling effort and show that the formation of heterogeneities in the anatomical connectivity of the network, due to the addition/strenghtening of a relatively small number of neural connections, can lead to the rapid formation of co-activating discrete neuronal ensembles, as well as their reactivation during sleep. This in turn, we hypothesize, leads to the formation of a distributed memory representation as is observed experimentally.

Specifically, we show that an increase in directional relationships between neurons corresponds to changes in neuronal dynamics that are apparent in the functional clustering of data obtained the mice as they learned a new environment. The directional interactions will be detected using causal entropies (CE) and clustering is determined by the FCA presented in the previous chapter. The use of the AMD in the algorithm allows for the calculation of distances within functional clusters and is used to quantify changes in clustering associated with memory consolidation. The measures are also be applied to data obtained from a simple STDP derived model of memory storage. The observed dynamical changes in the model data can be directly linked to the known structural changes in the model, suggesting that the measures are detecting the development of similar structural changes in the experimental case.

3.1 Methods: metrics and analysis

3.1.1 Directional interactions: causal entropies

We monitor the directional interactions between neurons over time using causal entropies (CE) [143, 153, 30]. CE are an asymmetric, time-adaptive metric, constructed to detect asymmetric locking between two spike trains based on the intervals between spiking events [142]. They are computed by first constructing two time-adaptive histograms of the inter-event intervals between the spike trains (P_{ij} and, separately, P_{ji}), then calculating the Shannon entropy.

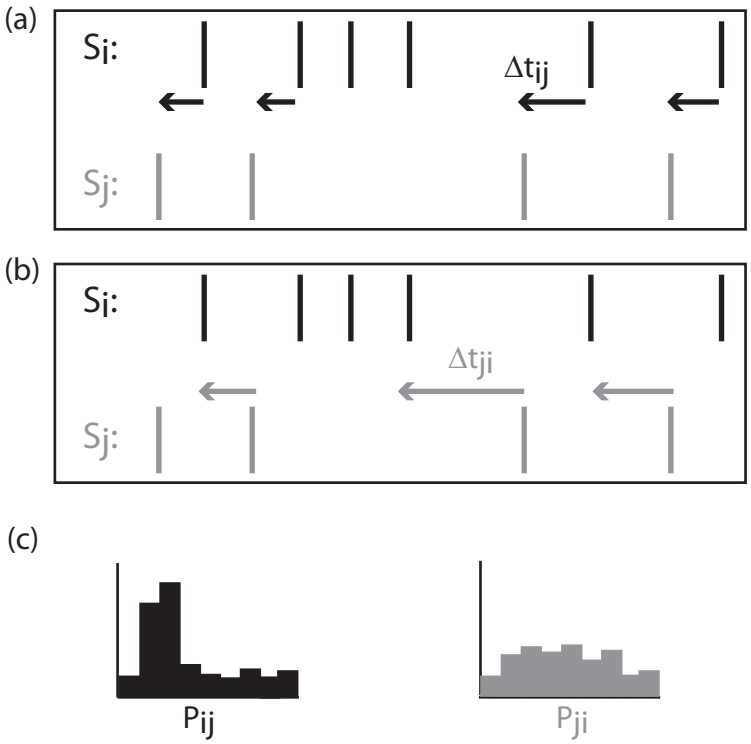

Figure 3.1: Example CE calculation. (a) Sample calculation of Δt_{ij} from spikes in train i to train j. (b)Sample calculation of Δt_{ji} from spikes in train j to train i. (c) Sample histograms for spike trains in which spikes in j lead spikes in i but there is no consistent relationship from spikes in i to spikes in j.

Briefly, let t_n^i be the time of the n^{th} spike for neuron i and $\tau_j(n)$ be the last time that neuron j fired before t_n^i. We then calculate $\Delta t_{ij}(n) = t_n^i - \tau_j(n)$. Note that if neuron i fires multiple times, $\Delta t_{ij}(n)$ is only calculated between the closest spike of neuron i and the previous spike of neuron j. Please see Fig. 3.1(a) for a schematic. We separately calculate Δt_{ji} (from spikes in j to spikes in i) in the same manner as shown in Fig. 3.1(b).

At t_n^i, we update the histogram P_{ij} by adding Δ_P to the bin corresponding to $\Delta t_{ij}(n)$ and then renormalizing the histogram. The parameter Δ_P is a free parameter which controls the effective length of history of the time-adaptive measure [142]. This process establishes an exponential attenuation to the memory of the histogram, allowing it to adapt to changes in synchrony over time. The causal entropy

$CE_{ij}(n) = -\sum_k P_{ij}(k) \cdot log(P_{ij}(k))$ is then computed, where k indexes the bins of the histogram. We then separately calculate CE_{ji} through the same procedure as above, interchanging the i and j in the prior description.

The advantage of CE is the ability to detect asymmetric locking between pairs of neurons. If neuron i regularly fires shortly after neuron j, but j does not regularly follow i, then CE_{ij} will become small, while CE_{ji} will remain relatively large. Therefore, one may take the causal entropy difference $CED_{ij}(n) = CE_{ij}(n) - CE_{ji}(n)$ to measure the degree and direction of locking between the two neurons. (See Fig. 3.1(c) for an example of histograms depicting this behavior.) For a detailed description of CE, see [142].

We track the number of significant CE pairs over time by computing $CED_{ij}(n)$ and comparing this to the same measure computed for surrogate data sets. Please see Sect. 3.1.4 for a description of the surrogate data. Significance is determined as being two standard deviations away from the mean. For the experimental data analyzed in the chapter, we calculated histograms for Δt within a window of 500 ms, using a bin size of 10 ms and $\Delta p = 0.05$. The model data was analyzed using a window of 400 time steps, a bin size of 1 time step, and $\Delta p = .005$.

3.1.2 Correlated activity: Functional Clustering Algorithm

In order to detect functionally correlated groups of neurons, we implement the Functional Clustering Algorithm (FCA) as described in the previous chapter. We again choose the AMD as our similarity metric in order to study the changes in functional distances between elements of the functional groupings throughout the learning of the environment.

3.1.3 Correlated activity: adjusted average minimum distance

One feature of the FCA is that the similarity associated with each joining step of the algorithm can be compared between different applications of the algorithm. When using the AMD as the chosen similarity measure, we must first introduce a frequency correction during the calculation of the D_{ij} values as this measure scales with the number of spikes in the trains otherwise. (Note that the effect of spiking frequency in the measure is accounted for in the algorithm through the comparison to surrogate data.)

Here, we normalize these distances by the average expected distance obtained from uniformly distributed spike trains having the same spike frequency: $D^{unif}_{ij/ji} = (\Delta T)/(N_{j/i}+1)$, where ΔT is the train length. Thus,

$$\tilde{D}_{ij/ji} = \frac{D_{ij/ji}}{D^{unif}_{ij/ji}}. \tag{3.1}$$

We then define the $\widetilde{AMD}$ between trains S_i and S_j to be

$$\widetilde{AMD}_{ij} = \frac{\tilde{D}_{ij} + \tilde{D}_{ji}}{2}. \tag{3.2}$$

Lower values of $\widetilde{AMD}$ indicate tighter functional clustering between the cells.

In Fig. 3.2 we show the average AMD and $\widetilde{AMD}$ values calculated between two random poisson trains as a function of the total number of spikes within the trains averaged over 100 trials. In this case, one spike train has a constant value of 50 spikes and the other train is varied from $2-200$ spikes over a constant window of time. In Fig. 3.2(a), we show the original AMD calculation between the trains. As expected, the AMD scales approximately as $1/N$ where N is the total number of spikes. In Fig. 3.2(b) we show the $\widetilde{AMD}$ calculated for the same spike trains. One can see that this first order correction effectively eliminates the dependence on spiking frequency as the measure is approximately constant over all frequencies.

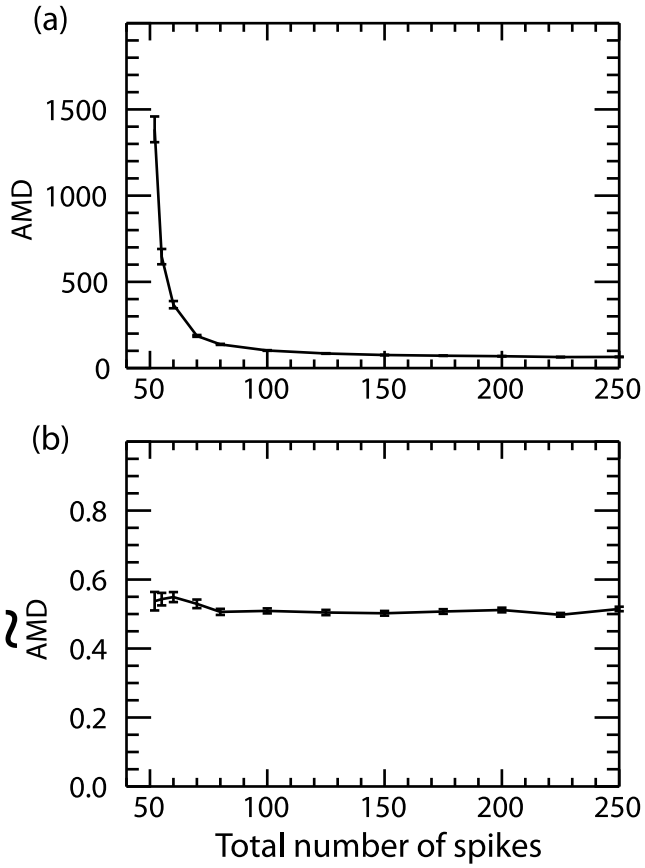

Figure 3.2: AMD and $\widetilde{AMD}$ comparison. (a) AMD and (b) $\widetilde{AMD}$ calculated between two random poisson trains as a function of the total number of spikes in the trains. One spike train contained a constant number of 50 spikes while the spiking frequency in the other was varied between 2 and 200 spikes. While the AMD scales with the number of spikes in the trains, the $\widetilde{AMD}$ remains constant as the number of spikes is varied.

3.1.4 Creation of surrogate data

In order to determine the significance of the above measures, we create surrogate data sets by adding a jitter to each spike in the train. This jitter is drawn from a uniform distribution [27] within a given window around each spike. This destroys correlations between firing events of neurons while preserving the number of spikes and average properties of the interspike interval distribution. For the experimental data, a jitter window of 2 s was used for the CE analysis, and a window of 20 s was used for the FCA analysis, with the exception of the data presented in Figs. 3.5 and 3.7, for which the jitter was drawn from a normal distribution with a standard

deviation of 10 s. For the model data, a window of 400 time steps was used for both calculations.

3.1.5 Experimental protocol

The experimental data presented in this paper was recorded using tetrode methods [14] from the hippocampus of freely moving mice as they explored a novel environment. The mice were placed in a novel rectangular track in which they underwent periods of exploration and sleep. The environment contained a textured floor and specific scent in order to ensure its novelty. Spatial cues were given by the location of the door through which the mouse entered. When placed in the track environment, the animal typically explored by running laps and then alternated between periods of exploration and sleep. Here, we analyze data from 77 pyramidal neurons in mouse 1 (42 CA1; 21 CA2; 14 CA3) and 28 pyramidal neurons in mouse 2 (14 CA1, 14 CA3). All animal experiments were performed in the laboratory of Joshua Berke at the University of Michigan and approved by the University of Michigan Committee on the Use and Care of Animals. The early exploration window was taken to be 100 s of exploration when the animal was initially placed in the environment whereas late exploration was defined to be 100 s of data taken from the end of the session after the animal had slept in the environment.

3.2 Modeling: understanding the structural basis of the observed temporal patterning

It has been shown that the hippocampus can rapidly form new memory representations and in a very short time period is able to generate experience-dependent reactivation during various stages of sleep [66, 18, 150, 21] and quiet waking periods [41]. During this reactivation, the spatio-temporal patterning of neuronal activity

is correlated with the patterning of the preceding awake activity [77]. Furthermore the correlation between cells co-active during waking is also higher during sleep [150, 106, 111]. We used a simple integrate-and-fire based model to show that local strengthening of network connectivity underlies the formation of localized network heterogeneity which, in turn, leads to rapidly increasing neuronal co-activation and potential formation of distributed memory representation. Furthermore, changes of global network excitability, driven, for example, through changes in the neurochemical environment during sleep [18, 80], can produce spontaneous reactivation of the previously co-active network regions. Thus, the structure of the activating regions in the network are inherently determined by the heterogeneities in network topology. Here, we show that this simple model coupled with an STDP based learning rule phenomenologically captures the processes observed experimentally.

3.2.1 Model details

The model uses leaky integrate-and-fire neurons given by

$$\tau_m \frac{dV^j_{i/e}}{dt} = -\alpha_j V^j_{i/e} + I_{i/e} + \sum_k w^{jk} I^k_{syn} \tag{3.3}$$

to represent the dynamics of the network elements, the e/i denoting either an excitatory or inhibitory neuron. $V^j_{i/e}$ is the membrane voltage of the j'th neuron; α_j is the membrane leak rate constant randomly distributed such that $\alpha_j \in [1, 1.3]$; $\tau_m = 30$ ms is the membrane time constant; I^k_{syn} is the incoming current to the j'th neuron from the k'th neuron; and w^{jk} is the connection strength between neurons j and k. The excitatory subnetwork of 500 cells is in a one-dimensional small-world formulation with periodic boundaries and has connectivity radius $R_e = 3$. Additionally, $p^e_g = 0.15$ is the rewiring parameter defining the fraction of the number of local connections to the number of random, long-range ones, with connections of strength

$w_{ex} = 2$. The inhibitory interneuron subnetwork of 100 cells has $R_i = 1$, $p_g^i = 1$, and $w_{in} = 10$, forming a random graph network. Every inhibitory cell receives input from $n_{ei} = 5$ neighboring excitatory neurons with strength $w_{ei} = 4$, and every excitatory neuron receives input from $n_{ie} = 10$ random inhibitory ones with strength $w_{ie} = 2$. Synaptic strengths were chosen to balance number of incoming connections so that the total possible input to all cells remains the same. The external current $I_{e/i}$ is uniform over the entire excitatory/inhibitory network and functions as a global control parameter that controls response transitions from low-frequency random activity, to spontaneous activation of localized network regions, and finally to global bursting. This network architecture promotes global inhibition driven by focal excitation that creates selective, persistent reactivation patterns [63]. For the simulations presented in this chapter, $I_e = 0.65$ and $I_i = 1.2$.

When the membrane potential of a given cell reaches a maximum value of $V_{reset} = 1$, the neuron emits an action potential, its membrane potential is reset to $V_{reset} = 0$, and the neuron enters a refractory period for $\tau_{refr} = 10$ ms. The synaptic current emitted by spiking neuron (k) is of the form

$$I_{syn}^k(t) = A * exp(\frac{-(t - t_{spike}^k)}{\tau_s}) - exp(\frac{-(t - t_{spike}^k)}{\tau_f}), \tag{3.4}$$

where $(t - t_{spike}^k)$ is the time since neuron k last spiked, $A = 1$ is the amplitude, $\tau_s = 1.5$ ms is the slow time constant, and $\tau_f = 0.15$ ms is the fast time constant. In addition to the synaptic current from other cells, all neurons have a $p_{fire} = 10^{-3}$ probability of firing spontaneously per millisecond.

The excitatory subnetwork undergoes synaptic modification based on spiking activity of these cells. This subnetwork is composed of 25% non-modifiable, homogeneous, active connections with strength $w_{ex} = 2$, in addition to 75% modifiable synapses, which are connections initially with weight 0 but can modulate their

strength based on neuronal activity between $w_{ex} = 0$ and $w_{ex} = 2$ [61]. The changes in synaptic strength of modifiable synapses are implemented based on a simplified neurobiological rule of spike timing dependent plasticity [12, 15, 79, 73]. Upon firing of neuron k, synaptic strength from neuron j to neuron k is incrementally increased if neuron j (pre-synaptic cell) fires before neuron k (post-synaptic cell) within a set interspike interval (ISI) of $T_L = 20$ ms. At the same time, synaptic strength from neuron k to neuron j is decreased by the same amount. Additionally, synaptic efficacy from the pre-synaptic to the post-synaptic cell is decreased by a smaller amount when the two cells do not activate congruously, i.e. their ISI is above the set threshold $T_F = 200$ ms. Formally,

$$\Delta w^*_{jk} = \begin{cases} \frac{w_{ex}}{\tau_{learn}} & \text{if } t_j - t_k < T_L \ ; \\ -\frac{w_{ex}}{\tau_{forget}} & \text{if } t_j - t_k > T_F \ ; \\ 0 & \text{if } T_L < t_j - t_k < T_F. \end{cases} \tag{3.5}$$

$$\Delta w^*_{kj} = \begin{cases} -\frac{w_{ex}}{\tau_{learn}} & \text{if } t_j - t_k < T_L \ ; \\ 0 & \text{otherwise.} \end{cases} \tag{3.6}$$

The w^*_{jk} indicates the weight of the modifiable synapse from neuron j to neuron k, $w_{ex} = 2$ is the strength of non-modifiable synapses in the excitatory network, $t_j - t_k$ is the ISI between neurons j and k, and $\tau_{learn} = 20$ and $\tau_{forget} = 70$ are the rates of learning and forgetting in the network. For comparison purposes, learning is not turned on until 3 s into the run. Calculations are performed using Euler's method and time steps of 0.05 ms.

To simulate external sensory input, a constant current of value 0.9 is fed into a localized subgroup of 100 neurons in the excitatory neuronal network (neuron IDs

201-300) at times 2-6 s and 9-12 s. A period of sleep is implemented between 6.5-8.5 s by raising I_e to 1.05 to represent biological neuromodulatory mechanisms during sleep.

The early plasticity window analyzed in the paper was defined to be from 3-4 s, just after plasticity had been turned on in the simulation. This was done in order to mimic the early exploration window for the mice when they were initially placed in the environment. Late plasticity was defined as 10-11 s (after the sleep period), again for comparison to the late exploration window in the experimental data. This model data was provided by Jane Wang in the Zochowski lab at the University of Michigan.

3.3 Results

We analyzed both experimental and model derived data to explore changes in network structure and dynamics as a result of synaptic modifications during exposure to a stimulus. In the experimental data, we analyze spike train data obtained from tetrode recordings of freely moving mice (see Sect. 3.1.5) as they learned a novel track environment. An example raster plot of the obtained recordings along with the mouse's behavioral state can been seen in Fig. 3.3(a).

This data is of interest for two reasons. Firstly, there are established differences in the functional organization of hippocampal networks between active exploration and slow-wave sleep [23]. These include the joint activation of pyramidal cell ensembles at timescales corresponding to gamma frequencies during awake movement [54], and the high speed replay of pyramidal cell sequences within ripple events that occur preferentially during slow-wave sleep and rest [41]. Secondly, the mouse learned a new spatial representation during exploration of the novel environment (as indicated by

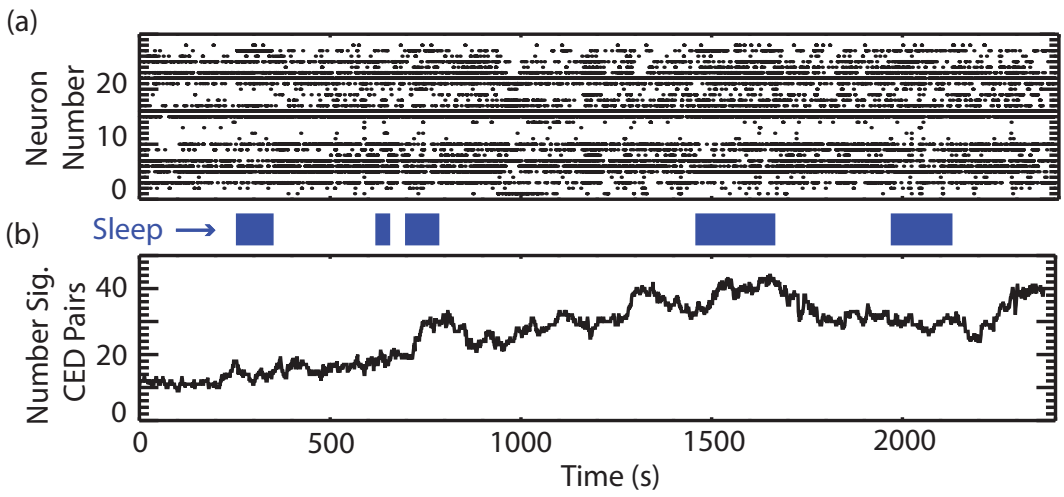

Figure 3.3: Experimental data and number of significant CED pairs. (a) Example raster plot of recordings from mouse 2 as it explores and sleeps in a novel environment. (b) Number of significant CED pairs as a function of the mouse's time in the environment. The rise in the number of significant pairs indicates the formation of directional lead/lag relationships between neurons as the mouse sleeps and continues to explore the environment.

the formation of "place fields" [14]) and the subsequent epoch of slow-wave sleep has been hypothesized to be a period of memory consolidation [21, 66], that is presumed to involve alterations in structural and thus functional network connectivity. These structural alterations involve the strengthening of existing monosynaptic connections between the neurons. Furthermore, recent experimental findings have shown that memory consolidation of the neural representation of novel stimuli results in two changes: neurons that are correlated during initial exposure progressively increase their co-firing, while the neurons that have shown a loose relation become further de-correlated [100]. In terms of network reorganization, this should lead to the tightening of the cluster of cells involved in the coding of the new environment and, at the same time, a functional decoupling from the other cells.

Given these functional differences between the various behavioral states of the mouse, we expected to see different clustering patterns during the exploration and

sleep phases, due to the known differences in network dynamics between these behavioral states.

To better understand the structural network changes which underlie the observed changes in dynamics, we also analyze data from a model of hippocampal memory formation (see Sect. 3.2). An example raster plot of the model data can be seen in Fig. 3.4(a). In this model, memories are formed by the stimulation of a selected group of neurons with modifiable synapses that can be strengthened/weakened through a learning rule implemented to simulate STDP processes. The modifiable synapses were initially silent [61] and became selectively active, driven by an activity-dependent synaptic modification process. After stimulation starts at 2 s, the external input given to neurons 201-300 induced these neurons to fire with spatio-temporal patterning that induced rapid strengthening of synapses when synaptic plasticity is turned on at 3 s. The synaptic plasticity continues until the stimulation is ceased at 6 s.

Below we compare and quantify the changes in directional neural interactions and evolution of functional clustering for the experimental data and model data.

3.3.1 Directional interactions

In order to quantify the changes in directional interactions between neurons in both experimental and model data, we analyzed pairwise interactions between neurons using causal entropies (see Sect. 3.1.1). This measure detects directional lead/lag patterning between spiking of neurons as a function of time. In Figs. 3.3(b) and 3.4(b) we show the number of significant CED pairs as calculated for the experimental and model data, respectively.

In the experimental data, we see that the number of significant CED pairs begins to grow during the first period of sleep and continues to increase as the mouse

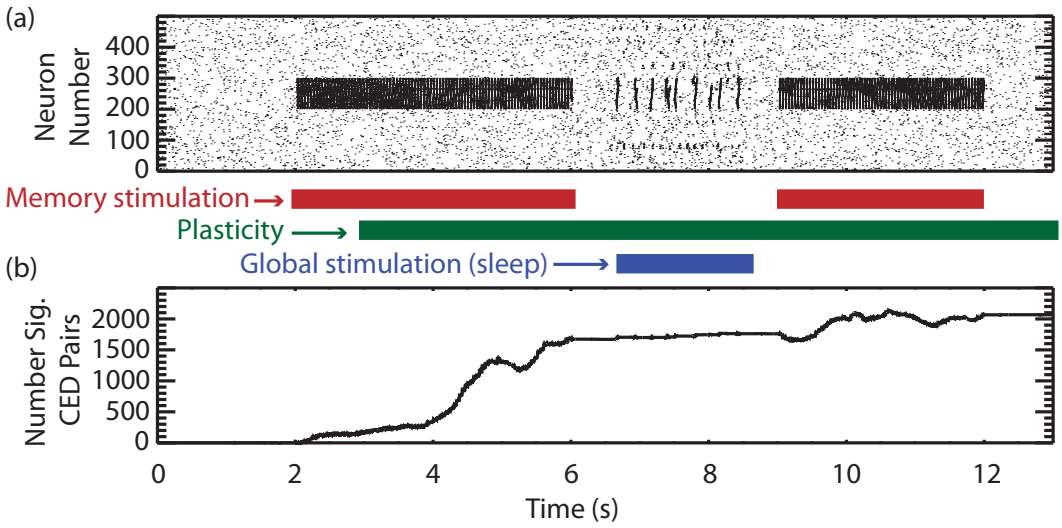

Figure 3.4: Model data and number of significant CED pairs. (a) Example raster plot of model data. Neurons 201-300 receive external input to simulate the presence of a stimulus as indicated by the red bar. An STDP rule is applied for the period marked by the green bar, and a global external input is applied to simulate sleep as indicated by the blue bar, causing reactivation in the previously stimulated neurons. (b) Number of significant CED pairs. Once plasticity is turned on, we see a rise in the number of significant directional relationships between neurons which continues to increase during the sleep period and persists during further stimulation.

further explores and learns the new environment. This corresponds to an increase in the number of significant directional (lead-lag) relationships between neurons, which is consistent with the development of enhanced connectivity between cells during memory consolidation [142].

We also see an increase in the number of directional relationships between neurons in the model data once plasticity has been turned on. Here, we calculate patterning only between the pairs of stimulated neurons. As the neurons comprising the memory are stimulated, the standard STDP rule strengthens directional connections between pre and post-synaptic neurons, leading to more reliable lead/lag patterning between the firing of the neurons. The increase in the number of significant CED pairs is thus a direct result of these known structural changes in the model topology. During the simulated sleep environment, the heterogeneity formed during the initial

Table 3.1: Percentage significant CED pairs and change in FCA significance

	CED: early exploration/plasticity	CED: late exploration/plasticity	FCA: significance change
experiment	$1.8 \pm 0.6\%$	$7.5 \pm 1.5\%$	0.54 ± 0.46
model	$8.3 \pm 1.5\%$	$56.4 \pm 9.1\%$	0.57 ± 0.03

stimulus presentation is more excitable as compared to other network regions and thus mediates reactivation. This reactivation exemplifies itself as an occurrence of synchronized bursts. As the stimulated region is reactivated during the sleep period, we see further increases in these interactions and these directional relationships persist through the second period of stimulation after sleep.

In table 3.1, we further quantify the increase in directional relationships by calculating the percentage of significant CED pairs during early exploration/plasticity and during late exploration/plasticity (after sleep). The data was averaged over $N = 2$ experimental trials and $N = 4$ simulated trials. The number of significant CED pairs was determined by the point at the end of the window designated as the early/late exploration/plasticity period described in Sects. 3.1.5 and 3.2.1. In both the experimental and model data, we see substantial increases in the percentage of significant CED pairs during the late exploration/plasticity stages, quantifying the increase of directional relationships between neurons as a result of memory consolidation and learning.

3.3.2 Functional groupings

In order to study the changes in functional groupings of neurons before and after learning, we implement the Functional Clustering Algorithm with the AMD similarity metric designed to detect co-firing events in neuronal activity. This algorithm not only parses the data into functional groupings, but also assigns values of similarity and significance to each joining step that combines groups of neurons (see

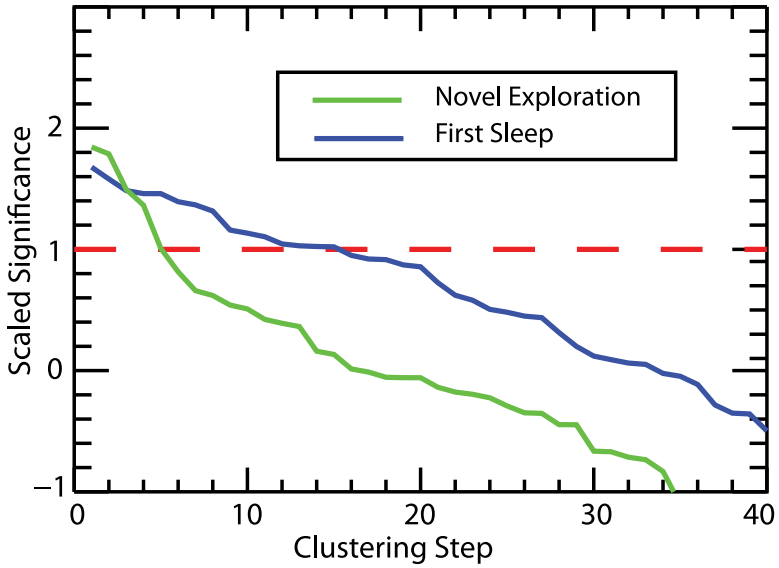

Figure 3.5: The scaled significance used in clustering calculated for novel exploration and the first sleep. Data is shown for mouse 1. The significance cutoff is shown by the dashed line. The FCA is able to detect the greater number of neurons involved in joint firing known to occur during sleep.

Sect. 3.1.2). It is therefore relevant to compare the properties of the similarities and significance for the joining steps in the algorithm during different stages of the mouse's behavior.

In Fig. 3.5 we show the scaled significance used in the FCA during the initial exploration as well as the first sleep period for mouse 1. The cutoff point in the algorithm occurs when the scaled significance drops below the dashed red line. The step in the algorithm at which this cutoff occurs indicates the number of neurons involved in the clustering. Thus, if a cutoff occurs for a late (as opposed to early) step in the clustering, more neurons are recruited into the clusters. One can see that there is an increase in the number of significant pairs being clustered during the sleep period (due to the later stage of cutoff), consistent with the increased co-activation of neurons known to occur during sleep ripples.

We also compare the scaled significance used in the clustering during the initial exploration and an exploration period that occurs later in the same trial, after a num-

ber of quiet waking and sleep periods. As functional groupings become increasingly coordinated in their activity, we expect to observe an increase in the significance of the joining steps indicating the decrease in temporal distance between firing times. Alternatively, neurons which become increasingly de-correlated in their activity will be indicated by a decrease in the amount of significance.

In Fig. 3.6(a), we plot the scaled significance used in each joining step of the FCA when applied to the data shown in Fig. 3.3. Examination of the scaled significance for this experimental data shows that we indeed see a change in the slopes of the curve between early and late exploration. The amount of significance increases for the initial steps of the algorithm which are indicative of the joining of correlated neurons. However, later in the algorithm (during the joining steps which are deemed insignificant, representing neurons which are less correlated), we see a decrease in the amount of significance. This indicates the expected loosening of functional interactions between neurons not involved in the coding of the environment.

In Fig. 3.6(b), we show the scaled significant for the early and late plasticity windows of the model data shown in Fig. 3.4. We again see that the amount of significance increases for the late plasticity window, indicating a tighter relationship between the firing of neurons.

We quantify the effect of the increase in functional correlations by measuring the area between the significance curve and the clustering cutoff line for the significant joining steps of the algorithm. This area is indicated by the shaded regions of Fig. 3.6(b). In order to normalize between data with different numbers of neurons, we quantify the change by calculating $(A_{late} - A_{early})/(A_{late} + A_{early})$. This measure is contained within $[-1, 1]$ and positive values indicate an increase in the scaled significance used to cluster the neurons. We show the results of this calculation for both

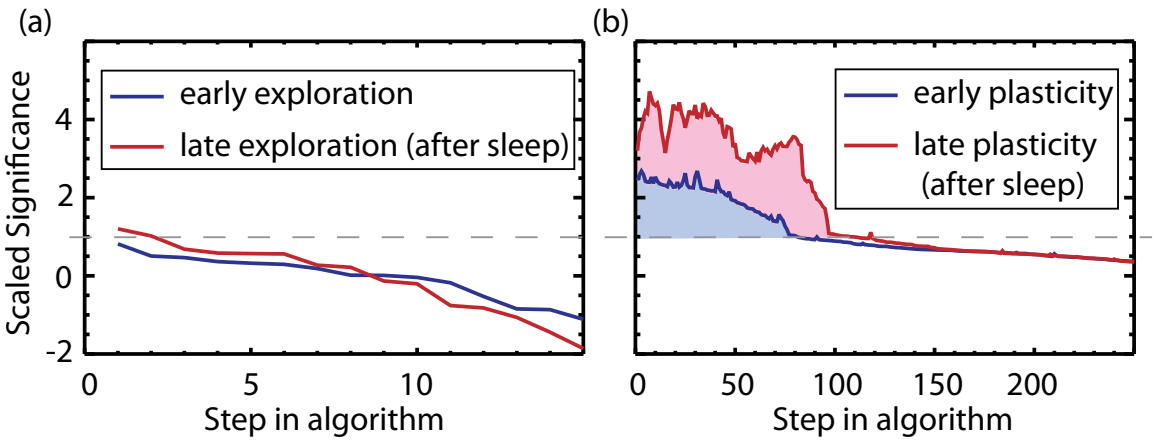

Figure 3.6: Scaled significance for early and late exploration periods. (a) The scaled significance used to join trains plotted as a function of joining steps in the FCA for the experimental data presented in Fig. 3.3 during the early and late exploration periods. (b) The scaled significance used in the FCA for the model data presented in Fig. 3.4 during early and late plasticity. The dashed grey line denotes the clustering cutoff. Values above this line are significant steps while values below this line are insignificant. The shaded regions denote the area between the significance curve and the clustering cutoff used to quantify changes in the amount of significance as described in the text.

experimental and model data in table 3.1. In both cases we are able to quantify the increase in significance used in the clustering steps of the algorithm.

It is also of interest to study the AMD values associated with the joining steps of the FCA before and after the environment has become familiar. We therefore compared the initial exploration of the novel environment to a subsequent exploration of the same environment (after the sleep epochs). Here, we hypothesized that, due to memory consolidation and the associated changes in correlations between neurons, we would observe a selective drop in the joining AMD when comparing the initial exposure to a novel environment to a subsequent exposure once the environment has become familiar. This drop should occur for initially small AMD values (initially correlated neurons) as these neurons become further correlated. However, for initially large (insignificant) AMD values, we expect an increase in the AMD values when comparing novel and familiar exploration. This growth occurs as the neurons with low correlations become further uncorrelated.

To assess any changes in the AMD values between initial (novel) and familiar exploration, we examine the $\widetilde{AMD}$ values (see section 3.1.3) used in the joining steps of the FCA when applied to data from each epoch. In Fig. 3.7(a), we show changes of the average $\widetilde{AMD}$s used to cluster the neurons for the clustering steps which have a significantly lower $\widetilde{AMD}$ than that obtained from surrogates (i.e. co-firing cells), during novel exploration and a subsequent familiar exploration of mouse 1. We indeed see that the average $\widetilde{AMD}$ value is lower for neurons during the familiar exploration indicating that the firing patterns of the neurons are more tightly correlated. Thus, as in the case of [100], the observed decrease of the $\widetilde{AMD}$ during the subsequent presentation of the novel environment occurs for neurons which fire in the same spatial locations of the maze. In Fig. 3.7(b), we show the average $\widetilde{AMD}$ distances for the non-significant clustering steps during the novel and familiar exploration. These distances are greater during the familiar exploration as the activity of the neurons having low correlation becomes even less correlated.

3.4 Discussion and summary

The observed changes in the neural patterning during the experiments support the underlying hypothesis is that as the mice explored the track, they learned a new spatial representation of the novel environment. While in the track, the mice underwent periods of sleep, followed by further exploration of the environment. These epochs of slow-wave sleep have been hypothesized to be a period of memory consolidation [21, 66], that is presumed to involve further alterations in structural as well as functional network connectivity. These structural alterations involve both the strengthening of existing monosynaptic connections between the neurons as well as the development of new connections. As a result of these changes, we observed

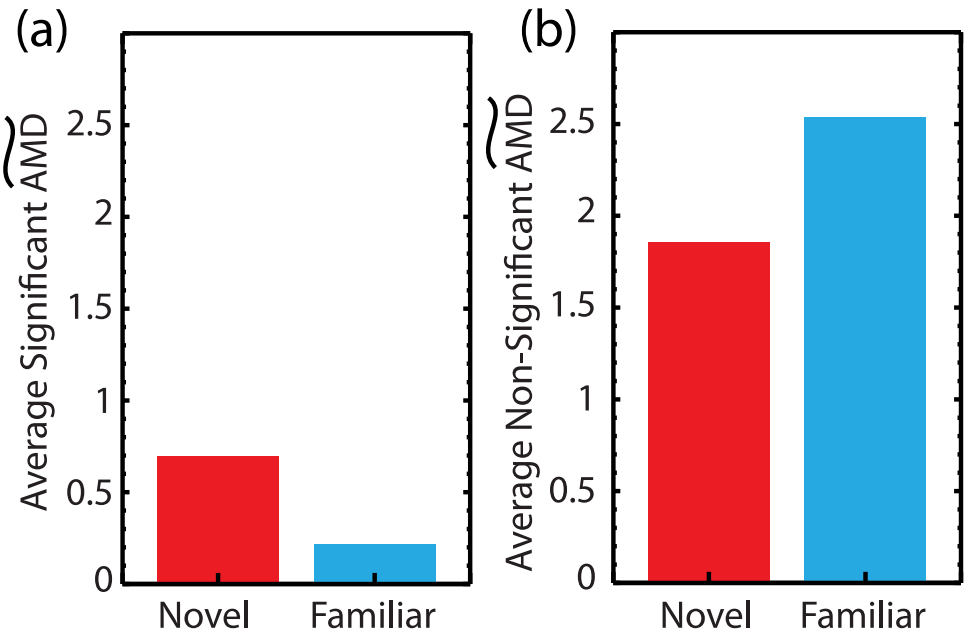

Figure 3.7: Changes in $\widetilde{AMD}$ values between novel and familiar exploration. (a) Comparison of the $\widetilde{AMD}$ averaged over significant clustering steps from novel exploration and a subsequent familiar exploration. We observe a decrease in this value during the familiar exploration as correlations between neurons become tighter. (b) Comparison of the $\widetilde{AMD}$ distances averaged over non-significant clustering steps during novel and familiar exploration. Here we see an increase in this value during familiar exploration as neurons which were uncorrelated become further de-correlated.

an increase in directional lead-lag patterning between cells as the mice learned the new environment. Since sleep is thought to play a focal role during memory consolidation, this directional patterning could appear during sleep phases and continue beyond them, as was observed in the data.

Additionally, recent experimental findings have shown that two changes in neural firing patterns correlate with the memory consolidation of neural representations of novel stimuli: neurons that are correlated during initial exposure progressively increase their co-firing, while the neurons that are initially less correlated in their activity become further de-correlated [100]. As predicted by this results we observe a tightening of functional interactions between initially correlated neurons as the neurons which code for the environment increase their co-firing activity.

In the model data, we show how the addition of an STDP motivated learning rule leads to synaptic modifications which, in turn, give rise to changes in neuronal dynamics. Here, a subset of the population is stimulated and the plastic synapses are allowed to evolve under the learning rule. The strengthening/weakening of synapses within this discrete region effectively creates a structural inhomogeneity of the network connectivity. Sleep is modeled as a global increase of network excitability, and during this period, the previously stimulated region is able to reactivate while suppressing surrounding areas due to the topological nature of the network which allows for focal excitation as well as global, random inhibition. The observed reactivation also allows synapses to further strengthen. When this external stimulation is repeated, we observe even further strengthening of synapses. These known changes in the network structure give rise to changes in neuronal dynamics which match the observed changes in the experimental data.

As the amount of experimental data depicting neural interactions during various cognitive tasks increases, it is becoming essential to develop metrics which quantify neural relationships during different behavioral states. Equally important is the ability to link these changes in neural relationships to underlying structural and/or neurobiological changes. This task of linking observed changes in dynamical behavior to structural changes implies a need to combine experimental data with extensive modeling where structural changes can be directly linked to dynamical changes. In this chapter, we have presented new methods which when applied to both experimental and model data, depict changes in neural dynamics and allow for explanation of the underlying structural changes which give rise to the observed dynamical changes.

Specifically, we tried to link the progressive functional clustering observed during exposition to a novel environment with the underlying structural network changes.

To do so we used two measures developed to: 1) quantify the emergence of directional dynamical interdependencies in the network which are indicative of the enhancement of network connectivity and, 2) monitor the emergence of functional clusters based on activity patterning of neurons. We applied these two measures to experimental data where they detected increases in directional relationships between neurons and a tightening of functional clusters as the mice explored, slept, and learned a novel environment. We then implemented the same measures in a simple model which implemented STDP processes during exposure to an external stimulus and periods of sleep. We observe very similar changes in the number of significant directional pairs as well as the emergence of of functional clusters during both stimulus presentation and sleep. These results are consistent with the hypothesis that the observed dynamical changes are a result of underlying structural changes induced through STDP processes as a function of learning.

CHAPTER IV

Interacting networks: a model of focal epilepsy

In the last chapter, I discussed the use of modeling to demonstrate the interplay of anatomical structure and neuronal dynamics through STDP. The behavior of the model was then compared to that of experimental data in an attempt to link changes in dynamics to underlying structural changes. In this chapter, I will again explore the relationship between structure and dynamics, this time through varying the neuronal properties (excitability) along with the network structure. This will be done in the context of a simple model of two coupled networks designed to study phase synchronization in focal epilepsy. In this case, I will show that the overall dynamics are robust to structural changes in the network coupling and largely determined by the relative relationship between the excitability of the networks. However, in this case, the excitability of each network is determined by the dynamics of the neurons within that network as opposed to the individual network structure. This result confirms that directly linking anatomical and functional structure is a non-trivial task.

Epilepsy, one of the most common neurological disorders, is characterized by the sudden onset of recurrent seizures due to a hypersynchronous firing of populations of neurons. Due to the debilitating nature of seizures and the fact that approximately

1% of the world population suffers from epilepsy, much research has investigated the dynamics of the onset of seizures with the hopes of developing methods of seizure prediction [85]. One of the most common types of epilepsy is focal epilepsy in which seizures originate from a circumscribed region within the brain. Since only about 2/3 of epilepsy patients will respond to medication, surgery to remove the focal region is another option for treatment [35]. In order to locate the focus, clinicians rely on information from electroencephalogram (EEG) recordings combined with various imaging techniques. The availability of EEG data from these patients has allowed researchers to study the dynamics of the EEG signal before and during a seizure in hopes of better understanding the seizure generating process with the ultimate goal of predicting seizures.

Through the analysis of EEG recordings, it has recently been shown that one can identify a preictal period before the onset of a seizure during which various properties of the EEG time series differ from those during interictal (activity between seizures) and ictal (seizure) periods [88]. Attempts have been made to characterize this preictal period using, among others, the largest Lyapunov exponent [60], correlation density [81], correlation dimension [71, 32], and dynamical similarity measures [68, 69, 90]. Other recent approaches utilize measures of phase synchrony which determines the degree of phase locking between two oscillatory signals. Although the concept of phase synchronization has long been known [59], it is only recently that it has been applied to nonlinear time series analysis [114] and biological data in the analysis of Parkinson's patients [136], the cardiovascular and respiratory systems [118], the calcium oscillations of epileptic cultures of astrocytes [6, 7], and in EEG recordings [89, 86, 87, 70].

Measures of phase and lag synchronization show a rather unexpected effect: a

significant decrease in synchronization between certain EEG channels during the preictal period. The patterning of channels that exhibit this drop is quite complicated and is not necessarily dependent upon spatial structure. It has been hypothesized that this is due to the fact that the spatial and functional structure of the brain do not overlap [87]. Specifically, structures that are far in terms of Euclidian distance may have strong functional links, while neighboring regions may be functionally independent. This leads one to believe that the drop in synchronization occurs in weakly connected, functionally different regions of the brain. Thus, while the cause of this decrease is unknown, it has been hypothesized [89, 87] that the recordings are performed in separate regions of synchronized activity where one site has become involved in the synchronous activity associated with the epileptic focus and onset of the seizure, while the other site has yet to become enveloped in this activity.

Testing this hypothesis experimentally as well as understanding its dynamical underpinnings is difficult since the EEG records the activity from a population of neurons, and while EEG recordings give important information about neural activity, the recorded signal can not be directly linked to the underlying dynamics of the brain. We thus turn to a modeling approach to gain further insight into the possible mechanisms for the increased synchrony observed during interictal periods as well as the drop in synchrony during the preictal period.

We study a computational model in which two coupled networks of integrate-and-fire neurons model separate EEG recording sites. We choose one network to be associated with the seizure generating region (epileptic focus) of the seizure and slowly drive this pathological network into a bursting (seizing) state by increasing the excitability of the neurons within that network over time. This method of transition into a seizure is chosen to mimic a class of cellular mechanisms thought to lead to a

seizure [50]. A model of this type allows for analysis of the levels of synchronization over the total population of the networks (similar to using intracranial EEG) as well as at the level of the individual neurons.

We observe changes within the collective dynamics of the pathological network as the neurons transition from the globally asynchronous firing state which we consider to represent normal neural dynamics into the bursting state of a seizure. If the collective dynamics of the networks share gross dynamical properties (i.e., the same excitability), the networks will enter a resonance state. This leads to an amplification of the intrinsic oscillatory rhythm and increased levels of locking between collective signals of the networks. However, as the network corresponding to the epileptic focus begins its transition into the seizing state (but before the network begins to burst), the networks stop resonating, resulting in an elimination of the oscillatory patterning and a subsequent drop in phase synchrony that marks the beginning of the preictal period. During this time, the neurons of the pathological network continue to fire asynchronously but begin to increasingly lock their frequencies. Once the pathological network reaches the bursting state, it begins to drive the other network into a bursting state and we again see the high levels of synchronization characteristic of the ictal period.

We thus postulate that the preictal period marks the beginning of the transition from normal neural dynamics into bursting dynamics, which is characterized by the steady increase and locking of neuronal frequencies that eventually leads to bursting. This transition in the "focal" network is accompanied by an initial lack of a similar transition in the "normal" network, which causes the divergence of intrinsic network properties and a drop in the phase synchrony between the two networks.

4.1 Methods

4.1.1 The model

The system studied in the paper consists of two inter-connected small-world networks (SWN) of integrate-and-fire neurons. Each network consists of 225 neurons situated on a 2D square lattice with a lattice constant of $a = 1$ and periodic boundary conditions. Neurons are initially locally connected to neighbors within a radius of $k = 2$. The connections are then rewired with a probability of $p = 0.3$, consistent with the Watts-Strogatz SW model [148]. The small-world architecture has been shown to produce self-sustained activity [117], increase the network's ability to synchronize [98, 9], and has previously been used for models of epileptic behavior [91, 108, 123].

We introduce connections between the two networks by selecting a fraction $f = 0.5$ of the neurons in each network to send synaptic current to a randomly chosen m neurons in the other network. Unless stated otherwise, $m = 15$. Connecting the networks in this manner causes the neurons in one network to receive, on average, seven random connections from the other network, representing the average activity of that network.

The dynamics of each neuron are governed by

$$\tau_m \frac{dV_i}{dt} = -\alpha_i V_i(t) + \sum_{j\in\delta} J_{ij}(t) + B\sum_{k\in\gamma} J_{ik}(t) + \xi_i(t) + E \tag{4.1}$$

where $\tau_m = 20$ ms, α_i is the leakage coefficient which is uniformly distributed in $[1, 1.1]$, δ represents the intra-network connections, γ represents the inter-network connections of the i^{th} neuron and we sum over the incoming synaptic current, J. B is the coupling parameter between the networks. For the simulations, we used $B = 0.4$ unless otherwise noted. The noise variable for each neuron $\xi_i(t)$ is uniformly

distributed in $[0, 0.5]$ and E is the excitability parameter which is constant for each neuron in a given network, but is allowed to vary between the networks. The neural excitability determines the amount of synaptic input needed to cause the neuron to fire and acts as a control parameter between the asynchronous firing of neurons within a network and bursting behavior where the population of neurons fires collectively. We use this parameter to induce bursting in one network by slowly raising its value over time, bringing the network from a non-bursting state into a bursting state. The level of excitability at which the network transitions into the bursting state is referred to as the bursting threshold. We will denote the two networks as $N1$ and $N2$ with respective excitability parameters E_1 and E_2.

Equation 4.1 was integrated using Euler's method and a neuron was said to fire an action potential when the membrane potential, V, reached a threshold value of 1. At this point, the neuron emits a spike of synaptic current that is sent to the neurons to whom it is connected. For this reason we use the term 'spike' to refer to the firing of a neuron. The incoming synaptic current to the i^{th} neuron from the j^{th} neuron is given by

$$J_{ij}(t) = A\left[exp\left(-\frac{t-t_j}{\tau_s}\right) - exp\left(-\frac{t-t_j}{\tau_f}\right)\right] \tag{4.2}$$

where t_j denotes the last time at which the j^{th} neuron spiked, $\tau_s = 0.2$ ms is the slow time constant, and $\tau_f = 0.02$ ms is the fast time constant. These two time constants determine the spike shape and are chosen to approximate a biological action potential [48]. The parameter $A = 1.8$ sets the amplitude of the spike. After firing, the membrane potential is reset to 0, and the neuron enters a refractory period of 8 ms under which it does not integrate incoming current. Moreover, when out of the refractory period, a neuron only integrates synaptic current if the total value is above a threshold level of 0.4. Each network has an intra-network synaptic delay of

0.6 ms and unless stated otherwise, the inter-network delay is 0.8 ms. These two constants define the spatial extent and the distance between the two networks.

For comparison with EEG recordings, we here consider the total current signal of each network which we define to be the sum of all synaptic currents of the neurons within the network at each point in time, as this tells us the collective activity of a population of neurons. We can then look at measures of phase and lag synchrony between the total current signals of our networks while varying their relative properties and compare the results to those obtained from EEG recordings of epileptic patients. Our model also allows us to monitor the firings of the individual neurons within the network and to study how the synchronization of the individual neurons leads to the observed signal. This allows for insight into the mechanisms behind the synchronization of the two networks on the neuronal level which is difficult to obtain from actual EEG recordings.

4.1.2 Mean phase coherence

We first examine the mean phase coherence in our system which is a measure of phase synchrony. Phase synchrony refers to the state where the phases of two oscillators become locked while their amplitudes remain uncorrelated [110]. This generally occurs in systems of weakly coupled, non-identical oscillators. We consider the brain to be an example of such systems, as a first order approximation, since each neuron is different, and the total number of synapses a given neuron has is small compared to the total number of neurons in the brain. The general definition of phase locking in noisy oscillators is

$$\Delta\phi_{1,2} = |k\phi_1 - l\phi_2| \cong constant \tag{4.3}$$

where ϕ denotes the phase of the oscillators and k and l are integers (here we use $k = l = 1$). The mean phase coherence examines the angular distribution of the difference in phase between two oscillators and is defined [89] as

$$R = \left| \frac{1}{N} \sum_{j=0}^{N-1} e^{i\Delta\phi_{1,2}(j\Delta t)} \right| \tag{4.4}$$

where N denotes the number of samples in a discrete time series and $1/\Delta t$ is the sampling rate. This definition restricts $R \in [0, 1]$ and phase locking occurs for $R = 1$ while $R = 0$ implies unsynchronized signals.

To calculate R for our simulations, we used a moving window technique in accordance with [86] with $k = l = 1$. The time series of the collective signal was divided into a series of windows composed of 4096 points or 819.2 ms with an overlap of 20%. First, the data in each window was demeaned (the mean value of the signal was subtracted, eliminating any DC component of the signal), and a Hanning window was applied. We then used the Hilbert transform [116] to define the analytic signal and calculate the instantaneous phase of the signal.

The Hilbert transform of a signal $s(t)$ is given by

$$\tilde{s}(t) = \frac{1}{\pi} P.V. \int_{-\infty}^{\infty} \frac{s(\tau)}{t - \tau} d\tau \tag{4.5}$$

(where P.V. denotes the Cauchy principal value) and the analytic signal is then defined as

$$\zeta(t) = s(t) + i\tilde{s}(t). \tag{4.6}$$

From this, we can uniquely define the instantaneous phase of our signal as

$$\phi(t) = arctan\left(\frac{\tilde{s}(t)}{s(t)}\right). \tag{4.7}$$

Finally, 10% of the signal was discarded at both ends to minimize the edge effects caused by applying the Hilbert transform to a finite signal. The resulting phases were used to calculate the phase difference between signals and the mean phase coherence.

4.1.3 Maximum linear cross correlation

We also examine the lag synchronization of the total current signal. Lag synchronization refers to the case when the state variables of two signals are the same but offset by a constant time lag [115]. A measure of lag synchronization between two signals, $s_{1,2}(t)$, at a time lag, τ, is the normalized cross correlation given by

$$\hat{C}(s_1, s_2)(\tau) = \left| \frac{C(s_1, s_2)(\tau)}{\sqrt{C(s_1, s_1)(0) \cdot C(s_2, s_2)(0)}} \right|, \tag{4.8}$$

where C is the linear cross correlation function

$$C(s_1, s_2)(\tau) = \int_{-\infty}^{\infty} s_1(t+\tau)\, s_2(t)\, dt. \tag{4.9}$$

In order to measure the lag synchronization of our system, we look at the maximum linear cross correlation [86] defined as

$$C_{max} = \max_{\tau} \{\hat{C}(s_1, s_2)(\tau)\}. \tag{4.10}$$

As with the case of the mean phase coherence, $C_{max} \in [0, 1]$, and $C_{max} = 1$ implies complete lag synchronization while $C_{max} = 0$ for unsynchronized signals. We use the moving window technique described above to calculate C_{max} over each window.

4.2 Results

We observe three different types of behavior in the total current signal of the modeled network as seen in Fig. 4.1. In an uncoupled system, the network will undergo random firing for low values of E as seen in Fig. 4.1(a). As the value of E is increased and the mean firing rates of the neurons increase, the network enters

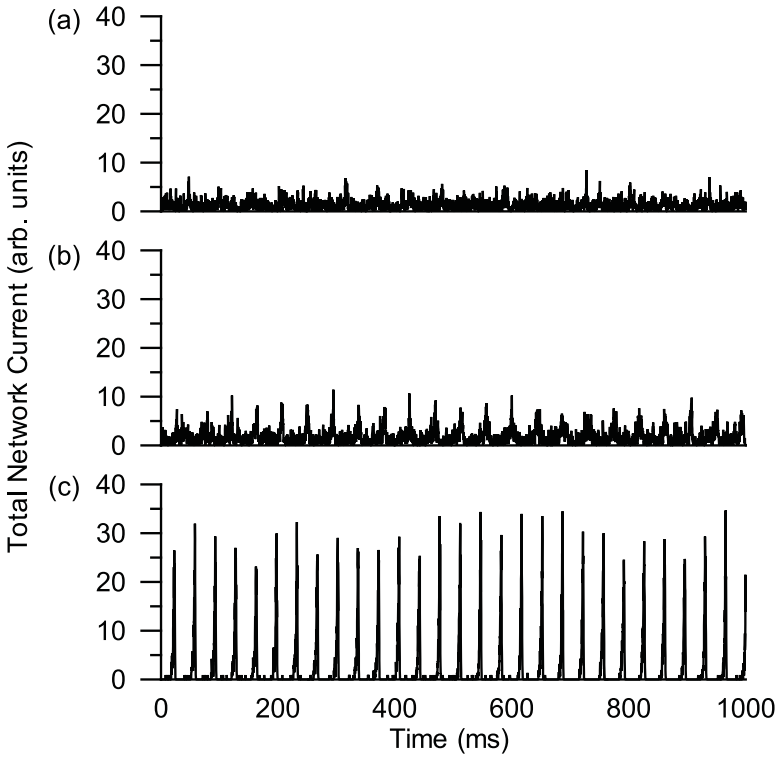

Figure 4.1: Examples of the different types of behavior of the collective current trace of a single, uncoupled network. (a) Random firing behavior seen below the bursting threshold. $E = 0.85$ (b) Fast oscillatory modulation just before the transition to bursting. $E = 0.95$ (c) Bursting behavior observed above the bursting threshold. $E = 1.1$

an oscillating stage where the total current signal undergoes oscillatory modulation as in Fig. 4.1(b). When E is increased further, the network reaches the bursting threshold where the neurons begin to fire synchronously, and the network enters the bursting stage of Fig. 4.1(c).

These results are consistent with the findings of [91], who studied single 1D SWN and induced bursting behavior by adding additional long range connections to the network while holding the excitability of the neurons constant. Here, we hold the topology constant and induce the transition to bursting by increasing the excitability of the neurons to mimic the transition from interictal to ictal dynamics. It has been shown [29] that slices from the CA3 region of the hippocampus exhibit population bursts when the mean firing rate of the neurons within a driver site is increased above

a threshold level. It has been hypothesized that bursting behavior within a neural network is thus the result of the increase in the mean firing rate of the neurons within a given region above some frequency threshold. This is precisely what we observe when increasing the excitability parameter due to the link between the excitability parameter and the firing rate of the neurons. In Fig. 4.2(a), we show this relationship between the average firing rate of 5 neurons and the excitability parameter. As we raise the excitability of the network, the neurons begin to fire more rapidly and the network enters a bursting state. As a result, there is also an increase in the mean current output by the network (Fig. 4.2(b)).

In a coupled network system, the excitability of $N2$ is held constant at $E_2 = 0.8$, representing a local network which is not a part of the epileptic focus. Conversely, $N1$ represents a local network that is part of the epileptic focus, and we step up the excitability of this network from $E_1 = 0.75$ to $E_1 = 1.1$ to obtain the transition to bursting, seizure-like dynamics. In Fig. 4.3 we show the mean phase coherence, R, and the maximum linear cross correlation, C_{max}, plotted as a function of the difference in excitability between the networks, $\Delta E = E_1 - E_2$, averaged over one hundred simulations. The average value of R and C_{max} were calculated for each simulation by iterating for 10 s at each value of ΔE and disregarding a transient time of 4 s.

We focus on the three dynamical regimes, when: (A) both networks are well below bursting threshold and have the same properties (same excitability, $\Delta E = 0$), (B) both networks are below bursting threshold and $\Delta E \neq 0$, and (C) the neural excitability of N1 is above the bursting threshold.

For low values of E, below the bursting threshold, when $E_1 = E_2$, the total current signal of both networks remains asynchronous but exhibits slow oscillatory

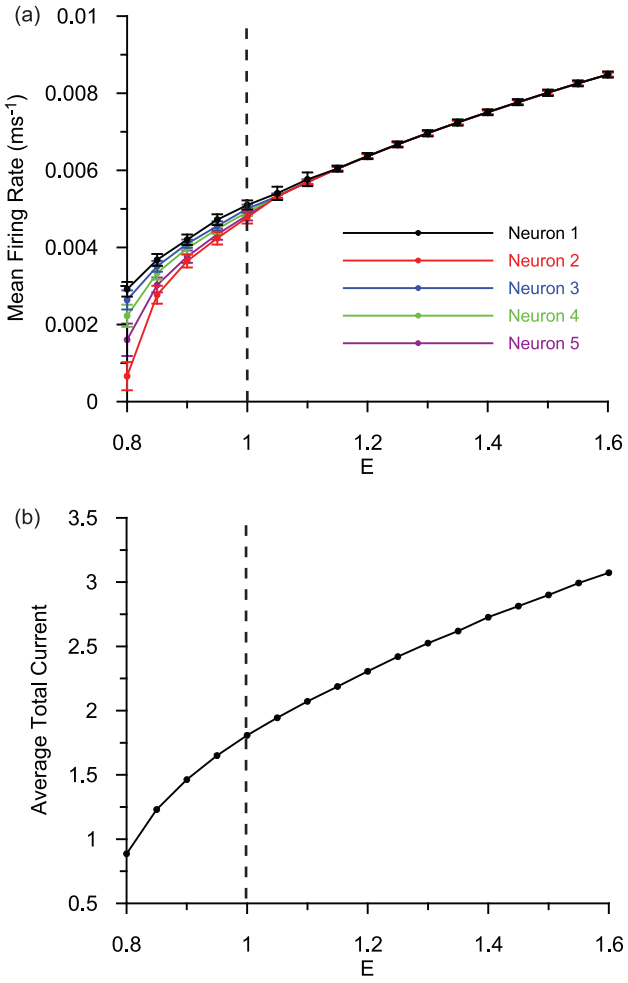

Figure 4.2: Effects of changing the excitability. (a) Relationship between the excitability parameter of a single network and the average firing rate of five different neurons within the network. Increasing the excitability of the network causes the neurons to fire more rapidly and to synchronize. (b) The average total current in a single network as a function of the excitability. As the excitability is increased, the total synaptic current in the network will raise. The dotted line denotes the bursting threshold.

modulation as observed in a single network for relatively high network excitability. However, the oscillatory modulation observed here is due to the resonance drive of both networks through the inter-network coupling. We associate this regime with the interictal dynamics observed in the epileptic brain.

When the networks are below the bursting threshold but have significantly different properties such that $E_1 \neq E_2$, even though the total input from N1 to N2 increases significantly as E_1 is increased, both networks still may exhibit asynchronous

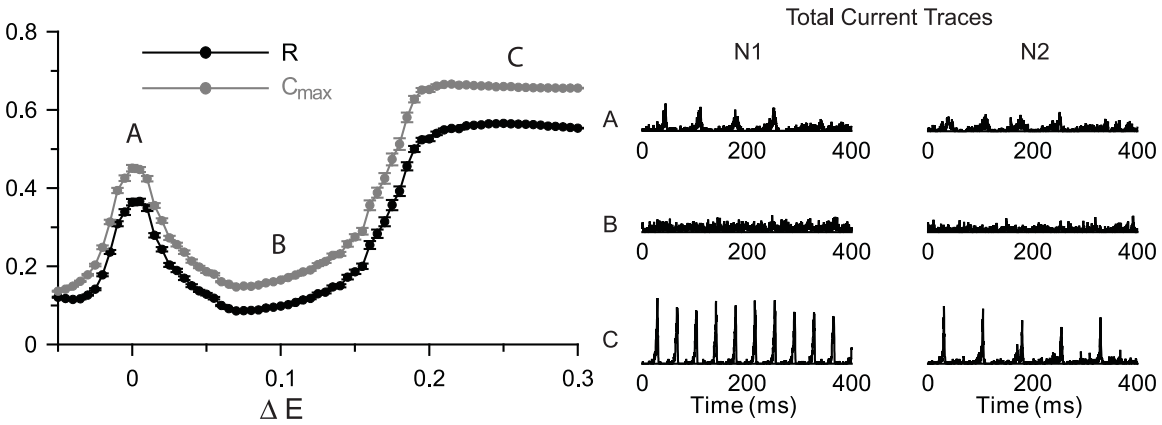

Figure 4.3: Average phase coherence and maximum cross correlation coefficient as a function of the mismatch between the excitability parameters in the networks. Values were averaged over one hundred simulations as described in the text. Sample current traces are shown for the different types of behavior seen during the resonance (A), random firing (B), and bursting regimes (C).

dynamics and, furthermore, the slow oscillatory modulation is abolished. We link this regime to the preictal state.

When $N1$ is above the bursting threshold, the bursting of that network will induce bursting behavior in $N2$. This driving interaction that occurs during the bursting regime represents the spread of bursting behavior throughout different regions of the brain during a seizure (the ictal state).

We thus observe a typical resonance curve centered on $\Delta E = 0$ which is where we see the oscillatory behavior of the networks that gives rise to the higher levels of synchronization. As ΔE is further increased, the frequency response of the two networks becomes mismatched, the slow oscillatory modulation is abolished, and there is a drop in the synchronization. The measures of synchronization rise again for large values of ΔE, as this is the region where E_1 crosses the bursting threshold and the networks enter the bursting regime, with $N1$ driving the bursting in $N2$.

We then studied the role of the coupling and delay between the networks on the observable drop of phase synchrony during the preictal period. Figure 4.4(a) shows

the average values of R and C_{max} for $\Delta E = 0$ (upper lines) and $\Delta E = 0.1$ (lower lines) calculated over twenty simulations in which the coupling parameter B was varied while number of connections between the networks was held constant at $m = 15$. As the coupling in the network increases, the level of synchrony at the resonance increases and for high levels of coupling, the synchrony during the parameter mismatch increases as well. We calculated the differences, $\Delta R = R\,(\Delta E = 0) - R\,(\Delta E = 0.1)$ and $\Delta C_{max} = C_{max}\,(\Delta E = 0) - C_{max}\,(\Delta E = 0.1)$ in Fig. 4.4(b). The peak in this curve is due to the interplay between the level of synchrony at resonance and the spread in the range of oscillations as the coupling is increased. We see that the difference between the synchrony at resonance and away from resonance remains high over a large range of coupling parameters. A similar effect was observed when we varied the number of connections, m, between the networks and kept the inter-network coupling strength constant at $B = 0.4$ (Fig. 4.4(c)-(d)). For large m, we see a decrease in the difference between synchrony levels. This is to be expected since as we add more inter-network connections, we are effectively losing the distinction of having two separate networks. We study the effects of inter-network delays on the observed phenomenon in Fig. 4.4 (e) and (f). Here we hold the coupling parameters constant at $B = 0.4$ and $m = 15$. One can see that as the delay between the networks is increased, there is a decrease in the observed resonance peak. However, the behavior is observed over a significant range of delays indicating that the two interacting networks can be positioned relatively far apart.

In order to better understand the behavior of the networks in terms of the underlying neuronal dynamics, we examined the behavior of the individual neurons within each network. Figure 4.5(a) and (d) show histograms of the interspike intervals (ISI) of the individual neurons within each network for four different values of ΔE in a

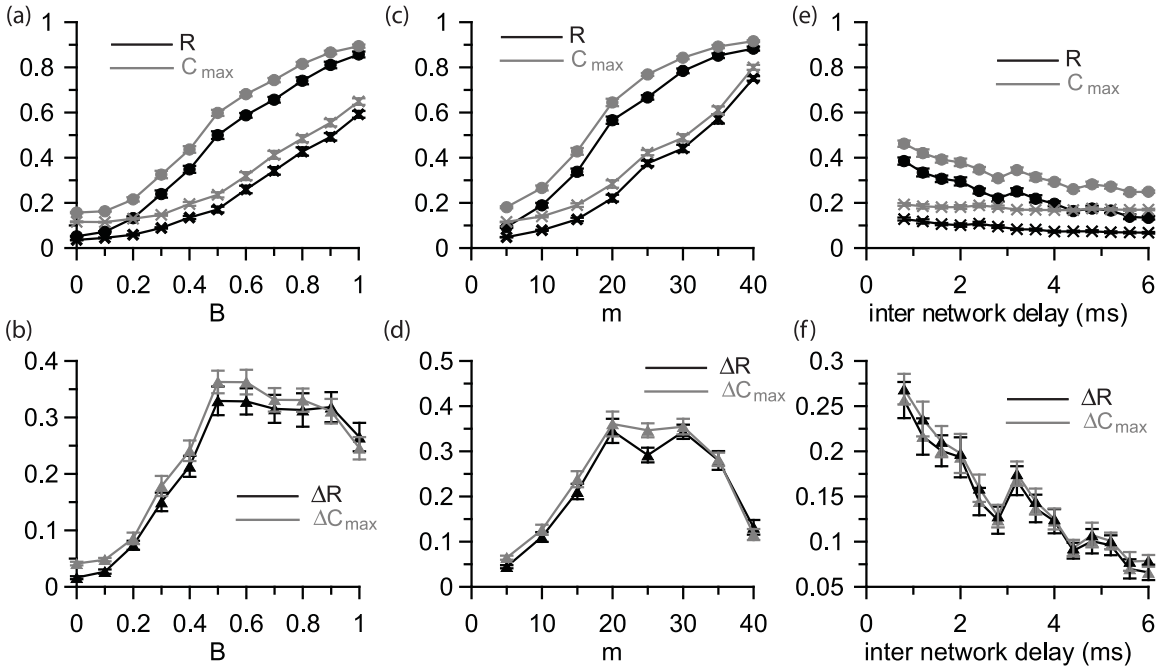

Figure 4.4: Synchronization as a function of network coupling. (a, c, e) Average synchronization as a function of the coupling parameters during two regimes: $\Delta E = 0$ - upper lines and $\Delta E = 0.1$ - lower lines. (b, d, f) Difference between the level of synchronization between the two regimes. (a) and (b) Calculated as a function B, with $m = 15$. (c) and (d) Calculated as a function of the number of connections between networks, m, with $B = 0.4$. (e) and (f) Calculated as a function of inter-network synaptic delay with $B = 0.4$ and $m = 15$ with a constant intra-network delay of 0.6 ms.

system with $B = 0.4$ and $m = 15$. We also performed a peak detection to detect bursts in the total current signal of each network (Fig. 4.5(b) and (e)) to create histograms of the interburst intervals (IBI). The peak detection was done by smoothing the signal over a window of 1.8 ms and a burst was said to occur when the smoothed signal increased above a threshold value of 3. These histograms of the networks' collective behavior are shown in Fig. 4.5(c) and (f). A bin size of 1 ms was used to create the histograms.

We first focus on the behavior of the network for values of E_1 below the bursting threshold. For the case of $\Delta E = 0$, we see that the ISI histograms of neurons in each network as well as IBI of each network have a similar distribution. The networks are operating at the same frequency. We observe slow oscillatory modulation in the total

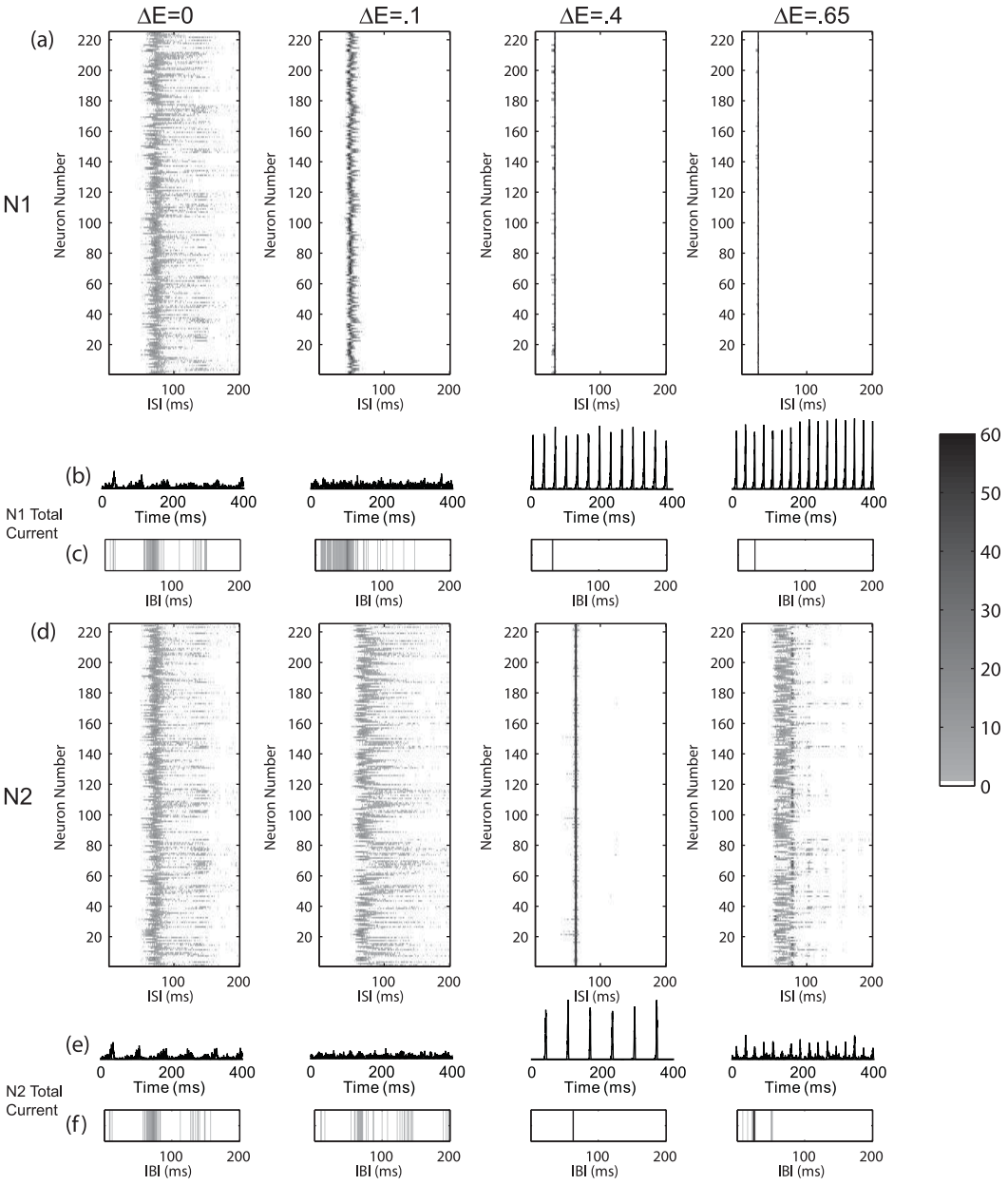

Figure 4.5: Interspike interval and interburst interval histograms. Panels (a)-(c) show the analysis for $N1$, panels (d)-(f) show the analysis for $N2$. (a) and (d) Interspike interval (ISI) histograms for each neuron shown for 4 levels of excitability mismatch. (b) and (e) Samples of corresponding collective signals. (c) and (f) Interburst interval (IBI) histograms of the collective signal during the same intervals as in (a) and (c). Histograms were created by running a peak detection program on the collective signal to determine population spikes. Note that the ISI and IBI histograms do not necessarily correspond indicating that the phase of the neuron plays a large role in the behavior of the network as a whole.

activity of the networks and consequently increased phase synchronization between the networks. When $\Delta E = 0.1$, we observe a different type of behavior. Although the individual neurons in $N1$ are firing at an approximately locked rate leading to the narrow ISI distribution, the total current signal of the network shows a broad IBI distribution indicating that the neural activity remains asynchronous, and the total current signal of the network undergoes occasional random, low activity bursts. The neurons in $N2$ show a virtually unchanged, wide distribution of ISI. The distribution of IBI is similar to that observed previously, but the slow oscillatory component in the total activity is no longer observed. Thus, the asynchronous dynamics of the first network do not significantly alter the temporal dynamics of the second network. This is due to the fact that the neurons in $N2$ receive a current input from $N1$ which increases, but remains temporally unstructured.

When the value of E_1 is above the bursting threshold we observe different behavior. Both networks start to burst with evolving locking patterns. In the case of $\Delta E = 0.4$, the ISI distributions of neurons in both $N1$ and $N2$ are highly peaked and the peaks correspond to those of the IBI distributions in the total activity of their respective networks, indicating that the neural populations within the networks are highly synchronized, and each network is now undergoing coherent bursting behavior. However, the value of ISI and IBI is different as the networks enter a 2:1 locking regime.

When E_1 is further increased ($\Delta E = 0.65$) , we observe a transition to another type of behavior. The neurons in $N1$ remain synchronized and the network bursts at a higher frequency due to the increase in the excitability. The neurons in $N2$ become unsynchronized and fire roughly at multiples of the period of the neurons in $N1$. This leads to relatively weaker bursting, as a limited numbers of neurons fire in

each cycle, but 1:1 locking can be observed.

Thus, even though the frequency of spiking and the average magnitude of the mean-field signal of $N1$ increases monotonically with changes of neuronal excitability, the slow oscillatory patterning in network activity observed when the networks have the same properties is initially abolished before the transition into bursting. This results in the drop of synchrony in the transitional period, before the onset of bursting. We thus hypothesize that the observed preictal drop in phase synchrony of the EEG is due to the abolition of resonant interaction between the two networks caused by changes in the frequency response of network that is associated with seizure generation. Therefore, we postulate that the observed drop in synchrony is in fact an early signature of the pathological changes in the dynamics of the focus that eventually lead to seizure-type dynamics.

To demonstrate this transition from normal to pathological dynamics, we hold the excitability of $N2$ constant at $E_2 = 0.8$ and slowly increase the excitability of $N1$ from $E_1 = 0.75$ to $E_1 = 1.1$ as shown in Fig. 4.6. The progression of the changes in synchrony, driven by incremental changes in excitability of $N1$, mimics those observed in epileptic patients during transitions from interictal to preictal and preictal to ictal states.

In Fig. 4.7 we show, for comparison, the temporal course of the mean phase coherence R estimated from EEG time series that were recorded intrahippocampally from an patient suffering from mesial temporal lobe epilepsy during the phase preceding an epileptic seizure. EEG signals were sampled at 260 Hz using a 12 bit analog-to-digital converter and filtered within a frequency band of 0.5 - 85 Hz. R values were calculated (see Sect. 4.1.2) using a moving-window technique with non-overlapping segments of 15.8 s corresponding to 4096 data points. In contrast to our model simu-

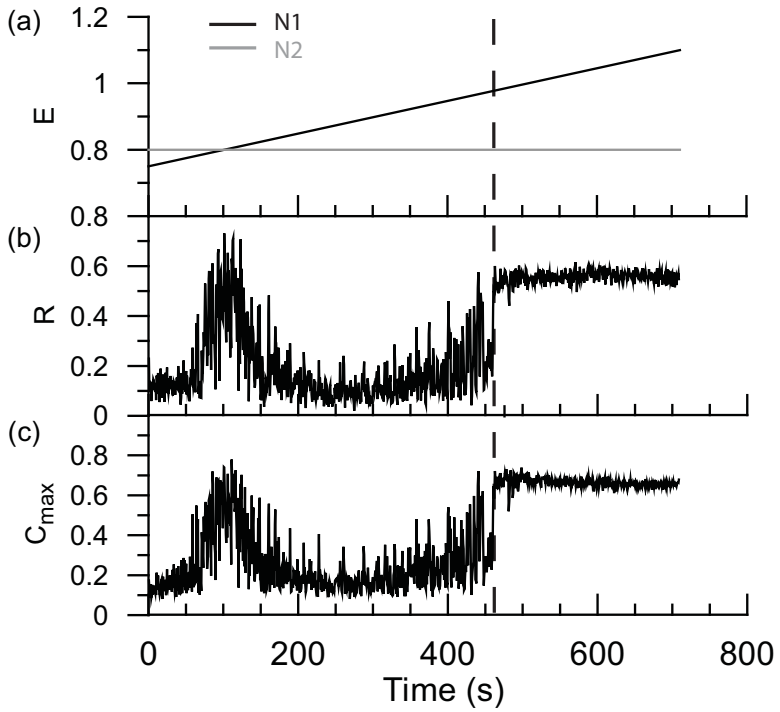

Figure 4.6: Measures of synchronization. The vertical dashed line represents the bursting threshold. (a) Excitability parameters as a function of time. N1 - black, N2 - gray. (b) Phase coherence, R, as a function of time. (c) Maximum cross correlation coefficient, C_{max}, as a function of time. High levels of synchronization occur during the region of parameter matching and during bursting behavior, while other regions exhibit low levels of synchronization.

lations, in the experimental setting we do not have access to the actual excitabilities of the network dynamics assessed by the respective EEG recordings. Nevertheless, we might speculate that the time course of R – in general – reflects fluctuations of the excitabilities of the network. Interestingly, during the time frame -100 to 0 min the course of R and the fact that a seizure occurs is consistent with what we observed in our model when monotonically increasing the excitability of the "focal" network.

Thus here we define the preictal length to be the time it takes for the networks to transition from the resonance state into the bursting state and study the distribution of these lengths over multiple realizations of a given network (i.e., different instances of a network with the same global statistical properties). This can be seen in Fig. 4.8 for four runs on 12 different network realizations. The start of the preictal period

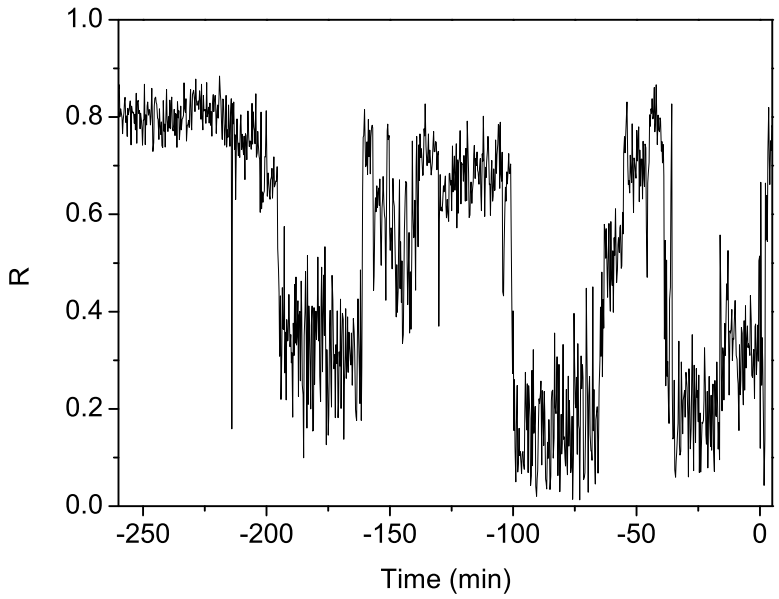

Figure 4.7: Comparison to experimental data. Profile of the mean phase coherence R for a pair of intrahippocampal EEG recordings from a patient suffering from mesial temporal lobe epilepsy. Seizure onset is at $t = 0$.

was marked by the point at which the mean phase coherence dropped below one standard deviation of its average value during the resonance state, and the end of preictal period was defined to be a point at which the networks first entered the bursting state. We see that although each realization displays the transition from resonance to bursting, the time course varies for different realizations. This variance in preictal lengths between patients has also been observed experimentally [86].

4.3 Discussion and summary

We have used a simple toy model of coupled networks to investigate the dynamical underpinnings of the drop in phase synchronization that is observed in epilepsy patients before a seizure. The observed regimes of high synchronization are the result of two types of interacting dynamics: a resonance interaction between the two networks when their properties are similar, and directional driving when the network associated with the focus drives the bursting in the other network.

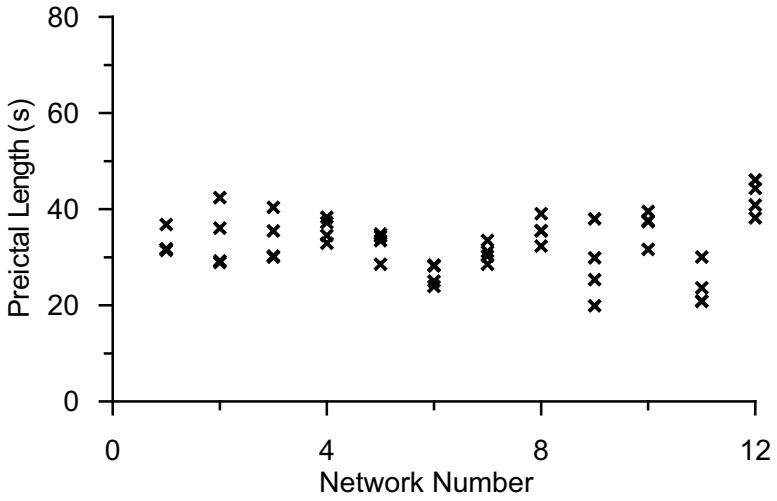

Figure 4.8: Calculated preictal lengths for 12 different realizations of a network. Four simulations were run for each network realization and the preictal length was calculated as described in the text.

We equate this resonance interaction between our networks to the normal dynamics of the brain during the interictal period and the directional driving to the propagation of the seizure during the ictal period. In between these two dynamical regions, we have an intermediate state which we equate to the preictal period where the dynamical properties of the interacting networks are mismatched, and the resonance interaction is abolished, while the directionally driven bursting is not yet present. While during both the resonance state and the driving state we see high levels of synchronization between the networks due to their similar dynamical properties, it is the mismatch of properties during the intermediate preictal state that leads to the observed decrease in the phase synchrony between the two networks.

We therefore compare the transition out of the resonance state and into the bursting state to the transition from normal neuronal dynamics to the pathological dynamics of a seizure. This implies that the observed drop in phase synchrony between certain EEG channels that defines the preictal period could be a result of the initial biological changes in the neurons associated with the focus and generation of the

seizure that occur long before the system actually reaches the seizing state.

For this transition scenario to happen one has to assume that in the interictal period the focal and normal networks in the brain have similar gross dynamic properties so that they enter the oscillatory resonant state. There is experimental evidence from phase synchronization measures that interictal synchronization is high between electrodes placed within the same structure of the brain [89]. Such interactions are also observed between the focus and other brain regions during the interictal period [67]. Furthermore, it has become an accepted view in neuroscience that "the perpetual interactions among the multiple network oscillators keep cortical systems in a highly sensitive 'metastable' state and provide energy-efficient synchronizing mechanisms via weak links" [22].

Although we have used a very simple model to explore a possible explanation for the underlying dynamics governing different areas of the brain before a seizure, our model shows the same behavior as observed in EEG recordings and has allowed us to make valuable insights at the neuronal level which can not be done through the analysis of EEG recordings. We conclude that it is possible that the observed preictal period is a manifestation of initial biological neuronal changes that begin before the start of seizing behavior and encourage further experimental work to explore this hypothesis.

CHAPTER V

Experimental approaches: glial and neuronal network interactions

In the previous chapters, I have analyzed experimental data recorded from tetrodes of freely moving mice (see Chapter III) and compared modeling results with EEG data recorded from epilepsy patients (see Chapter IV). In both of these cases, only the dynamics could be obtained experimentally; no structural data or properties of the neurons could be obtained due to the nature of the experiments. Thus, in order to explain the experimental results, I used modeling techniques to link structural or neuronal network changes with the observed changes in dynamics. However, it is imperative to also develop an experimental model in which structural network properties can be directly compared with neuronal dynamics. In this chapter, I will discuss experimental work from dissociated rat hippocampal cultures. Dissociated cultures are a good reduced system in which to study neuronal dynamics because they maintain many properties of neuronal interactions, but also have the advantage of the relative ease of structural and pharmacological manipulation. The gross structural properties of the culture can be observed using labeling techniques and dynamics of single neurons can be electrically recorded. They are therefore a useful tool to simultaneously study how anatomical connectivity, functional structure, and brain dynamics relate.

In this type of culture preparation, a single cell suspension of hippocampal cells is plated onto a culture dish. The neurons will attach to the surface of the dish and start to grow processes, forming synapses with other neurons and creating a two-dimensional network of neurons. After 3-7 days, these neurons will begin to spontaneously fire action potentials, and as the cultures age, the neural activity evolves into highly synchronous activity in the form of network bursts, during which almost all neurons will fire action potentials [25, 144]. The dynamics of these network bursts have been studied to examine burst patterning [113, 11, 53, 112, 104], learning [62, 75, 121, 10], and with pharmacological manipulation as a model of epilepsy [128, 132, 45].

The single cell suspension of hippocampal cells used to make these cultures is composed of both neural and glial cells. Neurons are the cells of the brain responsible for the firing of action potentials and processing of information, while the glial cells are generally considered to be the support cells for the neurons ('glia' is Greek for glue). In fact, there are 10-50 more glial cells than neurons in the brain [64]. The most common form of glial cells are called astrocytes. These cells can be identified by their star shaped cell body (as opposed to the round cell body of a neuron) and are thought to be important for the blood brain barrier and providing nutrition to neurons. It is also known that neurons need the presence of these glial cells to survive [64], and glial cells have been shown to aide neuronal development *in vitro* [109].

Because of the important supporting role played by the glial cells, neuronal cultures must be co-cultured with these cells. While neurons do not multiply, the glial cells do, and thus the glial cells initially plated with the neurons will quickly multiply, creating a confluent layer of support cells for the neurons. However, it is possible to inhibit the division of these cells through the addition of chemical blockers [145] or

type of media (nutritious solution in which the cultures are grown) used [20]. Different groups have studied the dynamics of the neurons in cultures grown under both types of conditions, although many studies allow the glial cells to multiply in order to provide a continuous layer of support for the neurons, [144, 53].

While the dynamics of the network bursts produced by the neurons in these cultures are often investigated, the impact of the glial network on the neuronal dynamics is less studied. The presence of glial cells is known to impact the development of neurons [109], which will certainly affect their dynamics, but astrocytes have also been shown to exhibit calcium oscillations which can affect intracellular calcium dynamics in neurons [92, 105, 138, 139]. As it was discussed earlier, calcium plays a role in the production of neuronal action potential, so these calcium oscillations likely contribute to the activity of the neurons. We are therefore interested in studying differences in the dynamics of the neuronal network in the presence of either a low or high density of glial cells.

In this chapter, I will present work relating differences in gross structural network properties to observed differences in neuronal dynamics for cultures grown with either a high or low density of glial cells. I show that the average neuronal process length is similar between the two conditions as the cultures age, indicating that the differences in the dynamics are likely due to the changes in the glial network as the glial cells multiply. I will then apply the Functional Clustering Algorithm presented in Chapter II to analyze the resulting functional structure obtained under the two conditions as the cultures age and relate this to observed structural changes. Finally, I show that the FCA can be used to study the temporal time scales involved in the bursting dynamics of the culture.

5.1 Experimental Setup

The cultures studied in this experiment were obtained from dissociated hippocampal cells of Wistar rats. For a complete description of the experimental protocol, please see Appendix A. Cells were plated at a density of 1400 cells/mm^2 on either culture dishes for structural staining, or on multi-electrode arrays (MEAs) which allow for the recording of neural dynamics. MEAs are glass dishes with embedded electrodes that record the local field potentials derived from the activity of neurons near the electrode. The recording region consists of 60 electrodes arranged in a square grid (8 x 8 grid with the corners removed). Electrodes are spaced 200 μm apart and have a 30 μm diameter, allowing for the detection of action potentials from $\sim$1-3 neurons per electrode. Upon plating, the neurons in the cultures begin to grow processes, forming a network, and between 3-7 days *in vitro* (DIV), the cells will begin to spontaneously fire action potentials. We recorded the dynamics from a total of 9 cultures at 8, 11, and 13 DIV. Recordings consisted of 5 minutes of spontaneous activity, which occurred in the form of network bursts. A typical recording of a network burst from 8 DIV can be seen in Fig. 5.1. In this figure, each window represents a 500 ms local field potential recording. The spatial organization of the pictures matches the placement of the electrodes on the array.

In order to analyze this data, spike detection was done on the recorded potentials using a threshold detection method. The threshold for spike detection was set to be 5 standard deviations above or below the baseline noise of the signal. Since we were interested in analyzing cumulative spiking patterns, no attempt was made to discriminate between multiple neurons recorded from the same electrode. Cultures used in structural staining were fixed at days 8, 11, and 13 to correspond to the

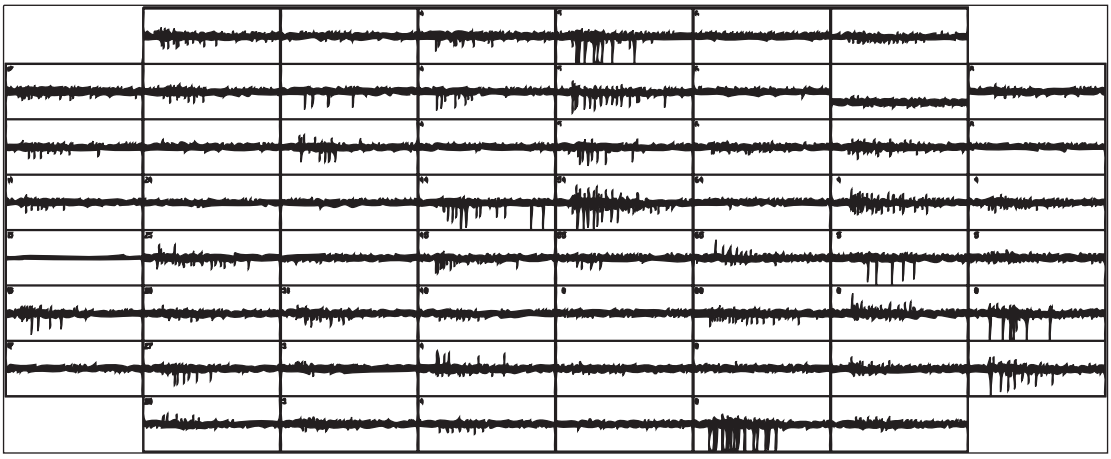

Figure 5.1: Example of a typical network burst. Recording taken from an MEA in the high glial group at 8 DIV. The signals are local filed potentials as recorded over 500 ms for the electrodes embedded in the MEA. The spatial organization of the windows represents the spatial layout of the electrodes on the array.

periods of recording.

The cultures were divided into two groups: a high density glial group (referred to as the high glial group, 5 MEAs) and a low density glial group (low glial group, 4 MEAs). Cultures in the high glial group were grown in Neurobasal media supplemented with horse serum which allows for the division and multiplication of glial cells [20], while cultures in the low glial group were grown in a sera-free media. Sera-free media has been shown to stop the multiplication of glial cells in the culture [20], meaning that the glial network remains constant over time. Neurons do not multiply over time, so their numbers are constant between the two groups.

5.2 Results

5.2.1 Anatomical Structure

We first examined the anatomic structural properties of the cultures. Although it is not feasible to determine the exact structure of the cultures (despite the reduction of the system, the resulting network is still quite complex), we are capable of studying gross properties of the network structure which could lead to differences in dynamics.

As discussed previously, it is known that the glial cells in the high glial group will multiply over time, while those in the low glial group will not. Although the neurons do not multiply over time, they do grow processes and synapses, changing the network structure as the cultures age. We therefore measured the average process length as a function of DIV for both groups using a fluorescent dye called di-I. The dye diffuses through the membrane of the cell, allowing for the staining of the cell body and processes of single neurons. The di-I was dissolved in oil and a micro-droplet of the dye was injected into a small cluster of neurons. After 5 days of diffusion, the cells were imaged and the process length of a neuron was measured to be the radius of a circle that was centered on the cell body and enclosed the processes.

Example images of staining for the two groups as a function of time can be seen in Fig. 5.2(a). The processes can be seen to grow over time, allowing the neurons to form increasingly global connections with other neurons. In Fig. 5.2(b), we quantify this affect, averaging over 4 stainings for cultures from 8, 11, and 13 DIV in each group. Both groups show an increase in process length over time. This increase in length of processes between days of recording should lead to a re-organization of network structure which will influence the dynamics over time.

It is also important to note that no difference was observed between the average process length of neurons between the two culture groups. This finding is indicative that the neuronal networks in the different culture groups are similar, meaning that differences in observed dynamics between groups is likely due to the known differences in the glial networks.

5.2.2 Dynamics

We studied the dynamics of the cultures as a function of age to determine the effects of the changing glial network and growth of neuronal processes. Cultures were

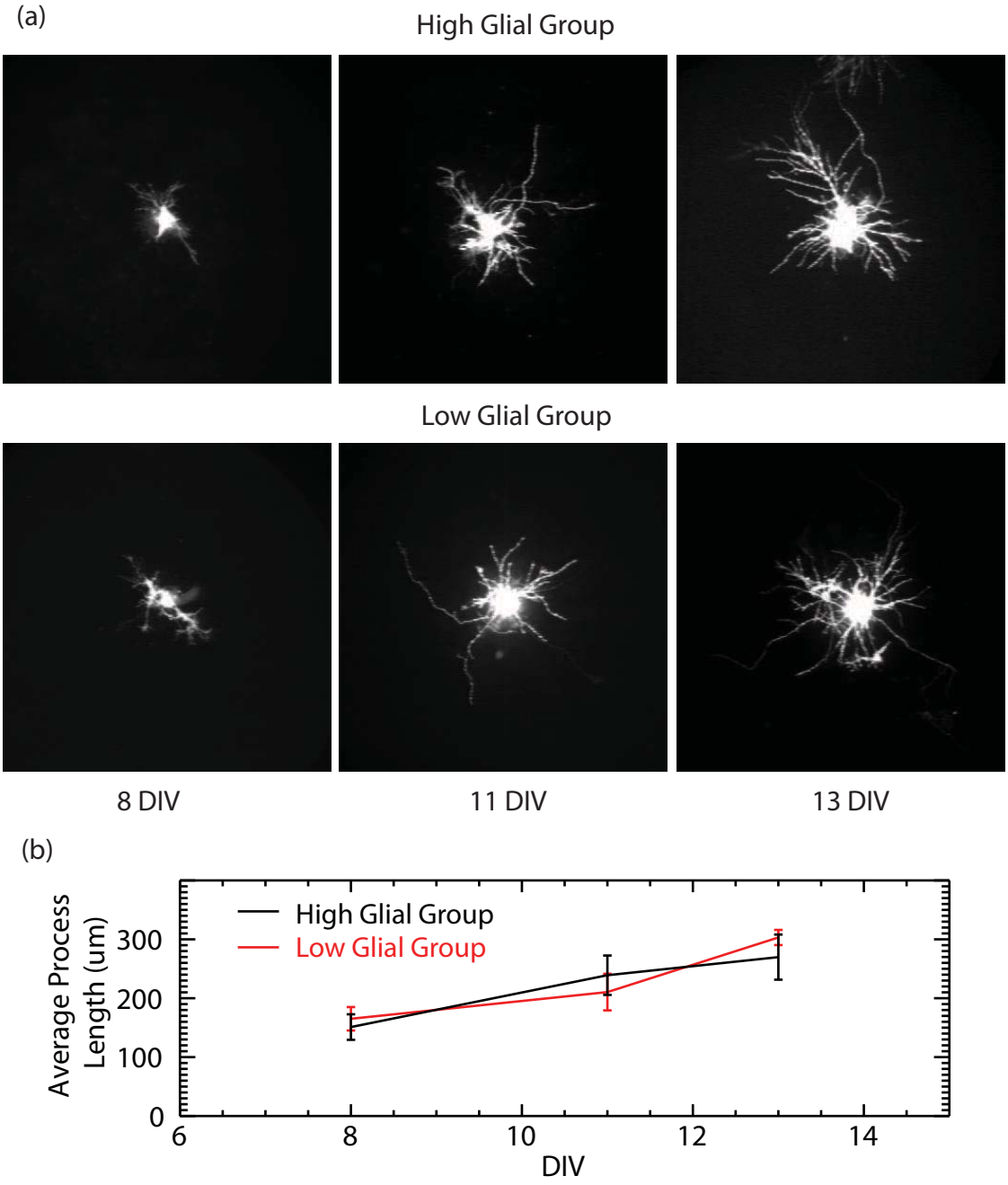

Figure 5.2: Di-I staining as a function of DIV for the two culture groups. (a) Example images of staining after 5 days of diffusion for cultures fixed on 8, 11, and 13 DIV for both high and low glial groups. (b) Quantification of the average process length as a function of DIV, averaged over 4 stainings for each group. The average process length increases over time, but shows no difference between neurons in the different groups.

recorded from at 8, 11, and 13 DIV as described in Sect. 5.1. Spike detection was done on the recorded signals and the resulting spike activity was analyzed as follows.

Visual observation of the recording sessions shows that cultures in the high glial group tend to persistently fire in network bursts with short silences in between bursts, while those in the low glial group tend to fire in longer bursts with longer quiescent periods between bursting events. These quiescent periods grow in length over time. We show these differences in dynamics by examining the interspike interval (ISI) as calculated for the net spiking activity in each culture. This result is shown in Fig. 5.3. In this plot, we examine the interspike interval of cultures as a function of DIV. The width of the ISI distribution for each culture group was increased for visualization purposes. Cultures from the high glial group are plotted in shades of red, and cultures from the low glial group are plotted in shades of blue. The shade of the dot indicates data from a specific culture within the respective group. Note the semi-log scale for visualization purposes of longer ISI events. Initially, the distributions are uniform, showing a mix of short and long ISI values. However, over time, one can see that in the low glial group (blue shades), the distribution becomes increasingly bi-modal. This indicates that firing events are consistently occurring within the bursts on short time scales, while the time between bursting events is becoming more polarized, with either short or long intervals between bursts and few quiescent periods of medium length. The cultures in the high glial group maintain a more evenly distributed arrangement of ISI times, although some polarization begins to appear at 13 DIV.

We then looked at the number of active electrode channels as a function of DIV. An active electrode was defined as a channel from which reliable spiking activity could be detected using the thresholding method. It should be noted that in order

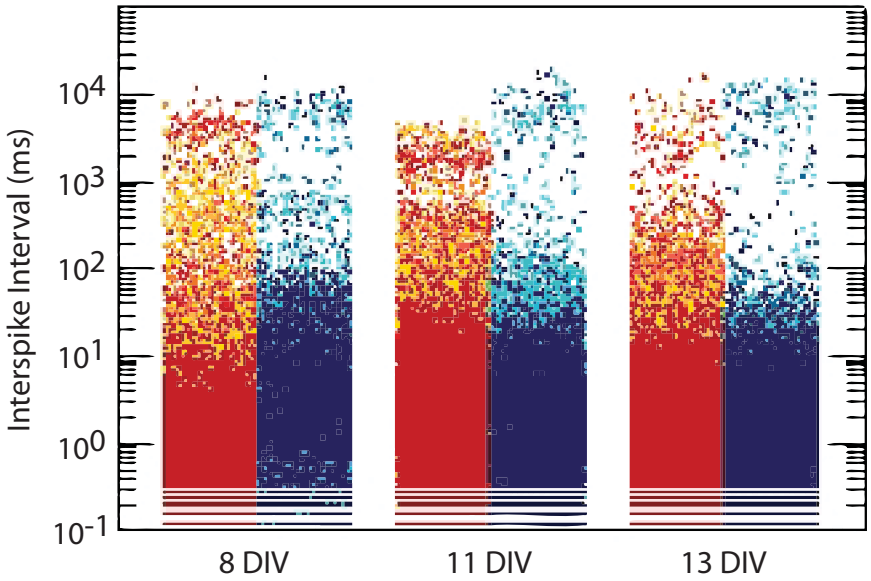

Figure 5.3: ISIs plotted as a function of DIV for high and low glial groups. The width of the distributions was increased for visualization purposes. Shades of red indicate data from the high glial group while blues denote the low glial group. The specific shade denotes data from a given culture in the group. One can see that the cultures in the low glial group show an increasingly polarized distribution of ISI indicating the development of long quiescent periods in between bursting events.

to record the activity from a neuron, the neuron must lie very near to the electrode and be well attached to the surface of the dish. As the network ages, some neurons die and others begin to fire, meaning that the active electrodes can change over time. However, one expects the overall number of active electrodes to increase over time as the neuronal processes increase in length, allowing for more neurons to be recruited into spontaneous activity. The number of active electrodes is plotted for both the high and low glial groups in Fig. 5.4(a). In both groups this number increases over time, yet is consistently higher for the high glial group. This indicates that the higher number of glial cells allows for the recruitment of more spatially separated sites into the bursting activity.

In Fig. 5.4(b), we plot the average number of spikes per active electrode as a function of time. Interestingly, we see no differences between the number of spikes emitted per channel between the two groups, indicating that unlike the number of

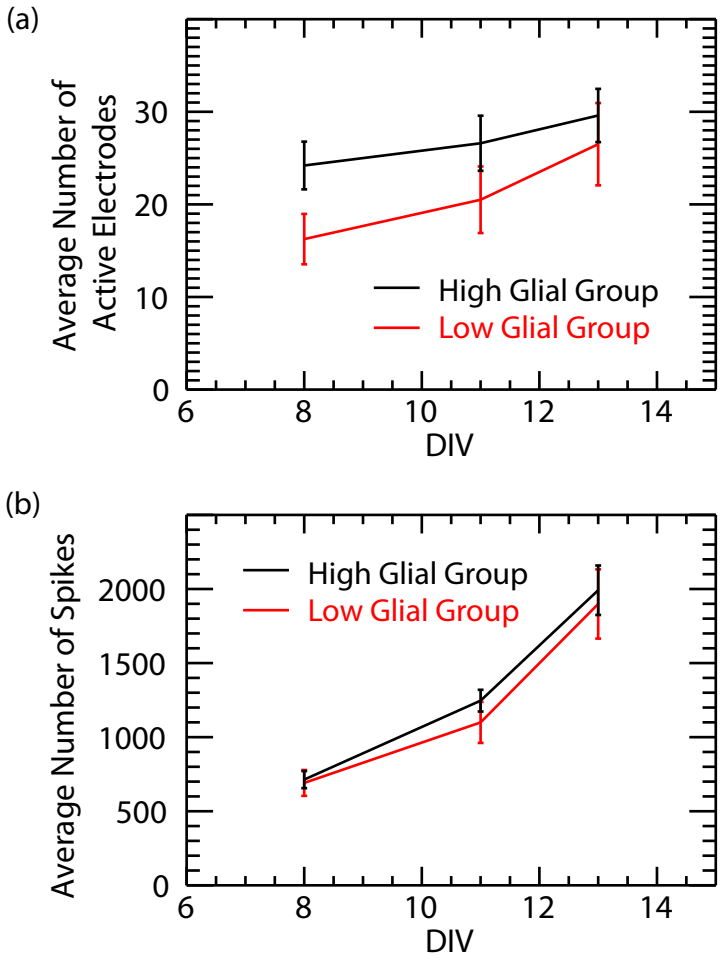

Figure 5.4: Number of active electrodes and spikes per active electrode as a function of DIV. (a) Number of active electrodes as a function of time for both high and low glial groups. While this number grows over time for both groups, it remains smaller for cultures in the low glial group indicating that the glial network seems to influence the recruitment of sites in the neuronal network. (b) Average number of spikes per active electrode as a function of DIV. This number grows as the culture becomes more active over time but is similar between the two groups of cultures, corresponding to changes in the neuronal network.

active sites, this value does not directly depend on glial interactions. Instead, it corresponds to the changes in neuronal network re-organization through the growth of neuronal processes.

5.2.3 Functional Structure

Since we observe difference in dynamics as a function of DIV as well as between culture groups, it is interesting to ask how these differences will be embodied in the functional structure of the network. To study the functional groupings of active sites, we implemented the FCA as described in Chapter II. We are therefore grouping electrodes based on synchronous activity within the network bursts. Unless otherwise stated, the jitter window used to create the surrogate data sets was a uniform window of 70 ms. The obtained clustering is shown for one culture from the high glial group and one culture from the low glial group.

We first explore the clustering as a function of time for cultures within each group. In Fig. 5.5(a) we show the spatial layout of the functional groupings. In this figure, each square represents the spatial location of an electrode as in the case of Fig. 5.1. Colored squares represent active electrodes, and squares of the same color belong to the same functional group. The dendrograms corresponding to the spatial clustering shown for the high glial group at 8 and 13 DIV are shown in Fig. 5.5(b-c) respectively. For the case of the high glial culture, we see that, initially, the culture contains multiple groups that largely represent local regions of the MEA. This indicates that only local groups of neurons are involved in synchronous activity during network bursts. However, as the culture ages, the synchronization becomes increasingly global, and more neurons are recruited into the largest cluster.

To quantify this effect, the percentage of electrodes that participate in the largest cluster is plotted as a function of DIV in Fig. 5.6. We do not see this increase in

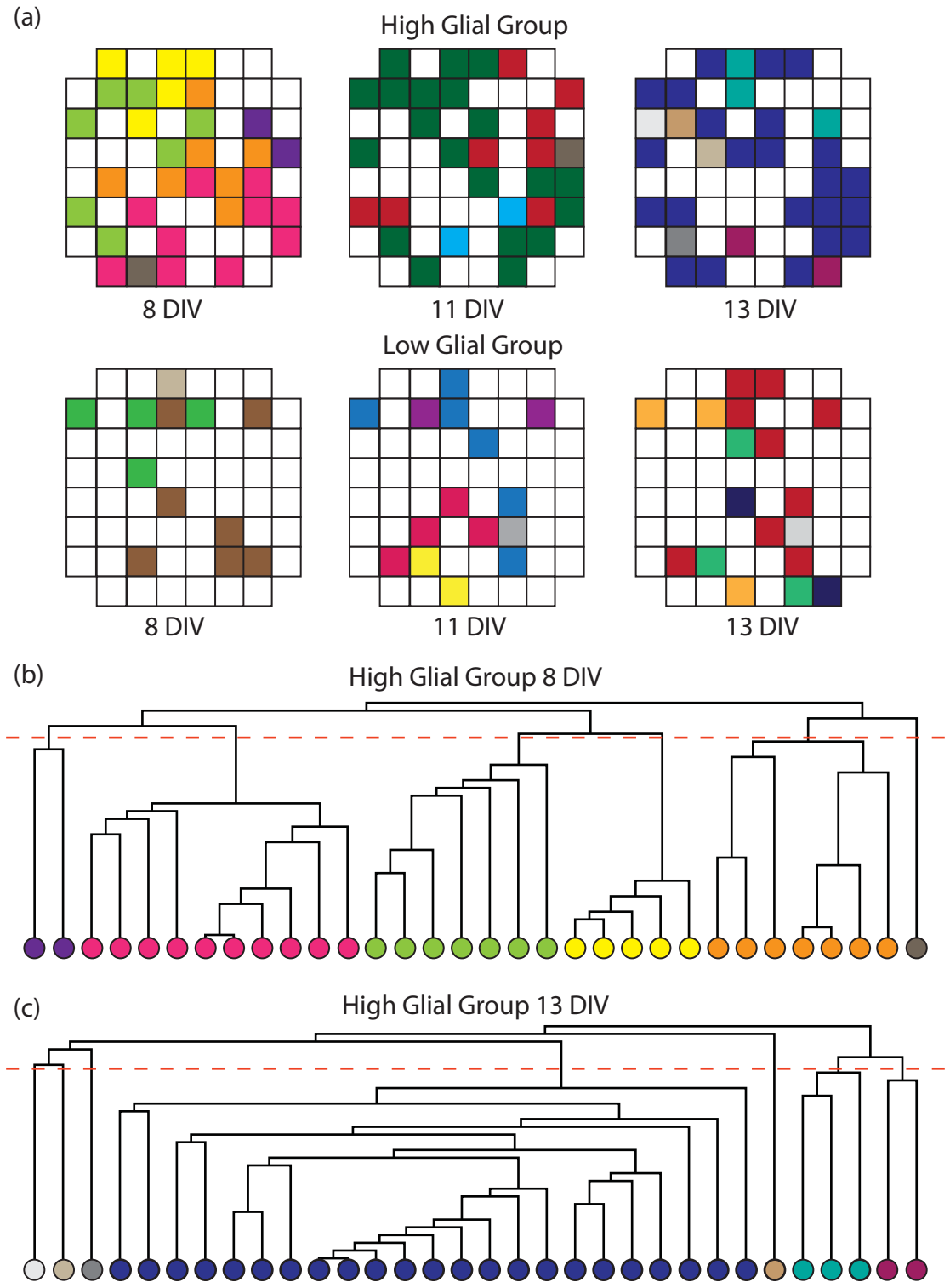

Figure 5.5: Functional groupings obtained from the application of the FCA to culture data. (a) Spatial representation of functional clusters. Colored squares indicate active electrodes and squares of the same color belong to the same functional group. The clustering becomes increasingly global over time for the high glial culture, while the clustering of the low glial culture becomes increasingly fragmented. Examples of the dendrogram corresponding to the spatial map are shown in (b-c) for the culture from the high glial group at 8 DIV (b) and 13 DIV (c).

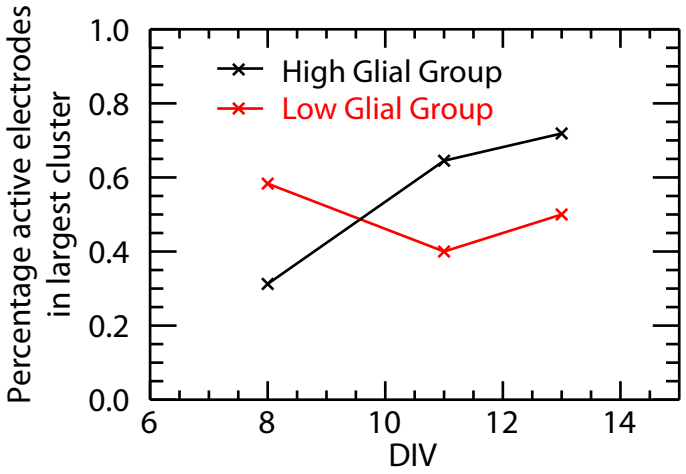

Figure 5.6: Percentage of electrodes participating in the largest functional cluster. The percentage increases over time for the high glial culture indicating the spread of global synchronization while this number decreases for the low glial culture as the groupings become increasingly fragmented.

cluster size in the case of the culture from the low glial group, as the clustering instead becomes fragmented over time as seen in Fig. 5.5. This increased fragmentation corresponds to the decrease in the percentage of electrodes that participate in the largest cluster seen in Fig. 5.6.

We are also interested in quantifying the level of synchronization present in the detected functional groupings. This is done through the examination of the scaled significance used in the joining steps of the FCA (please refer to Sect. 2.1.2). A higher scaled significance indicates a tighter relationship between spikes of electrodes. In Fig. 5.7(a-b), we show the scaled significance as a function of the step of the algorithm for clustering of the high and low glial cultures respectively. The dashed red line marks the clustering cutoff. These results are shown for the obtained clustering for each recording day (8, 11, 13 DIV). Note the different scaling on the y-axes of the figures. In each condition (high and low glial), the scaled significance used to group electrodes increases between recordings indicating that the firings of the neurons within the functional groups are becoming increasingly synchronous as the cultures

age. In Fig. 5.7(c) we show the average scaled significance used in the significant clustering steps (above the dashed red line) as a function of DIV for both the high and low glial cultures. The average scaled significance is greater for the high glial culture on each recording day, indicating that the high glial culture shows a tighter relationship between firing events during the bursts.

The analysis presented thus far has been done using a jitter window of 70 ms to create the surrogate data used to determine the significance of the clusterings in the FCA. This window size corresponds to timescales associated with the duration of network bursts. However, by varying the size of the jitter window, we can control the time scales involved in the detection of functional groupings due to the fact that the size of the jitter window determines the time scales of the correlations that are destroyed in the surrogate data [113, 107]. Thus, as we decrease the jitter size, we are able to examine the finer intraburst structure. In Fig. 5.8(a) we show the evolution of functional groupings for different sizes of jitter windows for the high glial culture recorded at 8 DIV. Functional groupings were analyzed for jitter windows of 20, 30, 40, 50, 60, and 70 ms. Again, the obtained clusterings are indicated by similar colors on the spatial representation of electrodes. For a small jitter window of 20 ms, we see many small functional groupings, indicated by the many colors on the map. As the jitter window is increased to 30 ms, we see that the previously obtained clusters begin to merge. For example, the electrodes that were previously light blue, indicating their own functional cluster, have now become part of the cluster labeled in orange. Additionally, two previously independent clusters have now joined to form a new cluster colored in neon blue, and the light green cluster now includes two previously independent electrodes. The dark blue cluster merges with the pink cluster at a jitter window of 40 ms and then this configuration is relatively stable.

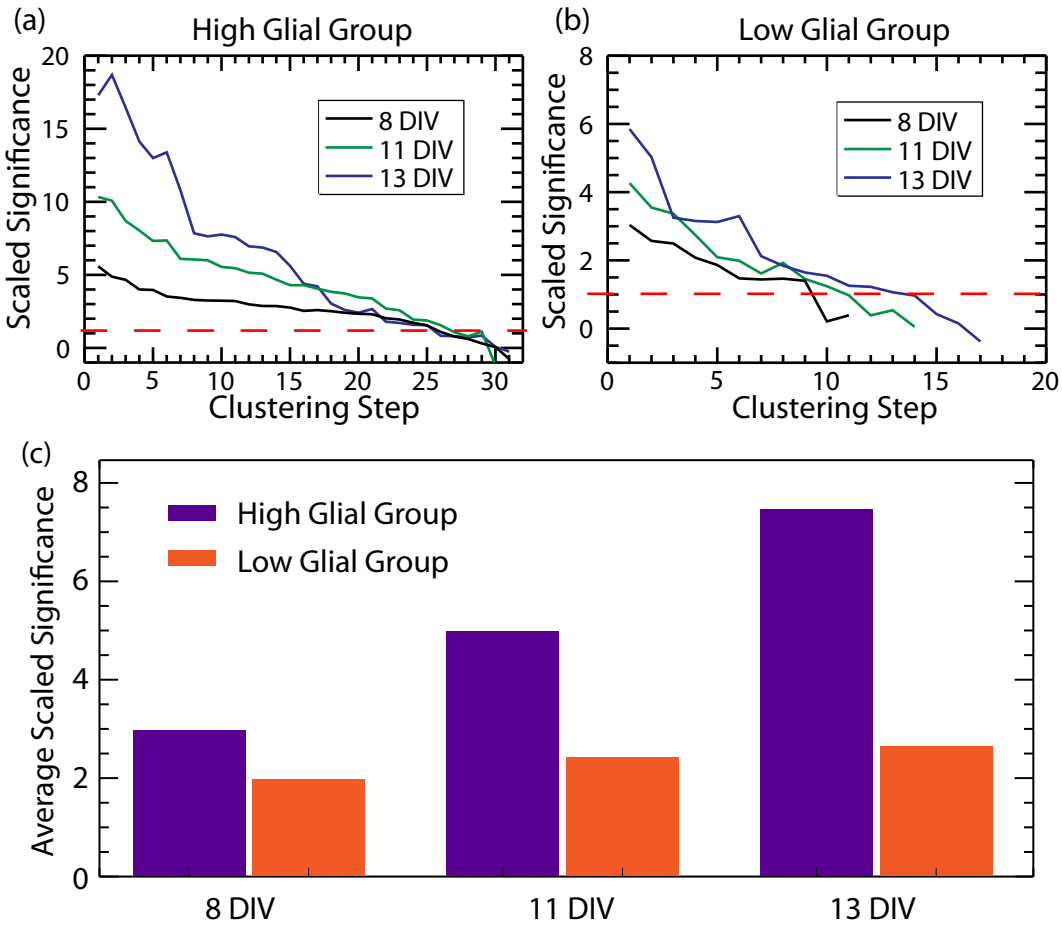

Figure 5.7: The scaled significance used to create functional groupings for the high and low glial cultures. (a) Scaled significance as a function of joining step for the different recording days of the high glial culture. (b) Scaled significance as a function of joining step for the different recording days of the low glial culture. Note the different scaling on the y-axis. The dashed red line denotes the clustering cutoff. (c) The average scaled significance used in the significant clustering steps of the data shown in (a) and (b). The significance increases as a function of time, indicating an increase in the synchronization of spiking within network bursts. The high glial culture also shows increased significance (synchronization) compared to the low glial culture.

We quantify this observation by plotting the number of independent clusters as a function of the jitter window size in Fig. 5.8(b). This indicates that while the bursts themselves are synchronized, there exists an additional hierarchy of temporal levels of synchronization within the bursting events. Previous work analyzing network bursts has also seen the emergence of different functional interactions between small and large time scales within the network bursts [135, 113].

5.3 Discussion and Summary

While previous work has studied either structural properties of cultured networks or analyzed the dynamics of these cultures, there is little work which attempts to link changes in structural network properties to the resulting dynamics and functional interactions. The work that has been done has focused on the effects of different substrates used to coat the dishes [131] or on patterned plating of cultures [24, 11]. Here we studied cultures grown with either a high density of glial cells or a low density of glial cells in order to relate the influence of the glial network on neuronal dynamics as a function of time (and therefore increasing density of glial cells). We showed that the average process length of the neurons appears constant between the two groups but grows over time, which can explain changes in neuronal dynamics over time, but not differences between the two culture groups. Thus, the observed differences in neuronal dynamics between the high and low glial groups is likely due to the influence of the glial network on the neuronal network.

Both culture groups displayed synchronized activity in the form of network bursts, but the specific form of these bursts varied between the two groups. The high glial cultures had more active electrodes, however, the total number of spikes per electrode was similar between the two groups for each recording session. The cultures became

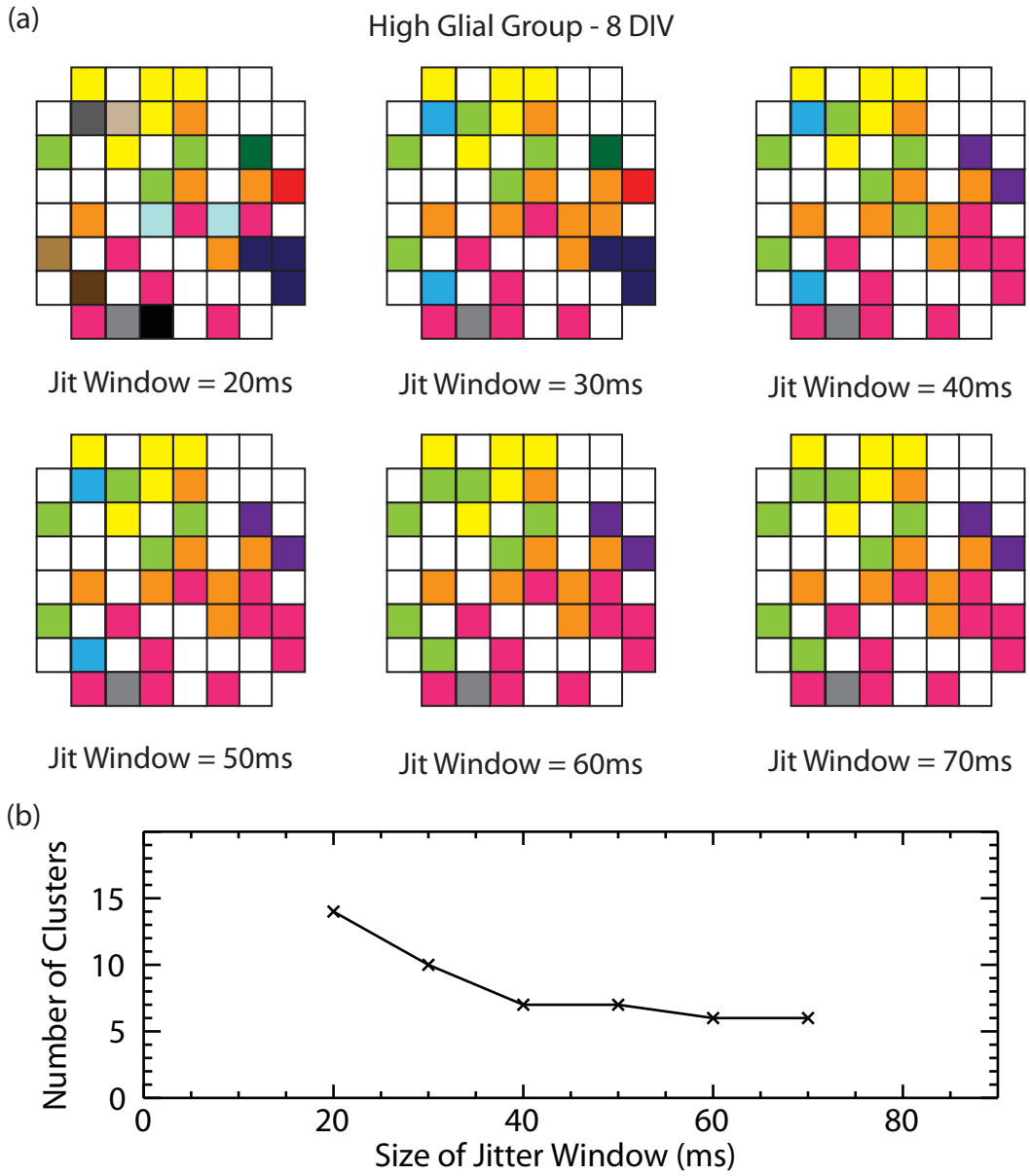

Figure 5.8: Functional groupings for different time scales of correlation within network bursts. (a) Spatial representations of obtained clusterings for different sizes of the jitter window used to create surrogate data sets. Squares of similar color indicate electrodes involved in the same functional group. As the jitter window increases, correlations are destroyed on larger time scales and we see the merging of functional clusters. These clusters become stable for larger jitter windows. This corresponds to the decrease in the total number of clusters detected as shown in (b).

increasingly active over time as seen in the rise of active electrodes and total spikes per electrode. However, the cultures from the high glial group displayed persistent bursting activity with a varied distribution of interspike intervals. Cultures from the low glial group displayed spiking patterns that became increasingly polarized towards either short or long intervals between spiking events, corresponding to an increase in the spiking frequency during a burst with larger intervals between bursting events.

The changes in neuronal dynamics over time led to a difference in functional classifications. We applied the FCA to detect neuronal groupings over time for a high glial and low glial culture. The high glial culture initially showed the formation of local clustering which became more global over time. The low glial culture showed a different behavior as the groupings became increasingly fragmented over time. These functional differences indicate that the cultures from the high glial group display bursting events which become increasingly globally synchronous while bursting events are consistently composed of smaller groups of synchronous activity in the low glial culture. We also quantified the amount of synchronization present within the functional clusters by comparing the scaled significance used in the joining steps of the FCA. Cultures from the high glial group showed greater values of significance indicating that the firing events within the bursts are more highly synchronized. The fact that these cultures have a higher glial density indicates that the glial network aids in the synchronization of the neuronal network. The significance used in clustering increased as a function of DIV in both groups indicating that as the neuronal networks evolve, the firing events become increasingly correlated. Thus the overall observed synchronization of bursts is the result of changes in both the neuronal network and the underlying glial network. We were also able to show that synchronization of these bursts is composed of hierarchy of synchronous activity operating

on multiple time scales as can be seen when varying the size of the jitter window used to determine the significance of the functional groupings obtained using the FCA.

Despite the fact that dissociated neuronal cultures are a simplified system and their structure and dynamics cannot be directly linked to brain dynamics, we have shown that they are a good reduced system in which to study the interplay of structure and dynamics in neuronal networks. Unlike neuronal data recorded from the intact brain of humans or animals where it is difficult to study the properties of the underlying network structure, we are able to manipulate gross properties of the anatomical network structure and observe how these changes affect neuronal dynamics. We can then apply methods developed to detect functional structure (such as the FCA) and relate the differences in the obtained clusterings to the known structural changes. This allows for the discovery of the important parameters that affect the relationships between structure and dynamics which can later be used to make inferences about network properties that can direct research in more complicated systems such as the brain.

CHAPTER VI

Summary and conclusions

The brain has an incredibly complex anatomical structure (even the small hippocampus of a rat contains $\sim 10^6$ interconnected neurons), making it incredibly difficult to study at the single neuron level. The synapses between neurons are plastic, neurons die, and new neurons are integrated into the existing network, adding to the difficulties in determining anatomical structure. Much work has thus focused on identifying gross structural properties between brain regions, but often one instead observes network dynamics since recent advances in recording techniques has made the identification of individual neuronal firing patterns possible. The recording of action potentials from single neurons involves only information from a sparse sample of neurons, but has the advantage that it is now possible to record from these neurons while an animal moves and performs certain tasks. This means that it is now possible to obtain dynamical information relating to specific features of brain function. It also introduces the need to develop new tools to extract functional relationships from observed neuronal dynamics.

In this dissertation, I've discussed the interplay between three features of neuronal networks: anatomical structure, neuronal dynamics, and functional structure. The anatomical structure provides the physical building blocks of the network in terms

of the properties of the connectivity between neurons. Since the neurons communicate through the firing of action potentials, which are transmitted through these physical connections, the anatomical structure impacts how information is passed through the network and therefore the dynamics of the network. Additionally, the firing patterns of the neurons can have an affect on atomical network structure, since neuronal synapses are plastic and can be modified through mechanisms such as spike timing dependent plasticity. The functional structure is obtained from the dynamics through the detection of correlated activity in the firing patterns, and is therefore coupled directly to the dynamics and indirectly to the underlying anatomical structure. However, it is important to remember that dynamical properties of neurons such as their excitability also have an influence on neuronal dynamics, meaning that it is not always straightforward to link functional and anatomical structure.

In Chapter II, I introduced a new algorithm called the Functional Clustering Algorithm designed to detect functional groupings from discrete event data. The FCA can be used with a variety of different similarity metrics, allowing the user to tailor the algorithm to detect specific temporal relationships between network elements. It also uses a comparison to surrogate data to determine the significance of the obtained groupings, giving the algorithm a natural stopping point. This also means that, unlike with many traditional clustering algorithms, no *a priori* knowledge of the number of functional groupings is required. Using simulated spike train data with a known structure, I compared the FCA to the gravitational method of clustering which looks for groups of neurons with similar firing patterns and clusters these particles in N-dimensional space. I showed that the lack of a stopping point and difficulty in visualizing the N-dimensional space makes the gravitational method difficult to utilize, especially in cases of low correlations between firing patterns. I

also used a standard hierarchical clustering method combined with a calculation of the modularity to determine functional groupings of the simulated data. Despite the clear correlation structure in the data, the modularity gave an unclear stopping point for the algorithm, as it is not optimized for all-to-all network connectivities. The FCA was able to correctly identify the known embedded clusters in the simulated data without any of these difficulties. This algorithm thus provides a novel method for linking neuronal dynamics to functional network structure.

After the FCA was verified on simulated data, the next step was to use the FCA to analyze neuronal dynamics and extract functional structure in experimental data. In Chapter III, I utilized the FCA along with causal entropies (a measure to detect the development of directional lead/lag relationships) to analyze experimental data obtained from the hippocampus of freely moving mice as they explored and learned a new environment. I showed that the FCA can detect a known increase in co-firing events due to ripple events during sleep periods, and that these periods of sleep also correspond to an increase in directional relationships between neurons that persists after the sleep period has ended. The FCA also showed an increase in the amount of scaled significance used in the joining steps of the algorithm when comparing early and late exploration periods (after sleep). This is representative of the tightening temporal correlations as the animal learned the environment. I showed that the average minimum distance used to cluster the data between the initial exploration of the environment and a separate familiar exploration decreases for significant clustering steps between initial and familiar exploration. These significant clustering steps correspond to neurons that were initially significantly correlated during the initial exploration. However, examination of the unsignificant clustering steps (neurons with low initial correlations) showed an increase in the AMD, representing that their

firing patterns were becoming increasingly uncorrelated. This finding is consistent with other recent experimental results [100] that have shown an increasing polarity between correlations of firing patterns as a result of memory consolidation.

I also applied the above methods to a simple model of memory formation. Since we are unable to obtain information about the underlying anatomic changes in network structure as a result of learning, the use of modeling is necessary to understand the structural changes that lead to differences in observed neuronal dynamics. When modeling, we can simultaneously monitor both network structure and dynamics under different conditions and link the changes in dynamics to those in structure. This can then be compared to similar changes in dynamics observed experimentally. In this model, synapses were plastic and allowed to evolved based on a simple STDP motivated learning rule in response to a stimulus. I showed that the development of lead/lag relationships and increase in significance of clustering was similar to that observed experimentally. This leads one to believe that the experimentally observed changes in dynamics and resulting functional groupings are due to synaptic modifications through STDP as a result of learning.

Although these results suggest that neuronal dynamics and underlying anatomical structure are always linked, the work of Chapter IV shows that the relationship is not as simple. Here, I studied two coupled networks as a model of focal epilepsy. One network represented the focus of a seizure and the excitability of the neurons in this network was increased over time, bringing the network from an asynchronous state to a bursting state representing a seizure. No anatomical structural changes were involved in this change of network dynamics. When the focal network was coupled to the other network, three different states of dynamics were observed through examination of the phase synchronization between the activity of each network: a resonance

state, a transition state, and a driving state. The resonance state occurred when the excitability of the networks was the same, and the transition state occurred when there was a mismatch in excitability between the networks before the focal network entered the bursting state. The driving state began when the focal network began to burst, as the bursting in this network drove the other network to a bursting state as well. These results were robust over a large range of network coupling parameters, meaning that structural modifications had little impact on the network dynamics. This indicates that one must be cautious when attributing changes in neuronal dynamics to changes in the underlying structure as other factors can contribute to network dynamics as well.

The above studies emphasize the fact that when analyzing brain dynamics, it is difficult to obtain simultaneous information about both anatomical structure and dynamics. It therefore becomes essential to use modeling techniques in an attempt to understand structural and neuronal effects on dynamics. Dissociated cell cultures offer an alternative scenario. Although the anatomic structure of cultures does not resemble that of the brain, the properties of the neurons are preserved, and upon plating the cells, the neurons will grow into a network and begin to fire action potentials. In Chapter V, I presented work studying dissociated rat hippocampal cultures. Cultures were divided into two conditions: a high glial group in which glial cells were allowed to divide and multiply, and a low glial group in which the number of glial cells was held constant. The dynamics of the cultures were recorded using multi-electrode arrays, and di-I staining was used to determine the average process length of neurons on days 8, 11, and 13 after plating. Differences in dynamics between the two groups could be linked to differences in the glial network, and the evolution of the dynamics as the culture aged corresponded to a growth of neuron

processes. I also used the FCA to study the functional structure resulting from the different conditions. Cultures in the high glial group showed an increase in global synchronization as the cultures aged, while those in the low glial group remained locally synchronized. The total level of synchronization in the high glial group was also shown to be stronger by examining the scaled significance used by the FCA to join groups. Additionally, the FCA proved a useful tool to investigate the dynamics of network bursts in the culture because by varying the size of the jitter window used to determine the significance of clustering, the different temporal levels of functional groupings could be determined.

Taken together, these projects address the need to develop new methods and tools to analyze the vast amount of data becoming available as new experimental techniques are developed to explore features of neuronal networks. The recent availability of tetrodes to record neuronal activity of freely moving animals and advances in fMRI technology have emphasized the importance of functional structure. The FCA provides a powerful tool to explore functional groupings in neuronal data. While all of the work presented in this dissertation used the AMD as a similarity metric to detect co-firing events in spike train data, the algorithm is not limited to the detection of co-firing events. For example, the CE metric used in Chapter III to detect directional relationships between pairs of neurons could be applied in the algorithm to detect sequences of neuronal activity. Other metrics could also be used, depending on the nature of the data and desired functional relationships.

This dissertation has also presented a methodology that combines both modeling and experimental approaches to explain observed relationships in neuronal dynamics. This combination of techniques and ideas will be essential to guide the efforts of understanding brain function and neuronal interactions. It is clear that there is much to

be learned about the complex network that comprises a brain, and our knowledge of the workings of neuronal networks and brain function is quickly evolving. This work presents a framework in which to link the important features of neuronal networks into a coherent whole.

APPENDIX

APPENDIX A

Dissociated culture protocol

A.0.1 Cell Culture Preparation

Dissociated cell cultures were prepared from neurons (and glia) obtained from the hippocampus of P1 Wistar rats (Harlan). Within 24 hours of birth, pups were decapitated and the hippocampi were removed and placed in 8 mL of cold PBS (Phosphate Buffered Saline with 20mM glucose). To aid in dissociation, 2 mL of trypsin (Sigma, St. Louis MO) was added (resulting in a .25% concentration of trypsin) and the solution was placed in a 37°C heat bath for 16 minutes, followed by the addition 2 mL of horse serum to stop the chemical digestion. The supernatant was then removed and replaced with warm PBS. Cells were mechanically dissociated through titration first with a 10 mL plastic pipette and followed by a flamed pasteur pipette. Cells were centrifuged and re-suspended in Neurobasal-A Medium (Gibco) supplemented with B-27, 5% heat activated horse serum, 0.5mM L-Glutamine, and 10mM HEPES. The solution was filtered using a 70μm strainer followed by a 40μm strainer. The cell density was determined using trypan blue (Invitrogen, Carlsbad, CA) staining and a Reichert counting chamber (Fisher Scientific, Chicago, IL). The density was adjusted by the addition of media such that the density upon plating would be $\sim$1400 cells/mm^2.

The cell suspension was plated on MEAs (Multi Channel Systems, Reutlingen, Germany) which had previously been coated with 0.05% poly-ethylene-imine (Sigma) in borate buffer followed by 20 μg/mL laminin (Roche Applied Science, Indianapolis, IN) solution in media. Cultures were maintained in a humidified incubator with a 95%O_2/5%CO_2 saturated atmosphere at 37°C.

Between 24-36 hours after plating (once cells had adhered to the surface of the MEA), cultures were split into high and low glial groups. Neurobasal-A media supplemented with horse serum as described above was added to cultures in the high glial group to allow for the proliferation of glial cells, while the media of the low glial group was replaced with Neurobasal-A media that had not been supplemented with horse serum. Following this, half of the media was replaced with fresh media once each week.

A.0.2 MEA Recordings

Cultures were recorded at 8, 11, and 13 DIV. During recordings, media was replaced with a recording buffer (140mM NaCl, 5 mM KCl, 1.5 mM $CaCl_2$, 0.75 mM $MgCl_2$, 1.25 mM NaH_2PO_4, 20 mM glucose, 15 mM HEPES/NaOH adjusted to 7.4pH) to maintain the pH of the culture. Cultures were recorded at 25 kHz using a Multi Channel Systems data acquisition card and MC-Rack software. During the recordings, cultures were maintained at 37°C and each recording lasted 5 minutes.

A.0.3 Spike Detection

The local field potential potential recorded from each electrode was assessed for spiking activity and active channels were selected for spike detection. Signals were first filtered through a high pass Butterworth filter at 250 Hz. Spike detection was done using a thresholding method, using 5 standard deviations of the baseline noise

as the threshold value. No attempt was made to distinguish between single neurons recorded by the same electrode. Spike times were saved and analyzed as described in Chapter V.

A.0.4 Di-I Staining

Cultures used in staining studies were fixed in 4% paraformaldehyde in PBS for 15 minutes at either 8, 11, or 13 DIV to correspond to the days of recordings. Di-I (1,1'-dioctadecyl-3,3,3',3'-tetramethylindo-carbocyanine perchlorate, Sigma) crystals were then dissolved to in cod liver oil to form a saturated solution. Micro-droplets of the oil solution were injected into cell bodies of neurons, and the dye was allowed to diffuse through the cell membrane for 5 days, staining the cell bodies and processes of single neurons. Cultures were then imaged using a fluorescent microscope (Olympus X-71). Pictures were analyzed using ImageJ software and average process length was determined to be the radius of a circle that was centered on the cell body and enclosed the processes.

BIBLIOGRAPHY

BIBLIOGRAPHY

[1] L. F. Abbott and S. B. Nelson. Synaptic plasticity: taming the beast. *Nat Neurosci*, 3 Suppl:1178–83, 2000.

[2] D. N. Abrous, M. Koehl, and M. Le Moal. Adult neurogenesis: from precursors to network and physiology. *Physiol Rev*, 85(2):523–69, 2005.

[3] R. Albert and A. L. Barabasi. Statistical mechanics of complex networks. *Reviews of Modern Physics*, 74(1):47–97, 2002.

[4] P. Anderson, R. Morris, D. Amaral, and J. O'Keefe. *The Hippocampus Book*. Oxford University Press, USA, 2007.

[5] S. N. Baker and G. L. Gerstein. Improvements to the sensitivity of gravitational clustering for multiple neuron recordings. *Neural Comput*, 12(11):2597–620, 2000.

[6] G. Balazsi, A. Cornell-Bell, A. B. Neiman, and F. Moss. Synchronization of hyperexcitable systems with phase-repulsive coupling. *Phys Rev E*, 64(4 Pt 1):041912, 2001.

[7] G. Balazsi, A. H. Cornell-Bell, and F. Moss. Increased phase synchronization of spontaneous calcium oscillations in epileptic human versus normal rat astrocyte cultures. *Chaos*, 13(2):515–8, 2003.

[8] G. H. Ball and D. J. Hall. A clustering technique for summarizing multivariate data. *Behav Sci*, 12(2):153–5, 1967.

[9] M. Barahona and L. M. Pecora. Synchronization in small-world systems. *Phys Rev Lett*, 89(5):054101, 2002.

[10] I. Baruchi and E. Ben-Jacob. Towards neuro-memory-chip: imprinting multiple memories in cultured neural networks. *Phys Rev E*, 75(5 Pt 1):050901, 2007.

[11] I. Baruchi, V. Volman, N. Raichman, M. Shein, and E. Ben-Jacob. The emergence and properties of mutual synchronization in in vitro coupled cortical networks. *Eur J Neurosci*, 28(9):1825–35, 2008.

[12] C. C. Bell, V. Z. Han, Y. Sugawara, and K. Grant. Synaptic plasticity in a cerebellum-like structure depends on temporal order. *Nature*, 387(6630):278–81, 1997.

[13] D. Berger, D. Warren, R. Normann, A. Arieli, and S. Grun. Spatially organized spike correlation in cat visual cortex. *Neurocomputing*, 70(10-12):2112–2116, 2007.

[14] J. D. Berke, V. Hetrick, J. Breck, and R. W. Greene. Transient 23-30 hz oscillations in mouse hippocampus during exploration of novel environments. *Hippocampus*, 18(5):519–29, 2008.

[15] G. Q. Bi and M. M. Poo. Synaptic modifications in cultured hippocampal neurons: dependence on spike timing, synaptic strength, and postsynaptic cell type. *J Neurosci*, 18(24):10464–72, 1998.

[16] S. Boccaletti. *The Synchronized Dynamics of Complex Systems*, volume 6 of *Monograph Series on Nonlinear Science and Complexity*. Elsevier, Amsterdam, 2008.

[17] S. Boccaletti, V. Latora, Y. Moreno, M. Chavez, and D. U. Hwang. Complex networks: Structure and dynamics. *Physics Reports*, 424(4-5):175–308, 2006.

[18] V. Booth and G. R. Poe. Input source and strength influences overall firing phase of model hippocampal ca1 pyramidal cells during theta: relevance to rem sleep reactivation and memory consolidation. *Hippocampus*, 16(2):161–73, 2006.

[19] S.P. Borgatti. How to explain hierarchical clustering. *Connections*, 17:78, 1994.

[20] G. J. Brewer, J. R. Torricelli, E. K. Evege, and P. J. Price. Optimized survival of hippocampal neurons in b27-supplemented neurobasal, a new serum-free medium combination. *J Neurosci Res*, 35(5):567–76, 1993.

[21] G. Buzsaki. Memory consolidation during sleep: a neurophysiological perspective. *J Sleep Res*, 7 Suppl 1:17–23, 1998.

[22] G. Buzsaki. *Rhythms of the Brain*. Oxford University Press, New York, 2006.

[23] G. Buzsaki, D. L. Buhl, K. D. Harris, J. Csicsvari, B. Czeh, and A. Morozov. Hippocampal network patterns of activity in the mouse. *Neuroscience*, 116(1):201–11, 2003.

[24] J. C. Chang, G. J. Brewer, and B. C. Wheeler. Neuronal network structuring induces greater neuronal activity through enhanced astroglial development. *J Neural Eng*, 3(3):217–26, 2006.

[25] E. Cohen, M. Ivenshitz, V. Amor-Baroukh, V. Greenberger, and M. Segal. Determinants of spontaneous activity in networks of cultured hippocampus. *Brain Res*, 1235:21–30, 2008.

[26] L. Danon, A. Diaz-Guilera, J. Duch, and A. Arenas. Comparing community structure identification. *Journal of Statistical Mechanics*, page P09008, 2005.

[27] Akira Date, Elie Bienenstock, and Stuart Geman. On the temporal resolution of neural activity. Technical report, Division of Applied Mathematics, Brown University, 1998.

[28] J. E. Dayhoff. Synchrony detection in neural assemblies. *Biol Cybern*, 71(3):263–70, 1994.

[29] L. M. de la Prida, G. Huberfeld, I. Cohen, and R. Miles. Threshold behavior in the initiation of hippocampal population bursts. *Neuron*, 49(1):131–42, 2006.

[30] R. Dzakpasu and M. Zochowski. Discriminating differing types of synchrony in neural systems. *Physica D*, 208(1-2):115–122, 2005.

[31] S. Eldawlatly, R. Jin, and K. G. Oweiss. Identifying functional connectivity in large-scale neural ensemble recordings: A multiscale data mining approach. *Neural Comput*, pages 450–477, 2008.

[32] C. E. Elger and K. Lehnertz. Seizure prediction by non-linear time series analysis of brain electrical activity. *Eur J Neurosci*, 10(2):786–9, 1998.

[33] A. K. Engel, P. Konig, and W. Singer. Direct physiological evidence for scene segmentation by temporal coding. *PNAS*, 88(20):9136–40, 1991.

[34] A. K. Engel and W. Singer. Temporal binding and the neural correlates of sensory awareness. *Trends Cogn Sci*, 5(1):16–25, 2001.

[35] J. Engel. *Surgical treatment of epilepsies*. Raven Press, New York, 1987.

[36] S. Feldt, H. Osterhage, F. Mormann, K. Lehnertz, and M. Zochowski. Internetwork and intranetwork communications during bursting dynamics: applications to seizure prediction. *Phys Rev E*, 76(2 Pt 1):021920, 2007.

[37] S. Feldt, J. Waddell, V.L. Hetrick, J. D. Berke, and M. Zochowski. A functional clustering algorithm for the analysis of dynamic network data. *Phys Rev E*, 79(5):056104, 2009.

[38] S. Feldt, J.X. Wang, V.L. Hetrick, J. D. Berke, and M. Zochowski. Memory formation: from network structure to neural dynamics. *submitted to Philsophical Transactions A*, 2009.

[39] A. A. Fingelkurts, A. A. Fingelkurts, and S. Kahkonen. Functional connectivity in the brain - is it an elusive concept? *Neuroscience and Biobehavioral Reviews*, 28(8):827–836, 2005.

[40] S. Fortunato, V. Latora, and M. Marchiori. Method to find community structures based on information centrality. *Phys. Rev. E*, 70(5 Pt 2):056104, 2004.

[41] D. J. Foster and M. A. Wilson. Reverse replay of behavioural sequences in hippocampal place cells during the awake state. *Nature*, 440(7084):680–3, 2006.

[42] A. L. N. Fred and A. K. Jain. Robust data clustering. *2003 IEEE Computer Society Conference on Computer Vision and Pattern Recognition, Vol II, Proceedings*, pages 128–133, 2003.

[43] K. J. Friston, C. D. Frith, P. F. Liddle, and R. S. J. Frackowiak. Functional connectivity - the principal-component analysis of large (pet) data sets. *Journal of Cerebral Blood Flow and Metabolism*, 13(1):5–14, 1993.

[44] S. Fujisawa, A. Amarasingham, M. T. Harrison, and G. Buzsaki. Behavior-dependent short-term assembly dynamics in the medial prefrontal cortex. *Nat Neurosci*, 11(7):823–33, 2008.

[45] E. J. Furshpan and D. D. Potter. Seizure-like activity and cellular damage in rat hippocampal neurons in cell culture. *Neuron*, 3(2):199–207, 1989.

[46] G. L. Gerstein, D. H. Perkel, and J. E. Dayhoff. Cooperative firing activity in simultaneously recorded populations of neurons: detection and measurement. *J Neurosci*, 5(4):881–9, 1985.

[47] G. L. Gerstein, D. H. Perkel, and K. N. Subramanian. Identification of functionally related neural assemblies. *Brain Res*, 140(1):43–62, 1978.

[48] W. Gerstner and W. Kistler. *Spiking Neuron Models: Single Neurons, Populations, Plasticity*. Cambridge University Press, Cambridge, 2002.

[49] M. Girvan and M.E.J. Newman. Community structure in social and biological networks. *PNAS*, 99(12):7821–6, 2002.

[50] J. A. Gorter, E. A. van Vliet, E. Aronica, and F. H. Lopes da Silva. Long-lasting increased excitability differs in dentate gyrus vs. ca1 in freely moving chronic epileptic rats after electrically induced status epilepticus. *Hippocampus*, 12(3):311–24, 2002.

[51] C. M. Gray. The temporal correlation hypothesis of visual feature integration: Still alive and well. *Neuron*, 24(1):31–47, 1999.

[52] R. Guimera, S. Mossa, A. Turtschi, and L. A. Amaral. The worldwide air transportation network: Anomalous centrality, community structure, and cities' global roles. *PNAS*, 102(22):7794–9, 2005.

[53] M. I. Ham, L. M. Bettencourt, F. D. McDaniel, and G. W. Gross. Spontaneous coordinated activity in cultured networks: analysis of multiple ignition sites, primary circuits, and burst phase delay distributions. *J Comput Neurosci*, 24(3):346–57, 2008.

[54] K. D. Harris, J. Csicsvari, H. Hirase, G. Dragoi, and G. Buzsaki. Organization of cell assemblies in the hippocampus. *Nature*, 424(6948):552–6, 2003.

[55] D.O. Hebb. *The Organization of Behavior*. Wiley, New York, 1949.

[56] W. J. Henneman, J. D. Sluimer, J. Barnes, W. M. van der Flier, I. C. Sluimer, N. C. Fox, P. Scheltens, H. Vrenken, and F. Barkhof. Hippocampal atrophy rates in alzheimer disease: added value over whole brain volume measures. *Neurology*, 72(11):999–1007, 2009.

[57] H. Hong, M. Y. Choi, and B. J. Kim. Synchronization on small-world networks. *Phys Rev E*, 65(2 Pt 2):026139, 2002.

[58] J. J. Hopfield. Neural networks and physical systems with emergent collective computational abilities. *PNAS*, 79(8):2554–8, 1982.

[59] Christiaan Huygens. *Horologium Oscillatorum*. Apud F. Muget, Paris, 1673.

[60] L. D. Iasemidis, J. C. Sackellares, H. P. Zaveri, and W. J. Williams. Phase space topography and the lyapunov exponent of electrocorticograms in partial seizures. *Brain Topogr*, 2(3):187–201, 1990.

[61] J. T. Isaac, R. A. Nicoll, and R. C. Malenka. Evidence for silent synapses: implications for the expression of ltp. *Neuron*, 15(2):427–34, 1995.

[62] M. Ivenshitz and M. Segal. Simultaneous nmda-dependent long-term potentiation of epscs and long-term depression of ipscs in cultured rat hippocampal neurons. *J Neurosci*, 26(4):1199–210, 2006.

[63] P. Jablonski, G. R. Poe, and M. Zochowski. Structural network heterogeneities and network dynamics: a possible dynamical mechanism for hippocampal memory reactivation. *Phys Rev E*, 75(1 Pt 1):011912, 2007.

[64] E.R. Kandel, J.H. Schwartz, and T.M. Jessell. *Principles of Neural Science*. McGraw-Hill, New York, 4 edition, 2000.

[65] T. Kreuz, J. S. Haas, A. Morelli, H. D. I. Abarbanel, and A. Politi. Measuring spike train synchrony. *Journal of Neuroscience Methods*, 165(1):151–161, 2007.

[66] H. S. Kudrimoti, C. A. Barnes, and B. L. McNaughton. Reactivation of hippocampal cell assemblies: effects of behavioral state, experience, and eeg dynamics. *J Neurosci*, 19(10):4090–101, 1999.

[67] M. Le van Quyen, J. Martinerie, C. Adam, and F. J. Varela. Nonlinear analyses of interictal eeg map the brain interdependences in human focal epilepsy. *Physica D*, 127(3-4):250–266, 1999.

[68] M. Le Van Quyen, J. Martinerie, M. Baulac, and F. Varela. Anticipating epileptic seizures in real time by a non-linear analysis of similarity between eeg recordings. *Neuroreport*, 10(10):2149–55, 1999.

[69] M. Le Van Quyen, J. Martinerie, V. Navarro, P. Boon, M. D'Have, C. Adam, B. Renault, F. Varela, and M. Baulac. Anticipation of epileptic seizures from standard eeg recordings. *Lancet*, 357(9251):183–8, 2001.

[70] M. Le Van Quyen, J. Soss, V. Navarro, R. Robertson, M. Chavez, M. Baulac, and J. Martinerie. Preictal state identification by synchronization changes in long-term intracranial eeg recordings. *Clin Neurophysiol*, 116(3):559–68, 2005.

[71] K. Lehnertz and C. E. Elger. Spatio-temporal dynamics of the primary epileptogenic area in temporal lobe epilepsy characterized by neuronal complexity loss. *Electroencephalogr Clin Neurophysiol*, 95(2):108–17, 1995.

[72] E. A. Leicht and M. E. J. Newman. Community structure in directed networks. *Phys Rev Lett*, 100(11):118703, 2008.

[73] M. Lengyel, J. Kwag, O. Paulsen, and P. Dayan. Matching storage and recall: hippocampal spike timing-dependent plasticity and phase response curves. *Nat Neurosci*, 8(12):1677–83, 2005.

[74] R. Lestienne. Spike timing, synchronization and information processing on the sensory side of the central nervous system. *Prog Neurobiol*, 65(6):545–91, 2001.

[75] Y. Li, W. Zhou, X. Li, S. Zeng, and Q. Luo. Dynamics of learning in cultured neuronal networks with antagonists of glutamate receptors. *Biophys J*, 93(12):4151–8, 2007.

[76] B. G. Lindsey and G. L. Gerstein. Two enhancements of the gravity algorithm for multiple spike train analysis. *J Neurosci Methods*, 150(1):116–27, 2006.

[77] K. Louie and M. A. Wilson. Temporally structured replay of awake hippocampal ensemble activity during rapid eye movement sleep. *Neuron*, 29(1):145–56, 2001.

[78] J. H. Lu, X. H. Yu, G. R. Chen, and D. Z. Cheng. Characterizing the synchronizability of small-world dynamical networks. *IEEE Transactions on Circuits and Systems I-Regular Papers*, 51(4):787–796, 2004.

[79] H. Markram, J. Lubke, M. Frotscher, and B. Sakmann. Regulation of synaptic efficacy by coincidence of postsynaptic aps and epsps. *Science*, 275(5297):213–5, 1997.

[80] F. Marrosu, C. Portas, M. S. Mascia, M. A. Casu, M. Fa, M. Giagheddu, A. Imperato, and G. L. Gessa. Microdialysis measurement of cortical and hippocampal acetylcholine release during sleep-wake cycle in freely moving cats. *Brain Res*, 671(2):329–32, 1995.

[81] J. Martinerie, C. Adam, M. Le Van Quyen, M. Baulac, S. Clemenceau, B. Renault, and F. J. Varela. Epileptic seizures can be anticipated by non-linear analysis. *Nat Med*, 4(10):1173–6, 1998.

[82] N. Masuda and K. Aihara. Duality of rate coding and temporal coding in multilayered feedforward networks. *Neural Comput*, 15(1):103–25, 2003.

[83] L. K. McEvoy, C. Fennema-Notestine, J. C. Roddey, Jr. Hagler, D. J., D. Holland, D. S. Karow, C. J. Pung, J. B. Brewer, and A. M. Dale. Alzheimer disease: quantitative structural neuroimaging for detection and prediction of clinical and structural changes in mild cognitive impairment. *Radiology*, 251(1):195–205, 2009.

[84] P. M. Milner. A model for visual shape recognition. *Psychol Rev*, 81(6):521–35, 1974.

[85] F. Mormann, R. G. Andrzejak, C. E. Elger, and K. Lehnertz. Seizure prediction: the long and winding road. *Brain*, 130(Pt 2):314–33, 2007.

[86] F. Mormann, R. G. Andrzejak, T. Kreuz, C. Rieke, P. David, C. E. Elger, and K. Lehnertz. Automated detection of a preseizure state based on a decrease in synchronization in intracranial electroencephalogram recordings from epilepsy patients. *Phys Rev E*, 67(2 Pt 1):021912, 2003.

[87] F. Mormann, T. Kreuz, R. G. Andrzejak, P. David, K. Lehnertz, and C. E. Elger. Epileptic seizures are preceded by a decrease in synchronization. *Epilepsy Res*, 53(3):173–85, 2003.

[88] F. Mormann, T. Kreuz, C. Rieke, R. G. Andrzejak, A. Kraskov, P. David, C. E. Elger, and K. Lehnertz. On the predictability of epileptic seizures. *Clin Neurophysiol*, 116(3):569–87, 2005.

[89] F. Mormann, K. Lehnertz, P. David, and C. E. Elger. Mean phase coherence as a measure for phase synchronization and its application to the eeg of epilepsy patients. *Physica D*, 144(3-4):358–369, 2000.

[90] V. Navarro, J. Martinerie, M. Le Van Quyen, S. Clemenceau, C. Adam, M. Baulac, and F. Varela. Seizure anticipation in human neocortical partial epilepsy. *Brain*, 125(Pt 3):640–55, 2002.

[91] T. I. Netoff, R. Clewley, S. Arno, T. Keck, and J. A. White. Epilepsy in small-world networks. *J Neurosci*, 24(37):8075–83, 2004.

[92] W. J. Nett, S. H. Oloff, and K. D. McCarthy. Hippocampal astrocytes in situ exhibit calcium oscillations that occur independent of neuronal activity. *J Neurophysiol*, 87(1):528–37, 2002.

[93] M. E. Newman. Fast algorithm for detecting community structure in networks. *Phys Rev E*, 69(6 Pt 2):066133, 2004.

[94] M. E. Newman and M. Girvan. Finding and evaluating community structure in networks. *Phys Rev E*, 69(2 Pt 2):026113, 2004.

[95] M. E. J. Newman. The structure and function of complex networks. *SIAM Review*, 45(2):167–256, 2003.

[96] M. E. J. Newman. Modularity and community structure in networks. *PNAS*, 103(23):8577–8582, 2006.

[97] M.E.J. Newman. Analysis of weighted networks. *Phys Rev E*, 70(5 Pt 2):056131, 2004.

[98] T. Nishikawa, A. E. Motter, Y. C. Lai, and F. C. Hoppensteadt. Heterogeneity in oscillator networks: are smaller worlds easier to synchronize? *Phys Rev Lett*, 91(1):014101, 2003.

[99] J. O'Keefe and N. Burgess. Dual phase and rate coding in hippocampal place cells: theoretical significance and relationship to entorhinal grid cells. *Hippocampus*, 15(7):853–66, 2005.

[100] J. O'Neill, T. J. Senior, K. Allen, J. R. Huxter, and J. Csicsvari. Reactivation of experience-dependent cell assembly patterns in the hippocampus. *Nat Neurosci*, 11(2):209–15, 2008.

[101] G.V. Osipov, J. Kurths, and C. Zhou. *Synchronization in Oscillatory Networks*. Springer Series in Synergetics. Springer-Verlag Berlin Heidelberg, New York, 2007.

[102] I. Ozden, H. M. Lee, M. R. Sullivan, and S. S. H. Wang. Identification and clustering of event patterns from in vivo multiphoton optical recordings of neuronal ensembles. *Journal of Neurophysiology*, 100(1):495–503, 2008.

[103] J. M. Parent and D. H. Lowenstein. Mossy fiber reorganization in the epileptic hippocampus. *Curr Opin Neurol*, 10(2):103–9, 1997.

[104] V. Pasquale, P. Massobrio, L. L. Bologna, M. Chiappalone, and S. Martinoia. Self-organization and neuronal avalanches in networks of dissociated cortical neurons. *Neuroscience*, 153(4):1354–69, 2008.

[105] L. Pasti, A. Volterra, T. Pozzan, and G. Carmignoto. Intracellular calcium oscillations in astrocytes: a highly plastic, bidirectional form of communication between neurons and astrocytes in situ. *J Neurosci*, 17(20):7817–30, 1997.

[106] C. Pavlides and J. Winson. Influences of hippocampal place cell firing in the awake state on the activity of these cells during subsequent sleep episodes. *J Neurosci*, 9(8):2907–18, 1989.

[107] A. Pazienti, P. E. Maldonado, M. Diesmann, and S. Grun. Effectiveness of systematic spike dithering depends on the precision of cortical synchronization. *Brain Res*, 1225:39–46, 2008.

[108] B. Percha, R. Dzakpasu, M. Zochowski, and J. Parent. Transition from local to global phase synchrony in small world neural network and its possible implications for epilepsy. *Phys Rev E*, 72(3 Pt 1):031909, 2005.

[109] F. W. Pfrieger and B. A. Barres. Synaptic efficacy enhanced by glial cells in vitro. *Science*, 277(5332):1684–7, 1997.

[110] Arkady Pikovsky, Michael Rosenblum, and Jurgen Kurths. *Synchronization: A universal concept in nonlinear sciences*, volume 12 of *Cambridge Nonlinear Science Series*. University Press, Cambridge, 2001.

[111] G. R. Poe, C. M. Thompson, B. T. Riley, M. K. Tysor, T. E. Bjorness, B. P. Steinhoff, and E. D. Ferluga. A spatial memory task appropriate for electrophysiological recordings. *J Neurosci Methods*, 121(1):65–74, 2002.

[112] N. Raichman and E. Ben-Jacob. Identifying repeating motifs in the activation of synchronized bursts in cultured neuronal networks. *J Neurosci Methods*, 170(1):96–110, 2008.

[113] J. D. Rolston, D. A. Wagenaar, and S. M. Potter. Precisely timed spatiotemporal patterns of neural activity in dissociated cortical cultures. *Neuroscience*, 148(1):294–303, 2007.

[114] M. G. Rosenblum, A. S. Pikovsky, and J. Kurths. Phase synchronization of chaotic oscillators. *Phys Rev Lett*, 76(11):1804–1807, 1996.

[115] M. G. Rosenblum, A. S. Pikovsky, and J. Kurths. From phase to lag synchronization in coupled chaotic oscillators. *Phys Rev Lett*, 78(22):4193–4196, 1997.

[116] Michael Rosenblum and Jurgen Kurths. Analyzing synchronization phenomena from bivariate data by means of the hilbert transform. In H. Kantz, J. Kurths, and G. Mayer-Kress, editors, *Nonlinear Analysis of Physiological Data*, pages 91–99. Springer, Berlin, 1998.

[117] A. Roxin, H. Riecke, and S. A. Solla. Self-sustained activity in a small-world network of excitable neurons. *Phys Rev Lett*, 92(19):198101, 2004.

[118] C. Schafer, M. G. Rosenblum, J. Kurths, and H. H. Abel. Heartbeat synchronized with ventilation. *Nature*, 392(6673):239–40, 1998.

[119] E. Schneidman, W. Bialek, and M.J. Berry II. An information theoretic approach to the functional classification of neurons. In S. Becker, S. Thrun, and K. Obermayer, editors, *Advances in Neural Information Processing 15*, pages 197–204. MIT Press, Cambridge, 2003.

[120] A. J. Schwarz, A. Gozzi, and A. Bifone. Community structure and modularity in networks of correlated brain activity. *Magnetic Resonance Imaging*, 26(7):914–920, 2008.

[121] G. Shahaf and S. Marom. Learning in networks of cortical neurons. *J Neurosci*, 21(22):8782–8, 2001.

[122] T. Shmiel, R. Drori, O. Shmiel, Y. Ben-Shaul, Z. Nadasdy, M. Shemesh, M. Teicher, and M. Abeles. Temporally precise cortical firing patterns are associated with distinct action segments. *Journal of Neurophysiology*, 96(5):2645–2652, 2006.

[123] B. H. Singer, M. Derchansky, P. L. Carlen, and M. Zochowski. Lag synchrony measures dynamical processes underlying progression of seizure states. *Phys Rev E*, 73(2 Pt 1):021910, 2006.

[124] W. Singer. Synchronization of cortical activity and its putative role in information processing and learning. *Annu Rev Physiol*, 55:349–74, 1993.

[125] W. Singer. Neuronal synchrony: a versatile code for the definition of relations? *Neuron*, 24(1):49–65, 111–25, 1999.

[126] W. Singer. Consciousness and the binding problem. *Ann NY Acad Sci*, 929:123–46, 2001.

[127] N. Slonim, G. S. Atwal, G. Tkacik, and W. Bialek. Information-based clustering. *PNAS*, 102(51):18297–302, 2005.

[128] S. Sombati and R. J. Delorenzo. Recurrent spontaneous seizure activity in hippocampal neuronal networks in culture. *J Neurophysiol*, 73(4):1706–11, 1995.

[129] S. Song and L. F. Abbott. Cortical development and remapping through spike timing-dependent plasticity. *Neuron*, 32(2):339–50, 2001.

[130] S. Song, K. D. Miller, and L. F. Abbott. Competitive hebbian learning through spike-timing-dependent synaptic plasticity. *Nat Neurosci*, 3(9):919–26, 2000.

[131] W. V. Soussou, G. J. Yoon, R. D. Brinton, and T. W. Berger. Neuronal network morphology and electrophysiologyof hippocampal neurons cultured on surface-treated multielectrode arrays. *IEEE Trans Biomed Eng*, 54(7):1309–20, 2007.

[132] K. V. Srinivas, R. Jain, S. Saurav, and S. K. Sikdar. Small-world network topology of hippocampal neuronal network is lost, in an in vitro glutamate injury model of epilepsy. *Eur J Neurosci*, 25(11):3276–86, 2007.

[133] S. H. Strogatz. Exploring complex networks. *Nature*, 410(6825):268–76, 2001.

[134] T. P. Sutula and F. E. Dudek. Unmasking recurrent excitation generated by mossy fiber sprouting in the epileptic dentate gyrus: an emergent property of a complex system. *Prog Brain Res*, 163:541–63, 2007.

[135] A. Tang, D. Jackson, J. Hobbs, W. Chen, J. L. Smith, H. Patel, A. Prieto, D. Petrusca, M. I. Grivich, A. Sher, P. Hottowy, W. Dabrowski, A. M. Litke, and J. M. Beggs. A maximum entropy model applied to spatial and temporal correlations from cortical networks in vitro. *J Neurosci*, 28(2):505–18, 2008.

[136] P. Tass, M. G. Rosenblum, J. Weule, J. Kurths, A. Pikovsky, J. Volkmann, A. Schnitzler, and H. J. Freund. Detection of n: m phase locking from noisy data: Application to magnetoencephalography. *Phys Rev Lett*, 81(15):3291–3294, 1998.

[137] M. Timme, T. Geisel, and F. Wolf. Speed of synchronization in complex networks of neural oscillators: analytic results based on random matrix theory. *Chaos*, 16(1):015108, 2006.

[138] C. Verderio, A. Bacci, S. Coco, E. Pravettoni, G. Fumagalli, and M. Matteoli. Astrocytes are required for the oscillatory activity in cultured hippocampal neurons. *Eur J Neurosci*, 11(8):2793–800, 1999.

[139] V. Volman, R. C. Gerkin, P. M. Lau, E. Ben-Jacob, and G. Q. Bi. Calcium and synaptic dynamics underlying reverberatory activity in neuronal networks. *Phys Biol*, 4(2):91–103, 2007.

[140] C. von der Malsburg. The correlation of brain function. Internal report, MPI Biophysical Chemistry, 1981.

[141] C. von der Malsburg. Binding in models of perception and brain function. *Curr Opin Neurobiol*, 5(4):520–6, 1995.

[142] J. Waddell, R. Dzakpasu, V. Booth, B. Riley, J. Reasor, G. Poe, and M. Zochowski. Causal entropies–a measure for determining changes in the temporal organization of neural systems. *J Neurosci Methods*, 162(1-2):320–32, 2007.

[143] J. Waddell and M. Zochowski. Intraburst versus interburst locking in networks of driven nonidentical oscillators. *Phys Rev E*, 76(5 Pt 2):056216, 2007.

[144] D. A. Wagenaar, J. Pine, and S. M. Potter. An extremely rich repertoire of bursting patterns during the development of cortical cultures. *BMC Neurosci*, 7:11, 2006.

[145] T. L. Wallace and Jr. Johnson, E. M. Cytosine arabinoside kills postmitotic neurons: evidence that deoxycytidine may have a role in neuronal survival that is independent of dna synthesis. *J Neurosci*, 9(1):115–24, 1989.

[146] J. Wang and P. De Wilde. Properties of evolving e-mail networks. *Phys Rev E*, 70(6 Pt 2):066121, 2004.

[147] X. F. Wang and G. R. Chen. Synchronization in small-world dynamical networks. *International Journal of Bifurcation and Chaos*, 12(1):187–192, 2002.

[148] D. J. Watts and S. H. Strogatz. Collective dynamics of 'small-world' networks. *Nature*, 393(6684):440–2, 1998.

[149] B. Wemmenhove and A. C. C. Coolen. Finite connectivity attractor neural networks. *Journal of Physics A*, 36(37):9617–9633, 2003.

[150] M. A. Wilson and B. L. McNaughton. Reactivation of hippocampal ensemble memories during sleep. *Science*, 265(5172):676–9, 1994.

[151] C. S. Zhou, L. Zemanova, G. Zamora-Lopez, C. C. Hilgetag, and J. Kurths. Structure-function relationship in complex brain networks expressed by hierarchical synchronization. *New Journal of Physics*, 9:178, 2007.

[152] H. Zhou. Network landscape from a brownian particle's perspective. *Phys Rev E*, 67(4 Pt 1):041908, 2003.

[153] M. Zochowski and R. Dzakpasu. Conditional entropies, phase synchronization and changes in the directionality of information flow in neural systems. *J Phys A*, 37(12):3823–3834, 2004.